NPS-69SL79011

NAVAL POSTGRADUATE SCHOOL

Monterey, California

A DISCRETE-VORTEX ANALYSIS OF FLOW ABOUT STATIONARY AND TRANSVERSELY OSCILLATING CIRCULAR CYLINDERS

T. SARPKAYA R. L. SHOAFF

January 1979

Approved for public release; distribution unlimited.

Prepared for:

Civil Engineering Laboratory
Naval Construction Battalion Center
Port Hueneme, California 93043

NPS-69SL79011

NAVAL POSTGRADUATE SCHOOL

Monterey, California

Rear Admiral T. F. Dedman
Superintendent

Jack R. Borsting
Provost

The work reported herein was supported by the Civil Engineering Laboratory of the Naval Construction Battalion Center, Port Hueneme, California 93043.

This report was prepared by:

Turgut Sarpkaya
Distinguished Professor of
Mechanical Engineering

Reviewed by:

Paul J. Marto, Chairman
Department of Mechanical
Engineering

Released by:

William Tolles
Dean of Research

NPS-69SL79011
January 1979

UNCLASSIFIED

(14) NPS-69SL-79-011

SECURITY CLASSIFICATION OF THIS PAGE (When Data Entered)

REPORT DOCUMENTATION PAGE

READ INSTRUCTIONS BEFORE COMPLETING FORM

1. REPORT NUMBER: NPS-69SL79011
2. GOVT ACCESSION NO.
3. RECIPIENT'S CATALOG NUMBER: rept.

(6) 4. TITLE (and Subtitle): A Discrete Vortex Analysis of Flow About Stationary and Transversely Oscillating Circular Cylinders.

(9) 5. TYPE OF REPORT & PERIOD COVERED: Interim Sept. 77- Dec. 78,

6. PERFORMING ORG. REPORT NUMBER

(10) 7. AUTHOR(s): T. Sarpkaya, Distinguished Professor of Mechanical Engineering
R.W. Shaaff
Sarpkaya

8. CONTRACT OR GRANT NUMBER(s): (12) 167p

9. PERFORMING ORGANIZATION NAME AND ADDRESS
Naval Postgraduate School
Monterey, California 93940

10. PROGRAM ELEMENT, PROJECT, TASK AREA & WORK UNIT NUMBERS
62759N, YF52.556
N68305 78 WR-8-0078

11. CONTROLLING OFFICE NAME AND ADDRESS
Civil Engineering Laboratory
NCBC, Port Hueneme, California 93043

(11) 12. REPORT DATE: January 1979

13. NUMBER OF PAGES: 166

14. MONITORING AGENCY NAME & ADDRESS (if different from Controlling Office)
(16) F52 556

15. SECURITY CLASS. (of this report): Unclassified

15a. DECLASSIFICATION/DOWNGRADING SCHEDULE

16. DISTRIBUTION STATEMENT (of this Report)

Approved for public release; distribution unlimited

17. DISTRIBUTION STATEMENT (of the abstract entered in Block 20, if different from Report)

18. SUPPLEMENTARY NOTES

19. KEY WORDS (Continue on reverse side if necessary and identify by block number)

Hydroelastic Oscillations, Analysis of Transverse Oscillations,
Cable Strumming, Discrete-Vortex Model.

20. ABSTRACT (Continue on reverse side if necessary and identify by block number)

A comprehensive numerical model has been developed to investigate the characteristics of flow about a circular cylinder undergoing synchronized transverse oscillations. The model is based on the rediscretization of the shear layers, wake-boundary-layer interaction, and the dissipation of vorticity.

The forces acting on the cylinder, rate of vorticity flux, Strouhal number, cylinder response, oscillations of the stagnation and separation

over

DD FORM 1 JAN 73 1473 EDITION OF 1 NOV 65 IS OBSOLETE
S/N 0102-014-6601

UNCLASSIFIED

SECURITY CLASSIFICATION OF THIS PAGE (When Data Entered)

251 450 79 02 02 066

points, longitudinal and transverse spacing of the vortices, and the base pressure have been calculated and shown to be in conformity with those obtained experimentally.

The model has been used to predict the characteristics of hydro-elastic oscillations of a cylinder in the range of synchronization. The numerical experiments shed considerable light on the interaction between the fluid motion in the wake and the dynamics of the body.

An extensive sensitivity analysis has been carried out to determine the stability of all the parameters and hence the stability of the numerical model itself.

TABLE OF CONTENTS

LIST OF FIGURES

LIST OF SYMBOLS

a_o	Mass parameter
c	Cylinder radius
C_D	Drag coefficient, $F_D/\rho U^2 c$
C_L	Lift coefficient, $F_L/\rho U^2 c$
C_L^*	Lift coefficient at perfect synchronization
C_{L_o}	Lift coefficient for stationary cylinder
C_M	Added mass coefficient
C_{pb}	Base pressure coefficient
D	Cylinder diameter, $D = 2c$
E	Energy imbalance parameter
F	Force
f	Frequency
f_c	Cylinder oscillation frequency
f_n	Natural frequency of oscillating cylinder
f_v	Vortex shedding frequency
f_{v_o}	Vortex shedding frequency for a stationary cylinder
h_v	Transverse vortex spacing
i	$= \sqrt{-1}$
L	Length of cylinder
ℓ_{fr}	Length of vortex-formation region
ℓ_{sr}	Length of stable wake region
ℓ_v	Longitudinal vortex spacing
m	Mass of the cylinder
p	Circulation reduction parameter

$q(z)$	Complex velocity
r	Radial distance
Re	Reynolds number, $Re = UD/\nu$
Re{ }	Real part of a complex quantity
rms	Root-mean-square
s_G	Response parameter, $s_G = \zeta/a_o$
s	Distance measured along vortex sheet
s_n	Distance measured along vortex sheet from the core of the spiral to the n-th vortex
St	Strouhal number, $St = f_v D/U$
S_o	Strouhal number for stationary cylinder
t	Time
T	Period
T_c	Period of cylinder oscillation, $1/f_c$
T_n	Natural cylinder oscillation period, $1/f_n$
T_v	Vortex shedding period, $1/f_v$
U	Ambient flow speed
u	x-component of velocity
U_M	Maximum velocity
U_r	Reduced velocity, $U_r = U/\omega_n D$
U_s	Outer flow speed at separation point
U_r^*	Reduced velocity at perfect synchronization
v	y-component of velocity
$w(z)$	Complex potential function
x	Longitudinal displacement
y	Transverse displacement
z	Complex variable, $z = x + iy$

z_o	Instantaneous position of cylinder center
Δx	Change in x displacement
Δt	Time step
$\gamma(s)$	Vorticity distribution function for a vortex sheet
γ_n	Value of vorticity distribution function at n-th vortex location
Γ	Total circulation of a vortex
Γ_n	Circulation of n-th point vortex
Γ_{nv}	Circulation of nascent vortex
δ	Boundary layer thickness
δs	Spacing between two adjacent point vortices on a sheet before rediscretization
δs_n	Length of sheet segment corresponding to n-th vortex
$\delta \hat{s}$	Spacing between two point vortices after rediscretization
ε	Radial distance to the nascent vortex from the cylinder
ζ	Material damping ratio
η	Normalized transverse cylinder displacement
η_M	Maximum value of η for a given value of ω_o or U_r
η_M^*	η_M at perfect synchronization
θ	Angle
θ_s	Separation angle measured from negative x-axis
$\overline{\theta}_s$	Average value of θ_s
θ_{stag}	Stagnation point measured from negative x-axis
ν	Kinematic viscosity of fluid
ξ	Distance along the cylinder surface measured from the forward stagnation point
ρ	Density
ρ_f	Fluid density
ϕ	Phase angle between lift force and cylinder displacement

ϕ^*	ϕ at perfect synchronization
ω	Circular frequency
ω_c	Cylinder oscillation frequency
ω_n	Natural frequency of oscillating cylinder
ω_o	Normalized frequency, $\omega_o = \omega_{v_o}/\omega_n$
ω_o^*	ω_o at perfect synchronization
ω_v	Vortex shedding frequency, $\omega_v = 2\pi f_v$
ω_v^*	ω_v at perfect synchronization
ω_{v_o}	ω_v for a stationary cylinder

ACKNOWLEDGMENTS

The work reported herein has been supported by the Civil Engineering Laboratory of the Naval Construction Battalion Center, Port Hueneme, Calif. This support and the continued encouragement of Mr. Dallas J. Meggitt are gratefully acknowledged.

The computer time has been donated by the Fleet Numerical Weather Central.

I. INTRODUCTION

A. FLOW SEPARATION

Real fluids flowing over bluff bodies separate under the influence of adverse pressure gradient as momentum is consumed by wall shear. Separation is best understood in terms of its consequences. In fact, it was the keen observations of separation in diffusers that led Prandtl to introduce the concept of transition or boundary layer theory. Even though the boundary layer theory has revolutionized fluid dynamics, the phenomenon which gave impetus to its discovery still remains an enigma.

Through the years various characteristics of separated flow about bluff bodies in general and about circular cylinders in particular have been partially understood through observations, measurements, and analyses.

The separation point may be mobile as on a circular cylinder or fixed along a line as on a wedge or blunt-based body. When a separation point is mobile, the pressure decreases up to the point of maximum velocity (slightly upstream of separation) and then increases up to the point of separation. When the separation point is fixed, the pressure continues to decrease up to the point of separation. Consequently, there are significant differences in the separation of flow about a circular cylinder and a sharp-edged body. In either case the velocity distribution, rate of vorticity flux, and the amplitude and frequency of oscillation of the separation points are not independent of the wake in the downstream side of the body. It is this interaction that makes the calculation of separated flows exceedingly complex. In other words, one needs the evolution of the boundary layer on the forebody (upstream of separation) of the

cylinder in order to determine the instantaneous position of the separation points. But, the characteristics of the boundary layer are, in turn, strongly affected by the fluid motion in the wake. Evidently, one needs some kind of an interactive mechanism whereby the effect of the wake on the boundary layer, and hence separation, can be given proper consideration. In mathematical terms one can state that the unseparated potential flow, or the d'Alembert flow, does not even constitute a first approximation to the separated real flow. Partly the realization of this fact, partly the difficulties associated with the integration of the Navier-Stokes equations across a singularity (separation point), and partly lack of sufficient computational capability have prevented the prediction of the kinematic and dynamic characteristics of separated flows about bluff bodies. In the following, the basic characteristics of flow about circular cylinders are described with special emphasis on those aspects which prepare the reader for the understanding of the numerical model developed during the course of this work and the assessment of the similarities and dissimilarities between the predictions and observations and measurements.

B. VORTEX SHEDDING

The separation of flow gives rise to alternate vortex shedding. This phenomenon is intrinsic to the flow itself and has been known at least since the times of Leonardo de Vinci. In 1878, almost exactly 100 years ago, Strouhal discovered that there is a relationship between the frequency of vortex shedding, the velocity of flow, and the diameter of the cylinder. This relationship, which is now known as the Strouhal Number, St, is given by $St = fD/U$. Strouhal's experiments gave an average value of $St = 0.185$. During the course of numerous experiments since then, it has been experimentally demonstrated that: (i) the Strouhal number is dependent on

the Reynolds number and, as first suggested by Lord Rayleigh, must be written as $f = St(Re)U/D$; (ii) the vortex shedding frequency is only an average quantity for a given flow and that there are always secondary and tertiary frequencies present; and finally, (iii) there are regions of flow such as the region of drag crisis where it is quite difficult to identify a particular frequency. It is evident from these facts that in some regions of flow one must speak of the spectral content of the wake fluctuations in assessing the value of the Strouhal number and the forces exerted on the cylinder. The foregoing discussion of the Strouhal number raises two questions: firstly, is it possible to devise a universal Strouhal number which would be applicable to all two and three-dimensional bluff bodies, and secondly, is it possible to theoretically predict the Strouhal number through, for example, the perturbation of the d'Alembert flow. An attempt along these lines has been made by Sacksteder [1] who found $St = 0.2028$ for an infinitely large Reynolds number. The reasoning behind this prediction and its validity will not be discussed here further.

The former question of the possibility of devising a universal Strouhal number has been of interest to various researchers. Table I, shown below, lists those definitions together with their originators.

TABLE I

St =	Value	Body Type	Originator
$f_v h'/UK$	0.163	two-dimensional bodies	Roshko [2]
$f_v \ell_v/U$	0.181	two-dimensional bodies	Bearman [3]
$f_v \ell_w/K \cdot U$	0.190	axisymmetric bodies	Calvert [4]
$f_v \ell_w/K \cdot U$	0.163	two-dimensional bodies	Simmons [5]

In Table I, h' represents the wake width as determined from Roshko's notched- hodograph theory [2]; ℓ_v, lateral spacing of the vortices as

determined by Kronauner's minimum drag criteria as reported by Bearman [3]; ℓ_w, the wake width at a distance of the wake establishment region; and $K = \sqrt{1-C_{pb}}$ where C_{pb} is the base pressure coefficient. All these definitions require either the measurement or the solution of one or more characteristics of the wake. Thus, their capability to predict a vortex shedding frequency is quite limited.

It is advantageous to note at an early stage those factors which influence the Strouhal number. Firstly, small amplitude transverse oscillation of cylinders or cables distinctly regularize the vortex shedding and hence the Strouhal number. For example, the experiments conducted at the National Physical Laboratory [6] have shown that the Strouhal number even in the drag crisis region remains perfectly constant and equal to about 0.21. Secondly, the vortices do not peel off from a cylinder as perfectly two-dimensional line vortices. As it was first shown by Humphreys [7], there is a cell pattern separated by a correlation length. The longer the cylinder the larger the number of cells. The consequences of the formation of such cells are that there are phase shifts in pressure along the cylinder and hence a reduction in the integrated transverse force. In other words, the transverse force calculated through the integration of the pressure distribution at a given section is not identical to the average transverse force determined experimentally. All numerical analyses which model the complex three-dimensional flow as a two-dimensional flow must necessarily predict a transverse force or lift coefficient somewhat larger than those found by measurements. Other consequences of the cell formation concern the strength of the vortices. The vortices are not necessarily oriented in a plane normal to the flow and the measurements (flow visualization or electro-optical techniques) yield only that

component of vorticity which is normal to the plane of flow. Additionally, experimental results necessarily depend on the length-to-diameter ratio, end conditions, intensity and scale of turbulence in the ambient flow, the rigidity of the cylinder mounting, and of course on Reynolds number and the surface conditions of the cylinder. Most recent experiments (Shih and Hove [8]) have shown that roughness affects the base pressure in the same manner as the small transverse oscillations (beyond a threshold limit of about 0.10 diameters). Uniform roughness yields a perfectly uniform base pressure and removes the cell pattern.

C. RESISTANCE IN STEADY FLOWS

1. In-Line Forces

The understanding of the fluid forces exerted on bluff bodies comes primarily from measurements. Of all bluff bodies, the circular cylinder has been subjected to the largest number of investigations. Those experiments which constitute milestones in the determination of the magnitude and characteristics of resistance are the works by Wieselsberger [9], Fage and Johansen [10], and Roshko [11]. A plot of the drag coefficient, C_D defined by $C_D = 2F/\rho LDU^2$, is shown in Fig. 1 as a function of the Reynolds number defined by $Re = UD/\nu$. It is a well known fact that for Reynolds numbers larger than about 10^4 and smaller than about 2×10^5, the drag coefficient for a circular cylinder remains essentially constant at a value of about 1.2. For $Re > 2\times10^5$, the shear layers emanating from the separation points become turbulent. Since a turbulent flow can exchange larger momentum between the inner and outer flow (i.e., between the boundary layer and external flow), it can sustain a larger adverse pressure gradient and even reattach to the cylinder. The reattachment of the turbulent shear layers gives rise to the formation of so called separation

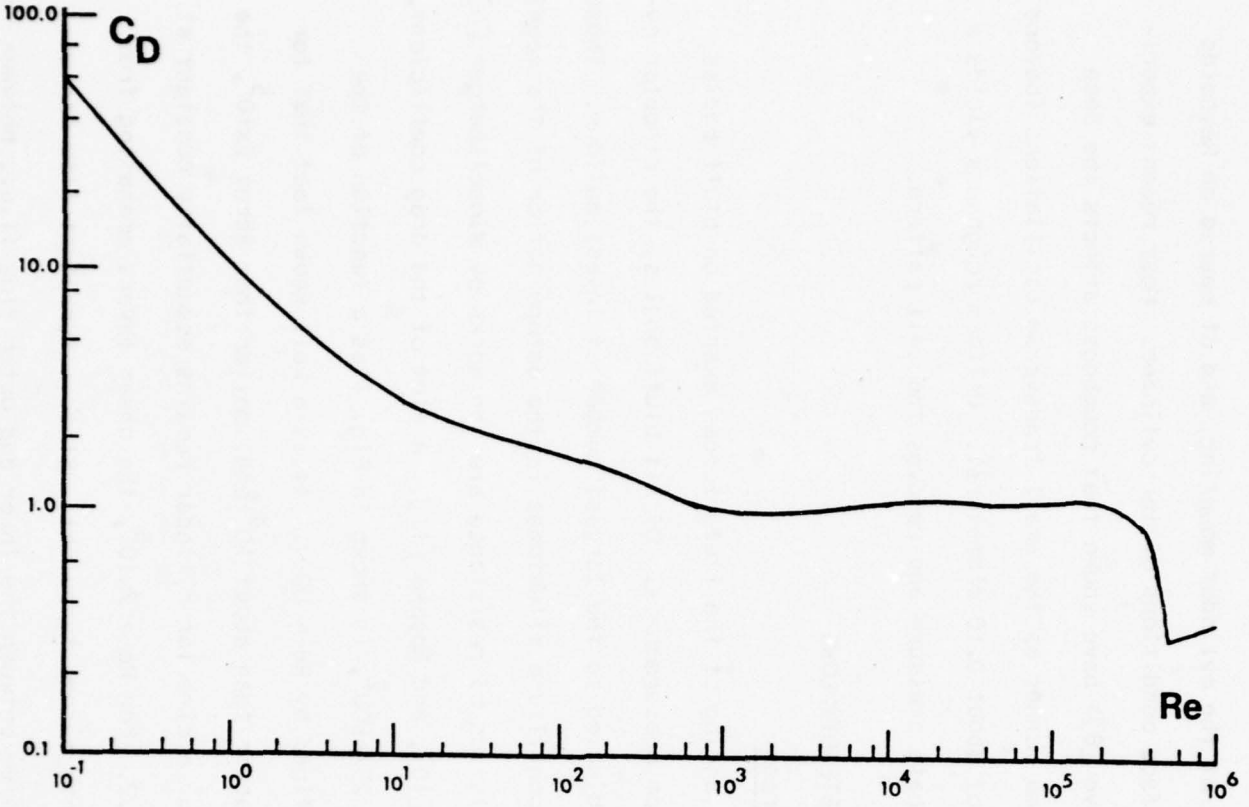

Fig. 1. Drag coefficient versus Reynolds number for a smooth circular cylinder.

bubbles and to the displacement of the attached flow further downstream from the first separation point. The reattached flow cannot continue to remain attached indefinitely and reseparates at an angle of about 130 degrees from the front stagnation point. Thus, the transition of the flow in the shear layers from a laminar to a turbulent state results in a considerably smaller wake and hence in a considerably reduced drag coefficient. This particular flow regime is commonly called the drag crisis region or the critical region. As the Reynolds number increases, parts of the boundary layer adjacent to the first separation point become turbulent and the second separation point begins to move gradually upstream. This region is called the transcritical region. At higher Reynolds numbers, the entire boundary layer becomes turbulent and the drag coefficient reaches a nearly constant value of about 0.6. There is considerable scatter in the data in the supercritical region because of the difficulties associated with flows at such high speeds.

The present knowledge of the drag coefficient for a smooth cylinder is limited to Reynolds numbers smaller than about 10^7. There is great practical interest in the determination of force coefficients, i.e., drag coefficient, lift coefficient, and the Strouhal number for projects such as ocean thermal energy conversion (OTEC), large cooling towers, high rise structures, etc. A careful consideration of the various possible methods to obtain data at Reynolds numbers in the order of 10^8 or 10^{10} shows that there are practically insurmountable difficulties. The existing wind and water tunnels are not capable of yielding such high Reynolds numbers without the adverse effects of blockage and compressibility. The pop-up and drop-down experiments with large cylinders are constrained by cavitation, weight, and stability conditions. It might be possible in the future to

close the high Reynolds number gap by building large cryogenic wind tunnels operating with freon or liquid helium.

The drag coefficient depicted in Fig. 1 may be influenced by a number of factors such as roughness and turbulence. Numerous investigators, notably Fage and Warsap [12], Achenbach [13], and Güven [14], have clearly demonstrated that the larger the surface roughness, the sooner is the occurrence of the critical region and the higher the dip in the drag coefficient (see Fig. 2). Turbulence plays a similar role in the evolution of the drag coefficients. It should be noted from Fig. 2 that the drag coefficient for a rough cylinder at supercritical Reynolds numbers is about twice that for a smooth cylinder. Furthermore, the experiments by Güven [14] and Szechenyi [15] have shown that at sufficiently high Reynolds numbers there is a Reynolds number independent region. This experimental fact has been termed the independence principle and used (Shih and Hove [8]) to extrapolate the drag coefficient data to Reynolds numbers in the order of 10^8. If the validity of the independence principle can be demonstrated unambiguously, it may obviate the need for difficult experiments in cryogenic tunnels.

2. Transverse Forces

Lift or transverse-force coefficient data are far less numerous and exhibit a great deal of scatter. Figure 3, which represents most of the existing lift coefficient data, shows that the lift coefficient, C_L defined by C_L = (amplitude of lift force)/$0.5\rho LDU^2$, may vary from 0.2 to 1.0 in the subcritical Reynolds number range. In the critical range it is impossible to define a lift coefficient without resorting to its root-mean-square (rms) values. It is for this reason that some of the data appearing in Fig. 3 are in terms of the rms values of the lift coefficients. For a more

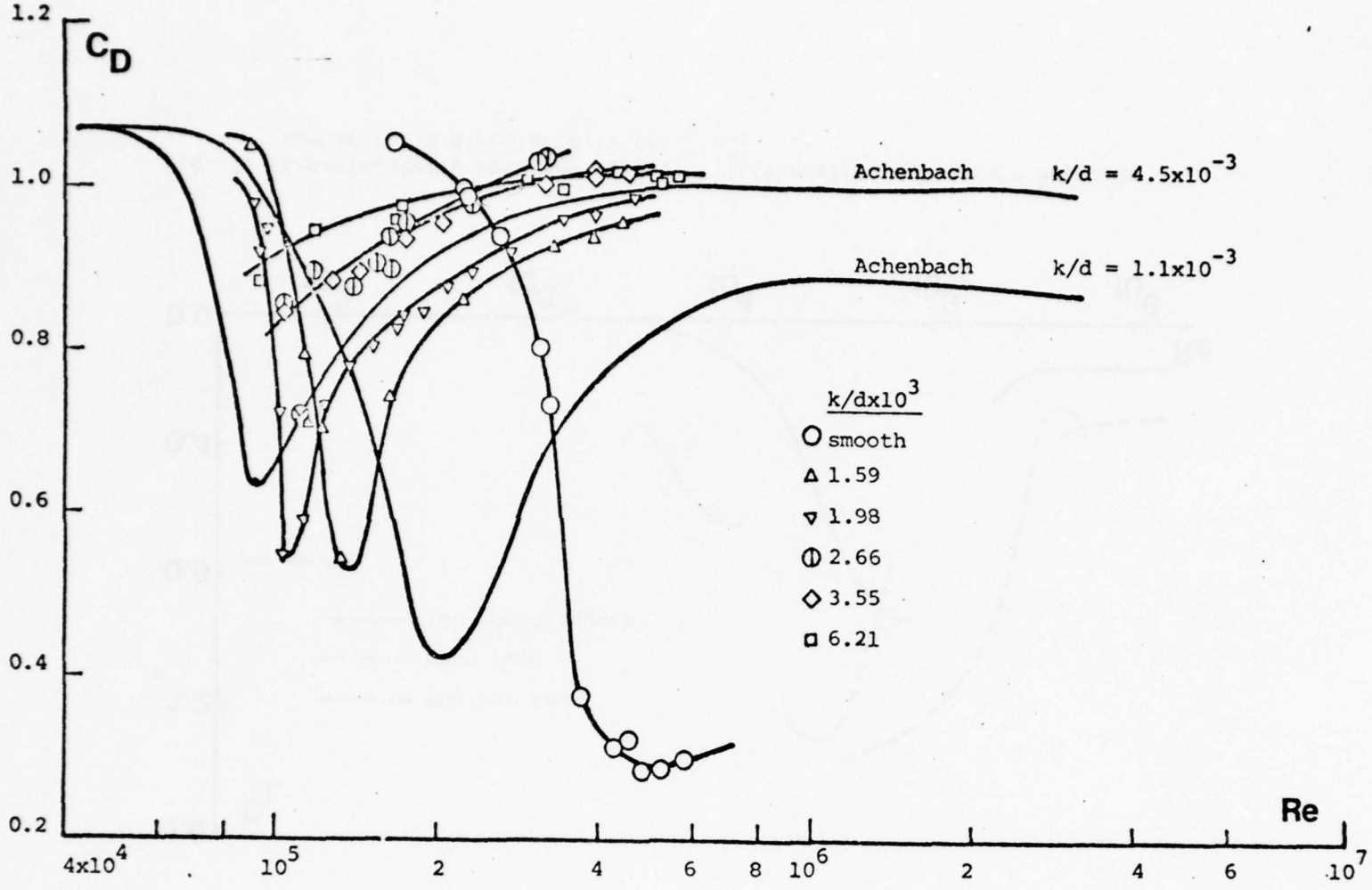

Fig. 2. Drag coefficient versus Reynolds number for a circular cylinder with distributed roughness [14].

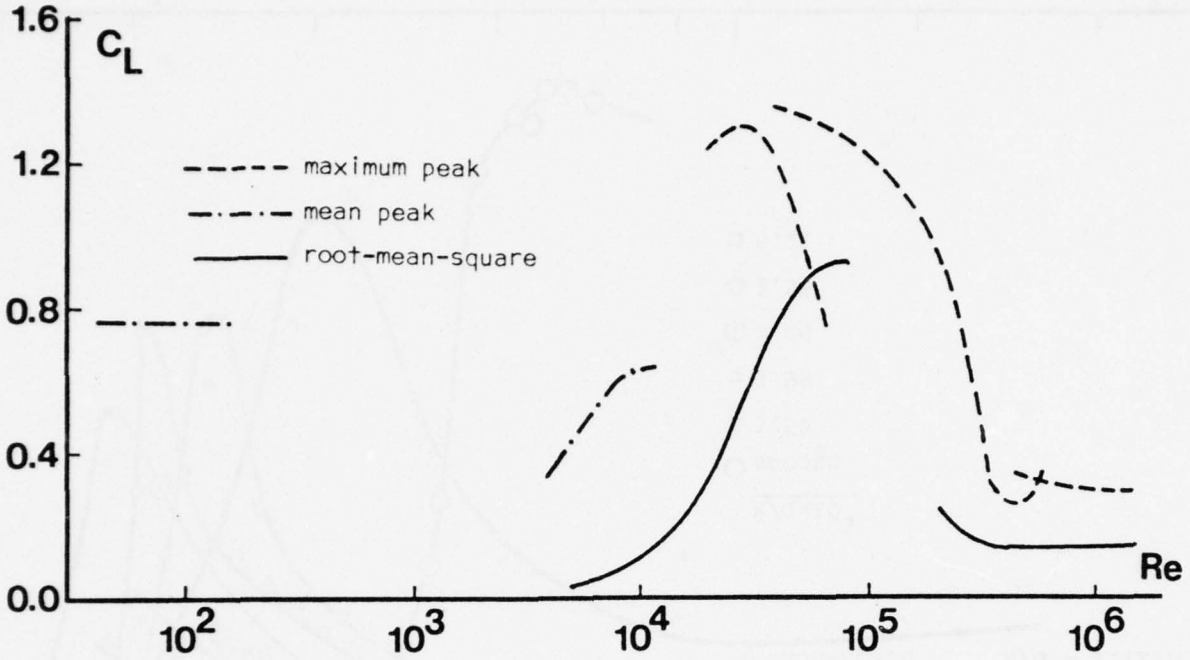

Fig. 3. Experimentally obtained values of lift coefficient versus Reynolds number for a circular cylinder [16].

detailed discussion of the spectral content of lift in the critical region see Bublitz [17].

The reasons associated with the large variations of the lift coefficient are directly related to the mobility of the separation points, formation of vortex cells, lack of spanwise correlation, end effects, turbulence present in the ambient flow, etc. Since each experiment is carried out with a different length-to-diameter ratio, blockage ratio, and end conditions, the number of vortex cells over the cylinder and the effect of the flow between the end of the cylinder and the tunnel wall give rise to widely different lift coefficients.

The effect of roughness on the lift coefficient is to reduce its scatter and to increase its magnitude. As noted earlier, roughness distinctly regularizes the vortex formation and the base pressure thereby eliminating the effect of phase shifts which cause the said scatter in lift. Data supporting the above experimental facts will not be reported here for sake of brevity. For additional details the reader is referred to the work by Szechenyi [15].

D. RESISTANCE IN TIME-DEPENDENT FLOWS

There are an infinite number of time dependent flows and it is impossible to discuss their characteristics in any unifying manner. One might obtain a clearer insight into such flows by considering only those cases which are relatively more manageable for numerical or laboratory experiments. Among such flows which have been subjected to extensive numerical analysis and experiments are the impulsively started flows, uniformly accelerating flows, and harmonically oscillating flows. Obviously, no distinction is made here between the said fluid flows about a body at rest and a body undergoing similar time dependent motions in a fluid otherwise at rest.

1. Impulsively Started Flows

The impulsively started flow has been by far the one most investigated numerically through the use of the Navier-Stokes equations. These investigations (Collins and Dennis [18], and Yang [19]) have been confined to the very early stages of the motion during which the separation points move from the rear stagnation point to about 109 degrees. An exception to the foregoing is the work reported by Thoman and Szewczyk [20]. They have solved the Navier-Stokes equations through the use of a suitable finite difference technique for various Reynolds numbers and found that the drag coefficient overshoots for a relative flow displacement (normalized time) of $Ut/c \cong 5$ and then gradually reaches steady state values.

Only two separate investigations of the impulsively started flow have been reported. The first is that carried out by Schwabe [21] upon Prandtl's suggestion and the other by Sarpkaya [22, 23]. Schwabe's experiments were conducted with a 9 cm diameter cylinder at a Reynolds number of about 600. His drag coefficient, calculated indirectly through the use of motion pictures, rapidly reaches a value of about 2.0 and remains constant thereafter. Schwabe's findings are not in conformity with either the numerical calculation or with the experimental results obtained by Sarpkaya. Figure 4 shows three sets of representative data at Reynolds numbers from 16000 to 35000 for the drag coefficient. Clearly, the very initial instants of the motion cannot be analyzed because of the problems associated with the generation of an impulsively started flow. At Ut/c slightly greater than zero, the force acting on the cylinder is almost entirely inertial. As the separation sets in at the rear stagnation point and rapidly moves upstream, the drag also increases rapidly and C_D reaches a value of about 1.5 at Ut/c between 4.0 and 5.0. Then C_D drops rapidly to the steady state value for smooth cylinders in steady uniform flows at

Ut/c larger than about 7.0. Detailed flow visualization experiments by Sarpkaya [22] have shown that the reason for the overshoot in C_D is the symmetric development of two vortices in the cylinder wake and the rapid accumulation of vorticity in each vortex. It must be noted that for such a symmetric vortex configuration, the only means by which the vorticity may be cancelled are the exchange of vorticity between the two vortices and the cancellation of vorticity with oppositely-signed vorticity, so called counter-vorticity, generated in the rear boundary layers. In other words, the rate of accumulation of vorticity in the vortices is considerably larger than that at any other time. Other vorticity cancellation mechanisms which come into play during the separation of the vortex from its feeding sheet, as proposed by Gerrard [24], do not play any role during the growth of the symmetric vortices. Thus, the rapid accumulation of vorticity gives rise to the drag overshoot. As the asymmetry sets in, vortices shed alternatingly and the flow gradually becomes asymptotically steady. The possible mechanisms which cause the asymmetry in an otherwise symmetrical flow about a symmetrical body are discussed in greater detail later. Suffice it to note that one of the fundamental facts of fluid flows is that symmetric causes do not give rise to symmetric effects, as most eloquently philosophized by Birkhoff [25].

Following the onset of asymmetry, the cylinder experiences a transverse force, as shown in Fig. 5, in terms of the lift coefficient and the normalized time Ut/c. The lift force fluctuates with the Strouhal frequency. The shedding of each vortex gives rise to a small fluctuation in C_D. The frequency of this fluctuation is twice the Strouhal frequency since two vortices (one from top and from bottom) are shed during a given cycle of lift oscillations.

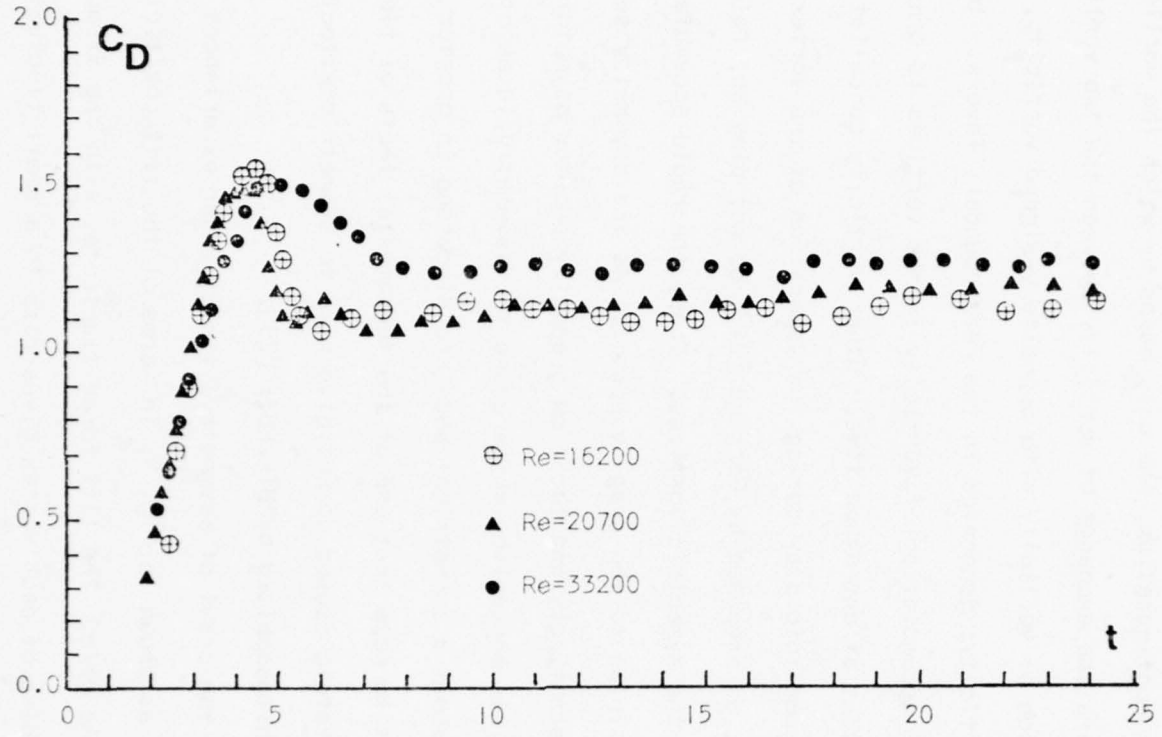

Fig. 4. Drag coefficient versus normalized time for impulsively-started flow about a circular cylinder [23].

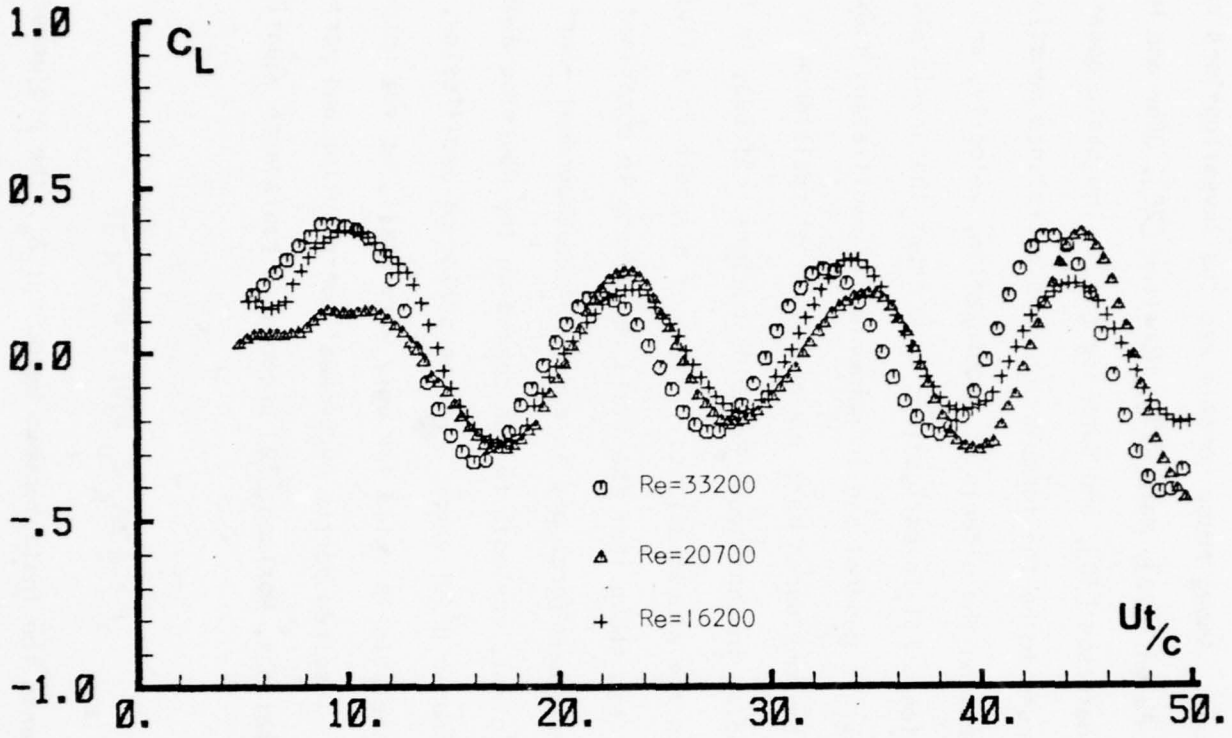

Fig. 5. Lift coefficient versus normalized time for impulsively-started flow about a circular cylinder [23].

2. Other Time-Dependent Flows

As noted earlier, the uniformly accelerating flows and harmonically oscillating flows have been subjected to numerous analytical and experimental investigations. Among those notable are the investigations carried out by Iverson and Balent [26], Keim [27], Hamilton [28], Odar and Hamilton [29], Sarpkaya and Garrison [30], and Sarpkaya [31]. The basic question has been and continues to be the formulation of a resistance equation which takes into consideration the effects of acceleration, velocity, and the history of the motion. All investigations have shown that resistance in time-dependent flows in general and in harmonically oscillating flows in particular cannot be considered as a juxtaposition of resistance in steady flows at corresponding instantaneous Reynolds numbers. Stokes, in his celebrated paper on the sinusoidal oscillation of a sphere in a fluid otherwise at rest, has shown that the fluid resistance is comprised of a linear velocity-dependent force and an acceleration-dependent inertial force. The coefficients for both forces depend on the Reynolds number and the frequency parameter $D^2/\nu T$ where T is the period of oscillation. Obviously, Stokes' analysis is valid for only very small, as yet unspecified, Reynolds numbers. Inspired partly by Stokes' contribution and partly by practical considerations, Morison [32] proposed a resistance equation which may be written as

$$F = \frac{1}{2} \rho A_p C_D U|U| + \rho \forall C_M \frac{dU}{dt} \qquad (1)$$

in which U represents the instantaneous velocity; A_p, the projected area; $\forall$, the displaced volume; and C_D and C_M, the drag and inertia coefficients respectively. For harmonically oscillating flow about a stationary cylinder where the fluid velocity is $U = -U_M \cos \theta$ (here $\theta = 2\pi t/T$) Eq. (1)

reduces to

$$\frac{F}{\frac{1}{2}\rho DL\, U_M^2} = -C_D|\cos\theta|\cos\theta + \frac{\pi}{U_M T/D} C_M \sin\theta \qquad (2)$$

The essence of this equation is that the resistance in harmonic flow is assumed to be equal to a linear combination of a velocity-squared dependent drag force and an acceleration-dependent inertia force. In the midst of insufficiently clear insight into the kinematics of the complex flow, it has not yet been possible to demonstrate the reasons for the differences between the measured force and that calculated from Morison's equation for $U_M T/D$ values in the vicinity of 15. Additional experiments and numerical analysis, possibly through the use of the discrete vortex model, might shed further light on the subject and into the overall understanding of resistance in time-dependent flows. It is evident from the discussion of both the steady and unsteady flows that analytical or numerical methods are urgently needed with which relatively inexpensive investigations can be conducted to clarify the complex wake-boundary-layer interaction mechanism. Of all the possible flows which might be considered as a candidate for such an analysis, the impulsively started flow is certainly the one most manageable and most fundamental to the understanding of all other flows.

E. METHODS OF NUMERICAL ANALYSIS

With the advent of high speed computers, numerical methods began to play a greater role in fluid dynamics. Currently four major methods of analysis are in use: finite difference, finite element, marker-cell technique, and the discrete vortex method.

Finite difference methods have been used for the solution of flow about a circular cylinder for relatively small Reynolds numbers ($Re \simeq 100$)

either through the use of the Navier-Stokes equations as they are commonly written or through the more frequently used vorticity equations. Ingham [33] calculated the steady flow past a circular cylinder at Re = 100. Thoman and Szewczyk [20], as noted earlier, carried out a similar numerical analysis of flow over stationary and rotating cylinders at Reynolds numbers as large as 10^6. There are a number of such examples in the literature but they are not cited here because of their lack of relevance to the subject under consideration.

The finite element method, which came into prominence first in the area of structural analysis and then permeated through heat transfer and fluid mechanics, has been primarily used for unseparated flows about bluff bodies. As far as fluid mechanics is concerned, the outstanding examples of such applications may be found in two recent volumes of work dealing with finite elements in fluid mechanics [34]. Bretanow and Ecer [35] made an attempt to calculate the separated flow about a circular cylinder at small Reynolds numbers but the results have been inconclusive. Applications of the finite element method to flows about foils where the flow remains attached have yielded results in conformity with experiments (Bretanow and Ecer [35]).

The marker-cell technique developed by the researchers at the Los Alamos Scientific Laboratory during the past 20 years uses the finite difference form of the Navier-Stokes equations and then adjusts the pressure in each cell to insure that the equation of continuity is satisfied. Numerous ingenious techniques have been developed by Fromm and Harlow [36] and Nichols and Hirt [37] for the efficient adjustment of pressure in each cell. Such techniques will not be dealt with here. The researchers of Los Alamos Scientific Laboratory have applied the marker-cell technique to the flow past cylinders, spheres, rectangular blocks and to various other

free-surface flows. These applications dealt with very low Reynolds numbers (in the order of 100). Even though the technique has considerably increased the understanding of the kinematics of the wake, the precise nature of the time-dependent force acting on any one of the bodies cited above remains obscure.

The discrete vortex model, which is included as one of the four major models, is the subject of extensive discussion in the next chapter. Therefore, the remainder of this section is confined to a discussion of the successes and shortcomings of the first three methods.

All numerical models are by their very nature approximate. They satisfy certain critical conditions only at discrete time steps. Secondly, they require mesh or element sizes which vary from one region of flow to another to insure that the characteristic gradients of the flow (such as velocity or pressure) do not significantly or abruptly change over any one element. For example, the finite difference method when applied to the viscous flow over a circular cylinder requires that the size of the elements on and near the cylinder be considerably smaller than the boundary layer thickness. Otherwise, the evolution of the boundary layer, the positions of the separation points, and the evolution of the wake cannot be accurately calculated. Since the boundary layer thickness for laminar flow is proportional to $Re^{-1/2}$, one realizes that only for relatively small Reynolds numbers can a sufficiently large boundary layer thickness and a correspondingly large mesh size be obtained. This fundamental difficulty has prevented the finite difference, finite element, and the marker-cell technique from making significant progress into the calculation of steady or time dependent flows about bluff bodies at Reynolds numbers of practical interest. None of the three techniques cited above has been applied to the solution of flow problems associated with oscillating bodies. The reasons for this are rather

self-evident since the solution requires not only a moving grid but also a grid whose mesh size must be varied with time to minimize the effect of sharp velocity and pressure gradients. Finally, it should be noted that all three numerical techniques present "stiffer" solutions and introduce an artificial numerical viscosity whose influence cannot be readily assessed. Not to be entirely critical of the said methods, for there are corresponding shortcomings of the discrete vortex model, one must note that in the wide spectrum of Reynolds numbers there will always be some interest in low Reynolds number flows. Thus, such numerical techniques will continue to play some role in separated flows where the discrete vortex model is not advantageously suited. It therefore appears that no one model will stand out as superior and universally applicable and that all methods will continue to complement each other.

II. FUNDAMENTALS OF THE DISCRETE VORTEX MODEL

A. INTRODUCTION

The discrete vortex model (DVM) is a potential flow representation of the shear layers emanating from the separation points. Any separated viscous flow is completely specified if the spatial and temporal distribution of vorticity in the entire flow field is known. For reasons described in the previous chapter, it has not yet been possible to achieve this objective through any exact or approximate methods. It has been observed and experimentally verified by Fage and Johansen [10] that the shear layers at sufficiently high Reynolds numbers are quite thin and the vorticity is confined into regions of tightly spiralled vortex sheets. This fact alone invites one to divide the shear layer into a number of small segments and concentrate the vorticity of each segment into a line vortex situated at the geometric center of the segment. This idealization permits one to use the powerful complex function theory to determine the kinematics and dynamics of the flow. Evidently, the validity of the results can only be judged in light of experimental facts.

In the following, only the gross features of the method are described and the details are presented following an historical résumé.

At a given time the separated shear layers are represented by vortices situated at the center of each segment. The potential flow theory permits one to calculate the velocity of each vortex induced at its center by all other vortices and the ambient flow. Then the vortices are convected for a short time interval Δt through the use of a suitable convection scheme to new positions. It is then necessary to introduce new vorticity into

the flow at or near the separation points to account for the vorticity generated in the boundary layer. The introduction of new vortices (nascent vortices) represents an addition to each set of vortex arrays. Then the process is repeated.

In spite of its apparent simplicity, there are a number of problems which must be resolved in carrying out the said calculations: (i) the vorticity introduced at each time step must be related to the characteristics of the boundary layers upstream of the separation points; (ii) one must insure that the point vortices continue to represent the vorticity at each segment in accordance with the fundamentals of hydrodynamics; (iii) allowance must be made for the interaction of oppositely-signed vorticity and the decay of vortices; (iv) methods must be devised to limit the number of the point vortices to minimize the computation time without affecting the kinematics and dynamics of the flow; and (v) procedures must be established for the flow to retain its inherent flexibility without introducing artificial stiffening effects (e.g., to allow for the mobility of stagnation and separation points).

The foregoing conveys the idea that the discrete vortex model is and will continue to rely on a strong interaction between potential and viscous flow theories. Neither is capable of providing a solution alone but together they can make inroads towards describing the basic features of the separated flow provided that sufficient ingenuity is incorporated into the said interaction. Lastly, it must be noted that all the numerical methods described above depend on the availability of a high-speed digital computer.

B. HISTORICAL DEVELOPMENT

The DVM has been in existence for the past 46 years since its inception by Rosenhead [38] in 1932. Rosenhead investigated the so-called

"Helmholtz instability" of a surface of discontinuity, separating two fluids of equal speed and density but moving in opposite directions. His primary objective was to give the shear layer between the two fluids an initial disturbance by situating the shear layer along the curve $y = 0.1 \sin(2\pi x/\lambda)$ and then observe the evolution of the sheet with time. To accomplish this, Rosenhead represented the shear layer by point vortices placed along the sheet at intervals such that their projections along the x-axis were equi-distant. Each vortex was assigned a strength of $U\lambda/6n$ where n is the number of vortices per wavelength, λ, and U the speed of the two fluids. Keeping the vortex strengths constant, Rosenhead followed the deformation of the sheet by convecting the vortices with a simple Eulerian integration of $\vec{r}^{\,j}_{t+\Delta t} = \vec{r}^{\,j}_{t} + \vec{q}^{\,j}_{t}\Delta t$ where $\vec{r}^{\,j}$ is the position vector of the j-th vortex; $\vec{q}^{\,j}$, the computed velocity vector; and Δt, the time interval. Using n = 2, 4, 8, and 12, Rosenhead observed that in each case the sheet rolled up smoothly into concentrated clusters of vortices positioned at intervals of λ along the x-axis. Rosenhead's results, which were computed using a desktop calculator, are shown in Fig. 6. The tendency of a distribution of point vortices to roll up in a manner consistent with observations is clearly evident.

Rosenhead's results remained undisputed until 1959 when the computational power of the digital computer was applied to the analysis. Birkhoff and Fisher [39] repeated Rosenhead's analysis using a Runge-Kutta integration scheme, 22 vortices per wavelength, and smaller time intervals. Instead of improved results they observed that the vortices took irregular paths and no longer rolled up smoothly. Birkhoff and Fisher concluded that, given sufficient time, an originally organized array of equi-strength point vortices would eventually become random and that the validity of representing a shear layer by point vortices is questionable.

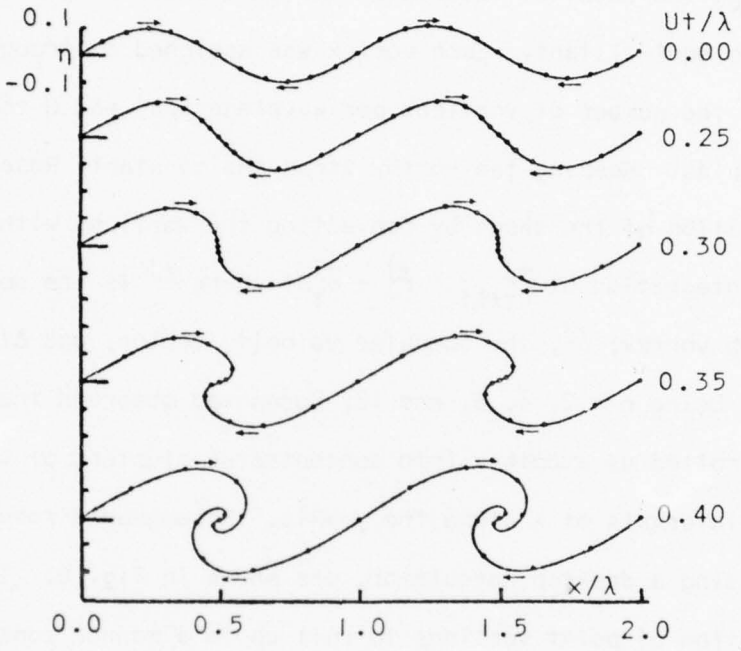

Fig. 6. Example of Rosenhead's calculations [38].

Shortly thereafter, Hama and Burke [40] undertook a similar computer study and verified the observations of Birkhoff and Fisher. However, Hama and Burke noted a conceptual error in Rosenhead's original method of placing the discrete vortices along the shear layer. Specifically, if the initial vortex sheet was to have a constant vorticity per unit distance along its length and be represented by equi-strength vortices, then the vortices should be placed at equal distances measured along the sheet vice at equal x increments. Using this arrangement Hama and Burke repeated their calculations and found that the onset of irregular vortex motion was significantly delayed. Eventually, however, a random pattern did result. Thus, at this point it was hypothesized that the onset of instability could be delayed although the questions of why it occurred and how it could be controlled were still a mystery.

Without fully realizing the consequences of sheet instability (the result of which is discussed later), the DVM continued in its evolution relying on the assumption that meaningful results could be obtained up to the onset of irregular vortex motions. In 1962 Abernathy and Kronauer [41] applied the method to investigate the motion of two shear layers of oppositely-signed vorticity separated by a distance h_v and each given an initial perturbation as in Rosenhead's work. They observed that the vortices accumulated into clusters resembling the pattern of a vortex street. An example of their results is shown in Fig. 7.

Encouraged by the demonstrated ability of the DVM to represent a vortex street, the next logical extension of the method was to analyze the flow past a bluff body. However, the inclusion of a solid body in the flow field necessitated new considerations. Specifically, the previous analyses had begun with a discretized sheet having a preassigned initial position and vorticity distribution along its length (usually taken as

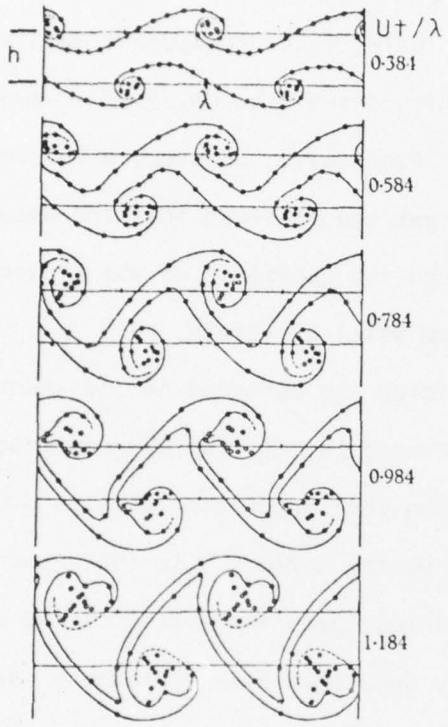

Fig. 7. Example of Abernathy and Kronauer's calculations ($h/\lambda=0.34$) [41].

constant). The application of the DVM to flow past a bluff body required that the discretized shear layers be generated continuously by adding additional point vortices into the flow at regular time intervals and at locations representative of where the shear layers actually emanate from the body. The requirement for some method to account for vorticity generation and introduction in an otherwise potential flow model posed a significant problem. Compounding the difficulty was the time dependent nature of both the generation rate and its point of introduction.

The first DVM analysis to include a bluff body was performed by Gerrard [42] for a circular cylinder. Although a circular cylinder was of great practical interest it was also the most difficult one to analyze because of the unsteady vorticity generation and mobile separation points. Gerrard was forced to adopt a rather arbitrary method of introducing new vortices which severely influenced the results of his analysis, although it still represented a noteworthy application of the DVM. Noting the difficulties associated with the mobile separation points and the vorticity introduction, Sarpkaya [43] introduced a mobile separation region represented by an infinite number of vortex sheets of vanishingly small vorticity connected to the nascent vortex. This analysis was restricted to impulsively started symmetric flow about a circular cylinder. In the ensuing years many investigators bypassed the difficulty introduced by the mobility of the separation points and dealt with bodies with sharp edges (e.g., inclined plates, blunt-based bodies, wedges, etc.) where the separation points are fixed. Despite the growing number of applications of the DVM, a number of disturbing difficulties remained unresolved and a full interaction between the boundary layer, separation points, and the wake had not been established. These difficulties required the use of a number of nondisposable parameters. Consequently, the proper balance between

heuristic reasoning and computational formulation had to evolve through the recognition of the reasons underlying the basic difficulties.

Briefly, the most important of these difficulties stemmed from the proximity of the vortices to each other and to the solid boundary, and from the necessity of representing the continuous process of vorticity generation at the singular separation points by a discrete process. The occasional proximity of two point vortices resulted in large mutually-induced velocities and hence the shooting of the two vortices rapidly away from the flow field. This was particularly true when the vortices ceased to be located at the geometric center of the sheet segment which they were supposed to represent. Furthermore, the spiralling of the sheets brought vortices on two adjacent spirals close to each other and gave rise to a traveling and growing instability. Thus, it was not possible to correctly represent the core of tightly spiralled sheets. The proximity of the vortices to the boundary and hence to their images inside the body resulted not only in similar instabilities but also in unrealistic local pressures. This, in turn, resulted in unnatural fluctuations in drag and lift forces.

Faced with the problems just cited and the desire to enhance the applicability of the method, various investigators devised several numerical cures. Chorin and Bernard [44] introduced a cut-off distance from the center of each vortex beyond which the vortices were to behave like potential vortices. For radial distances smaller than the cut-off distance the vortices were assumed to exhibit a solid body rotation. Their calculations did not, however, result in an improvement of the analysis of separated flow about a circular cylinder. Moore [45], in dealing with two vortex sheets emanating from a plane lifting surface, introduced the method of amalgamation. When a vortex sheet was spiralled tightly enough,

the last vortex on the sheet was connected to a core vortex. At each time step the last vortex was amalgamated into the core vortex increasing its strength. This procedure partly avoided the difficulties stemming from the proximity problems of the adjacent coils of the spiralling sheet. Both investigations dealt with the devising of methods to overcome the instability problems rather than with the understanding of the real cause of the difficulty.

The basic question of why an initially equidistant set of vortices should after several convections come in close proximity of each other was resolved by Fink and Soh [46] who demonstrated that the primary source of the difficulty was in failing to rediscretize the sheet at each time interval of the calculation. In other words, it is necessary to insure that the point vortices are always located at the geometric center of the segment of the sheet which they are supposed to represent. The complex conjugate velocity $\bar{q}(z_j)$ at a point z_j due to a single vortex of strength Γ_k located at z_k is given by[1]

$$\bar{q}(z_j) = \frac{1}{2i\pi} \frac{\Gamma_k}{z_j - z_k} \tag{3}$$

For a series of N discrete vortices on a vortex sheet, the same velocity at a point z_j becomes [46]

$$\bar{q}(z_j) = \frac{1}{2i\pi} \sum_{k\neq j}^{N} \frac{\Gamma_k}{z_j - z_k} - \frac{1}{2i\pi} \frac{\Gamma_k e^{-i\theta_j}}{|s_{j+1/2} - s_{j-1/2}|} \ell n \left| \frac{z_j - z_{j+1/2}}{z_j - z_{j-1/2}} \right| \tag{4}$$

---

[1] Mathematical details of the relevant potential flow theory will be presented in Chp. III. Here no attempt is made to introduce the precise definitions of the variables appearing.

Equation (4) resembles Eq. (3) for the induced velocity field due to point vortices except for the logarithmic term. The point z_j lies within the segment $(s_{j+1/2}, s_{j-1/2})$ without necessarily bisecting it at all times, and s measures the distance along the sheet. The consequences of Eq. (4) are that: (i) if the equivalent point vortex is not placed at the midpoint of its segment through rediscretization of the sheet at each time interval, then the logarithmic term does not vanish and the computational error increases depending on the number of vortices, the time interval used, and the total time of computation; (ii) the vortices, which initially bisect the segment which they are to represent, do not continue to do so at the succeeding time intervals; (iii) the use of finite vortex cores, amalgamation of vortices at the center of the spiral, or other techniques only delay or minimize the accumulation of the errors resulting from the logarithmic term in an amount related to the distance between z_j and the center of the segment; and that (iv) the growth of the computational error may be significantly reduced by placing each discrete vortex at the midpoint of its segment, i.e., by placing the vortex at $z_j = 0.5(z_{j+1/2}+z_{j-1/2})$ at each time interval. Only through such a procedure can one make the logarithmic term vanish.

The calculations are then carried out at each time step by representing the vorticity density by an entirely new set of equidistant vortices whose strengths are adjusted to give a good representation of that density.

The foregoing procedure does not resolve all of the computational errors particularly in regions where the radius of curvature of the sheet is small. Fink and Soh applied this technique to the early stages of relatively simple flows with fixed separation points. Their examples did not deal with the alternate shedding of vortices.

Even though the method of rediscretization essentially resolved the problems stemming from the proximity effects, two fundamental links between the potential flow model and the behavior of real fluids remained unresolved. The first of these is the relationship between the vorticity to be introduced at each time step and the boundary layer which generates it. The second is the decay of vortices by various mechanisms. The first question was initially considered by Deffenbaugh and Marshall [47] who investigated the impulsively started flow about a circular cylinder (without recourse to rediscretization). They used Pohlhausen's boundary-layer approximation method to determine the position of the separation point and the vorticity to be introduced at each time interval. Their analysis predicted a separation angle of θ_s = 64 degrees, which is considerably smaller than the commonly accepted experimental value of θ_s = 81 degrees.

The question concerning the decay of vortices has remained practically obscure. Although several researchers employed methods to cancel oppositely-signed vortices whenever they came within a prespecified distance of each other, no systematic investigation of the effect of decay of vorticity was conducted. Often recourse was made to Prandtl's suggestion that individual vortices in a vortex street retain only about 60 percent of the vorticity generated in the boundary layer during a period required to shed a single vortex. Some investigators, in efforts to obtain results in partial conformity with Prandtl's suggestion, automatically applied a 40 percent reduction to the strength of each nascent vortex. Seldom was mention made of the experimentally observed fact that the rate of decay of vortex strengths varies with distance behind the cylinder.

The foregoing represents the state-of-the-art prior to the beginning of the present investigation. A relatively more detailed account of the historical evolution of the DVM is found in Clements and Maull [48] and Fink and Soh [46].

III. THEORETICAL AND PHENOMONOLOGICAL FOUNDATIONS OF THE DISCRETE VORTEX MODEL

A. INTRODUCTION

This chapter deals with the characteristics of inviscid and viscous flows about a circular cylinder from the forward stagnation point to the vortices in the far wake. Mathematical principles, boundary layer concepts, and relevant hypotheses are introduced in preparation for the discussion of the details of the discrete vortex model developed in the present study.

B. FLOW KINEMATICS

The complex potential for a two-dimensional inviscid flow is given by

$$w(z) = \phi + i\psi$$

where ϕ and ψ represent, respectively, the velocity potential and the stream function. The velocity components which satisfy the Cauchy-Riemman conditions are given by

$$u = -\frac{\partial \phi}{\partial x} = -\frac{\partial \psi}{\partial y} \quad \text{and} \quad v = -\frac{\partial \phi}{\partial y} = \frac{\partial \psi}{\partial x} \tag{5}$$

In terms of the complex potential, one has

$$\frac{dw(z)}{dz} = -u + iv \tag{6}$$

The flow about a circular cylinder is generated by combining a uniform flow with a doublet at the center of the cylinder (see e.g., Milne-Thomson [49]). This yields

$$w(z) = w = -U(z + c^2/z) \tag{7}$$

in which -Uz represents the uniform flow and the remainder the doublet. The introduction of a vortex into the flow field exterior to the cylinder requires, by virtue of the circle theorem, the introduction of an image vortex interior to the circle. Thus, the flow about a circular cylinder with N number of real vortices is given by

$$w = -U(z + \frac{c^2}{z}) + \frac{i}{2\pi}\sum_{n=1}^{N} \Gamma_n\{\ell n(z-z_n) - \ell n(z - \frac{c^2}{\bar{z}_n})\} \qquad (8)$$

It should be noted that a real vortex located at $z = z_n$ has an image at $z = c^2/\bar{z}_n$ and at $z = 0$. The image at the center of the circle, which gives rise to terms like $\Gamma\ell n(z)$, must be excluded due to the condition that the vortices shed from the cylinder leave a circulation opposite to their own on the cylinder. Clearly, the absence or presence of an image vortex at the center of the circle does not alter the boundary condition $(\partial\phi/\partial n\big|_{|z|=c} = 0)$ since the streamlines of a vortex are circles. No restriction has been imposed regarding the time dependence of the velocity U other than that it be uniform.

Substituting Eq. (8) into Eq. (6), one obtains the velocity at any point z as

$$-u+iv = \frac{dw}{dz} = -U(1- \frac{c^2}{z^2}) + \frac{i}{2\pi}\sum_{n=1}^{N} \Gamma_n\{\frac{1}{z-z_n} - \frac{1}{z - \frac{c^2}{\bar{z}_n}}\} \qquad (9)$$

Equation (9) may also be used to evaluate the convective velocity of a vortex at $z = z_n$ provided that the singular term $\Gamma_n/(z-z_n)$ is omitted by virtue of the condition that a vortex cannot impart a velocity on itself.

It is advantageous to work with dimensionless parameters by introducing the following change of variables:

$$z' = z/c,\quad u' + iv' = (u+iv)/U,\quad \Gamma' = \Gamma/Uc \tag{10}$$

$$w'(z) = w(z)/Uc \qquad t' = Ut/c$$

Substituting into Eqs. (8) and (9), letting U = 1.0, c = 1.0, and dropping the primes for sake of simplicity, one has

$$w(z) = -(z+\frac{1}{z}) + \frac{i}{2\pi}\sum_{n=1}^{N} \Gamma_n\{\ell n(z-z_n) - \ell n(z-1/\bar{z}_n)\} \tag{11}$$

and

$$-u+iv = \frac{1}{z^2} - 1 + \frac{i}{2\pi}\sum_{n=1}^{N} \Gamma_n\{\frac{1}{z-z_n} - \frac{1}{z-1/\bar{z}_n}\} \tag{12}$$

where u, v, Γ and z are now the normalized variables and w the normalized complex potential function. Hereafter, all measures of distance, time, velocity and circulation are given in terms of the above normalized variables. Any exceptions are clearly specified.

Equation (12) is used extensively in convecting the vortices and in calculating the lift and drag forces. In fact, about 90 percent of the computation time of the present model is consumed in the evaluation of complex velocities. This points out the necessity of keeping the number of discrete vortices as small as possible while maintaining a sufficiently small time interval to insure that the characteristics of flow are faithfully reproduced. The selection of the time interval, like the selection of the mesh size, is one of the subjective items of the method and

requires a careful parametric analysis. This is addressed to in a later section.

In general, the calculation of velocities and the convection of vortices are straightforward and noniterative. Under certain circumstances vortex-vortex proximity between adjacent spirals and the vortex-boundary proximity may require special attention. The resolution of such secondary issues is deferred to another section since they are not of any major consequence either theoretically or practically.

C. FORMULATION OF THE RESISTANCE EQUATIONS

The forces acting on a stationary circular cylinder of unit length by a time-dependent flow containing N vortices of strengths Γ_n and locations z_n can be calculated from the normalized form of the generalized Blasius theorem (Milne-Thomson [49]) to give

$$\overline{C_D + iC_L} = \frac{i}{2} \oint \left(\frac{dw}{dz}\right)^2 dz + i \frac{\partial}{\partial t} \oint w dz \qquad (13)$$

where C_D and C_L represent the drag and lift coefficients respectively. Inserting Eq. (11) into Eq. (13) and evaluating the residues, Sarpkaya [50] has shown that

$$C_D + iC_L = \sum_{n=1}^{N} \Gamma_n \{(iu_n - v_n) - (iu_n^i - v_n^i)\} \qquad (14)$$

in which u_n and v_n represent the velocity components of the n-th real vortex and u_n^i and v_n^i, the velocity components of the image of the n-th vortex.

Equation (14) may be written in a more compact and computationally more suitable form as

$$C_D + iC_L = i \sum_{n=1}^{N} \Gamma_n (\dot{z}_n - \dot{z}_n^i) \qquad (15)$$

where the dot denotes derivative with respect to time such that

$$\dot{z}_n = q_n = u_n + iv_n \tag{16a}$$

and

$$\dot{z}_n{}^i = q_n{}^i = u_n{}^i + iv_n{}^i \tag{16b}$$

The complex velocities q_n and $q_n{}^i$ may easily be shown to be related by

$$q_n{}^i = -\frac{\overline{q_n}}{z_n{}^2} \tag{17a}$$

or by

$$u_n{}^i + iv_n{}^i = \frac{-u_n + iv_n}{\bar{z}_n{}^2} \tag{17b}$$

The normalized force given by Eqs. (14) or (15) can also be evaluated indirectly through the use of surface pressures and the unsteady form of Bernoulli's equation. In either case the results are identical and the use of one method or the other is simply one of personal choice and programming efficiency.

D. GENERATION AND INTRODUCTION OF VORTICITY

The vorticity per unit length of a thin shear layer separating two streams with velocities U_1 and U_2 is equal to the difference of the velocities U_1-U_2. This vorticity is transported with the average velocity of the two streams, i.e., $(U_1 + U_2)/2$. This is a continuous process and the amount of vorticity transported during a time Δt becomes

$$\Delta\Gamma = (U_1-U_2)(U_1+U_2)\ \Delta t/2 = (U_1{}^2-U_2{}^2)/2 \cdot \Delta t \tag{18}$$

The discrete vortex model represents the continuous generation and flux of vorticity into the outer flow by introducing point vortices at discrete time intervals. The strength and position of introduction of each vortex must depend on the interaction of the unsteady vorticity distribution in the wake and on the appropriate boundary-layer considerations necessary to determine where the separation occurs. Those applications of the DVM which consider the separation points fixed ignore not only the said interaction but also artificially constrain the evolution of the flow.

In the present analysis the instantaneous position of the separation points is determined through the use of an approximate boundary layer analysis. At a given instant the velocity distribution on the forebody of the cylinder is calculated and the corresponding pressure distribution is assumed to be impressed on the boundary layer. This fundamental feature of the boundary layer theory together with the integral momentum equation of von Karman permits the use of a number of separation prediction methods. Among the most notable of such methods are those given by Pohlhausen [51], Stratford [52], Thwaites [53], Curle and Skan [54], Timman [55], and Loitsianski [56]. All of these methods exhibit varying degrees of sensitivity to the external velocity distribution and may not all yield identical or uniformly consistent results.

It is important to note that the combination of potential and viscous flow methods cannot establish a one-to-one relationship between the Reynolds number and the flow characteristics. It is only the kind of separation criteria used (laminar or turbulent) that determines whether the flow is subcritical, critical, or turbulent. The fact that the use of the DVM becomes increasingly more accurate with decreasing shear layer thickness makes one realize that the results obtained with a laminar separation criteria correspond to moderate to high subcritical Reynolds numbers.

The integral-momentum methods such as that of Pohlhausen require that the velocity outside the boundary layer be given and that the separation points be either fixed or fluctuate with small amplitudes and velocities about a mean position. In other words, the changes in the outer flow and the separation points should be such that the flow may be treated as quasi-steady.

The outer velocity distribution may be calculated either numerically through the use of an interactive scheme between the wake and the boundary layer or through the use of experimentally determined pressure distribution. Hiemenz [57] used the measured pressure distribution about a circular cylinder and approximated the velocity distribution at the edge of the boundary layer by

$$U(\xi) = 1.8348\xi - 0.27422\xi^3 - 0.04782\xi^5 \qquad (19)$$

where ξ represents the arc length measured along the cylinder from the stagnation point. Hiemenz's solution indicates that separation occurs at an angle θ_s = 82 degrees, measured from the stagnation point. This celebrated result has often been taken as proof that in subcritical flows separation occurs at θ_s = 82 degrees. The fact has not been realized that the entire velocity distribution and in particular that portion between the maximum velocity and the separation point (i.e., from $\theta \simeq 70$ to $\theta \simeq$ 80 degrees) dramatically affect the position of the separation point. In fact, Meksyn [58] has shown that the higher order derivatives of Hiemenz's velocity profile do not satisfy certain fundamental criteria regarding the separation point. At present there is no completely satisfactory velocity distribution for the forebody of a circular cylinder either in subcritical or in the supercritical regimes. Additional discussion of this subject is found in Meksyn [58].

Numerous experiments have yielded laminar separation points ranging from θ_s = 70 degrees to θ_s = 90 degrees. The commonly accepted value is about 80 degrees. Fage and Johansen's [10] experiments, and others since then, have shown that the separation point is in reality a separation zone which extends over a finite region and that spanwise and chordwise fluctuation of this region do not permit a precise determination of the mean position, amplitude, and period of oscillation of the separation point.

The purpose of the foregoing brief discussion is to point out both the theoretical and experimental difficulties encountered in the determination of the separation point and the inadequacies of the appropriate laminar boundary layer methods. The prediction of the separation of turbulent boundary layers is even more uncertain (Stratford [52], Takada [59]) and are not discussed herein. Instead, attention is focused on Pohlhausen's method for time-dependent boundary layers. The former is more appropriate to the flow conditions where the motion of the separation point and the velocity at the edge of the boundary layer may be treated as quasi-steady. Schuh's [60] method is more appropriate for the initial instants of motion where the separation points move rapidly from θ_s = 180 degrees to about θ_s = 110 degrees. The motion of the separation point commences after a relative fluid displacement of (Schlichting [61])

$$t = \frac{1}{2(1 + 4/3\pi)} = 0.351 \qquad (20)$$

The reason for this is that in impulsively started flows about rounded bluff bodies the separation does not begin until the fluid moves some distance past the body. The only exception to that is the flow about bodies with sharp corners in which case the separation begins at $t = 0.0$.

For the case of impulsively started flow about a cylinder, the time in the boundary layer calculations is measured from the instant of the

inception of separation. Thus, a relative time of $t = 0.351$ must be added to that used in the boundary layer calculations in order to match the starting times.

Pohlhausen's method is well described in the literature (Schlichting [61]) and only the highlights of the method are presented herein. Assuming a fourth order polynomial for the velocity distribution within the boundary layer, Pohlhausen has shown that von Karman's integral momentum equation may be reduced to

$$\frac{dZ}{d\xi} = \frac{F(K)}{U(\xi)} \quad \text{and} \quad K = Z \frac{dU(\xi)}{d\xi} \tag{21}$$

in which

$$K = \left(\frac{37}{315} - \frac{1}{945}\Lambda - \frac{1}{9072}\Lambda^2\right)^2 \Lambda \tag{22}$$

with

$$\Lambda = \frac{\delta^2}{\nu} \frac{dU(\xi)}{d\xi} \tag{23}$$

Other variables appearing in Eqs. (21), (22) and (23) are

$U(\xi)$: the normalized velocity on the cylinder

ξ: the arc length measured along the cylinder from the stagnation point

δ: the boundary layer thickness normalized by the cylinder radius

ν: viscosity normalized by the ambient velocity and the cylinder radius (sometimes referred to as the unit Reynolds number).

The values of K and F(K) are tabulated in terms of Λ (Schlichting [61]). Similar tables are provided for other boundary layer approximations cited previously.

Integration of the coupled Eqs. (21) begins at the front stagnation point and proceeds along both sides of the cylinder independently until

the separation criteria ($\Lambda = -12$) is satisfied for each layer. This results in two distinct separation points which in general are not at identical angular distances from the mobile stagnation point.

As noted earlier, the foregoing method is applicable only to the relatively established flow where the velocity at the edge of the boundary layer and the separation point do not significantly vary with time. During the early stages of motion, however, the time dependence of the said parameters is very strong and must be treated through the use of the time dependent integral boundary-layer equations. Schuh [60] has extended Pohlhausen's method for the general calculation of the unsteady boundary layer. The details of his method are not presented here. The results obtained by Schuh for an impulsively started flow about a circular cylinder are shown in Fig. 8. These results, based on the classical potential flow velocity distribution about a circle, show that the separation point rapidly approaches a value of about $\theta_s = 109$ degrees. Schuh's method is not capable of incorporating the growth of the symmetric wake and the subsequent motion of the separation points and thus is not valid at large times. Thoman and Szewczyk [20] employed the finite difference form of the full Navier-Stokes equations and obtained results identical to those shown in Fig. 8 for the initial instants of flow. They have further shown that the separation point once having reached an angular position of about 110 degrees moves gradually to the final value of the separation angle (about 80 degrees). Partly to confirm this conclusion and partly to assess the significance of time dependence on the instantaneous position of the separation points, two sets of calculations are performed. Both use the time-dependent velocity distribution available through the model and both begin with an initial separation point of $\theta_s = 109$ degrees. The first calculation uses Pohlhausen's steady-state separation criteria with the in-

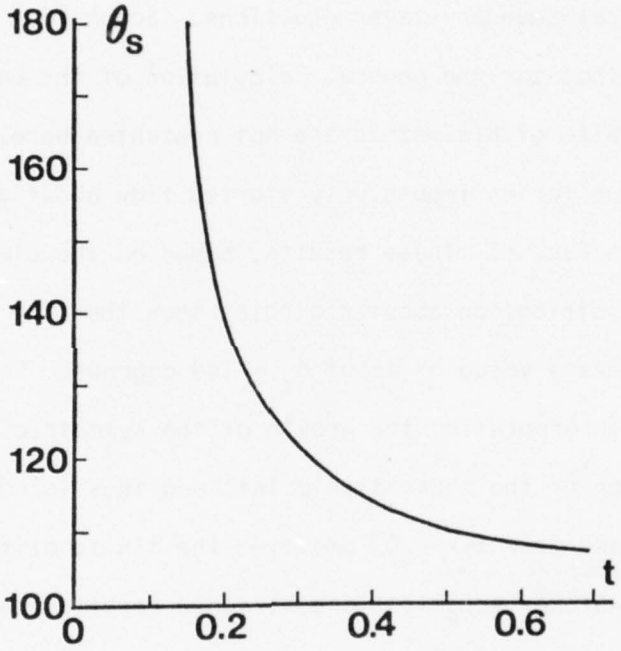

Fig. 8. Separation angle versus time [60].

stantaneous velocity distribution. The second calculation uses the unsteady integral-momentum equations given by Schuh [60], including those terms associated with the unsteady velocity distribution. The results obtained from both sets of calculations are shown in Fig. 9. Evidently the two calculations yield almost identical results, pointing out the fact that the separation point moves rather slowly and that the contribution of the time dependent terms in the unsteady form of the equations are negligible. It is because of this reason that all calculations are based on Pohlhausen's separation criteria assuming the flow to be quasi-steady. This assumption improves as one approaches steady state. Figure 9 indicates that the angular speed of the separation point is about 10 degrees per second. The same speed about the mean position of the separation point is about 2 degrees per second. (As is shown later, the separation point oscillates about a mean position of θ_s = 77 degrees with an amplitude of 3 degrees and a period of about 10.) Based on the foregoing, an amplitude of oscillation as much as 15 degrees can be performed without the inclusion of time-dependent terms.

In the present model the calculations begin at the time of $t = 1.0$ when the separation point is at θ_s = 109 degrees. It should be noted that a straightforward application of Pohlhausen's method with a potential flow velocity distribution ($U = 2 \sin \theta$) yields a separation angle of θ_s = 109.5 degrees.

Once the position of the separation points is determined, the rate of generation of vorticity is easily determined by writing

$$\frac{d\Gamma}{dt} = \int_0^\delta \frac{\partial u}{\partial y}\, u\, dy \qquad (24)$$

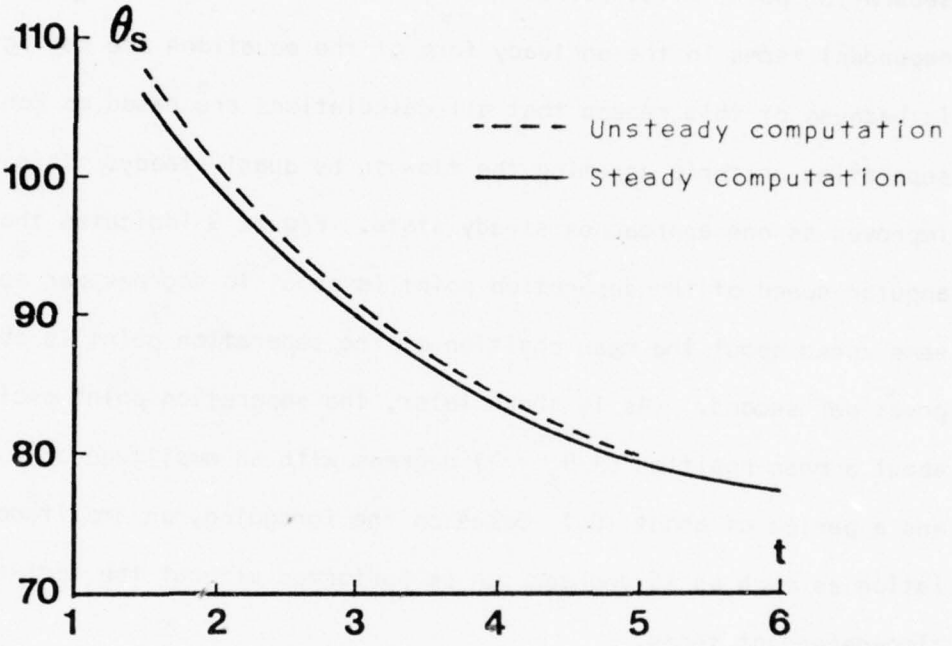

Fig. 9. Comparison of steady and unsteady separation point calculations.

where δ is the boundary layer thickness; u, the velocity within the boundary layer; and y, the distance along the outward normal. The contribution of $\partial v/\partial x$ is excluded from the vorticity expression in conformity with the approximations of the boundary layer theory.

The integration of Eq. (24) to obtain the circulation flux at a separation point yields

$$\frac{d\Gamma}{dt} = \frac{U_s^2}{2} \tag{25}$$

where U_s is the tangential velocity at the predicted separation point. Ordinarily the rate of change of circulation should be written as

$$\frac{d\Gamma}{dt} = \frac{U_1^2 - U_2^2}{2} \tag{26}$$

where U_1 and U_2 represent respectively the velocities at the outer and inner edges of the separating shear layer. Extensive experiments with various bluff bodies by Fage and Johansen [10] have shown that U_2 is about 5 percent of U_1 and that $\frac{d\Gamma}{dt}$ is correctly represented by $U_s^2/2$. This is a universally accepted experimental and theoretical fact.

In numerical calculations $\frac{d\Gamma}{dt}$ is replaced by $\Delta\Gamma/\Delta t$ and the strength of the nascent vortex is calculated from

$$\Gamma_{nv} = \frac{U_s^2 \Delta t}{2} \tag{27}$$

The placement of nascent vortices into the flow to adequately represent the separating shear layers has been a source of difficulty. This is primarily because the discretization of a continuous process near a singular region (separation point) is an exceedingly complex problem. In the present analysis, no new procedures are needed for the determination of the strength

and position of the nascent vortex because the separation point is obtained from the boundary layer analysis. By virtue of its definition, the separation point must be the point at which both the velocity and the shear stress on the cylinder are zero[2]. Thus, the nascent vortex of known strength must be placed on a radial line passing through the separation point at a distance m, i.e., at $z_{nv} = (1+\varepsilon) \exp [i(\pi-\theta_s)]$, to render the tangential velocity on the cylinder at the separation point equal to zero. This yields a unique value for ε as

$$\varepsilon = \frac{1 + |\Gamma_{nv}|/2\pi U_s}{1 - |\Gamma_{nv}|/2\pi U_s} - 1 \qquad (28)$$

The use of the boundary layer theory and the separation condition uniquely specifies the strength and position of the nascent vortices and allows the separation points to move along the cylinder as required by the interaction between the wake and the boundary layer. It is of importance to note that the no-slip condition is satisfied only at discrete time steps. Efforts to satisfy the said condition in a more continuous manner are counterproductive because the decrease in Δt calls for unacceptably large computation times. One of the essential features of the model is the bracketing of a suitable interval for Δt, which provides an adequate scale of discretization without excessive computation time.

The method described above properly accounts for the vorticity generated on the forebody of the cylinder. However, the flow in the wake of the cylinder develops a boundary layer on the afterbody which generates

---

[2] A lengthy discussion may be made regarding the difference between the definitions of steady and time dependent separation criteria. However, a numerical analysis such as the DVM does not warrant the consideration of the distinction between the results stemming from the use of different separation criteria.

countervorticity. Procedures by which this relatively small amount of vorticity generation may be accounted for are far from simple. The velocity distribution on the afterbody has strong spatial and temporal gradients due to the immediate proximity of the fluctuating wake. These gradients render useless the separation prediction methods described earlier.

Davis [62] attempted to account for countervorticity effects by using four separation points (two for the forebody and two for the afterbody boundary layers) but his method required the assumption of fixed separation points. Deffenbaugh and Marshall [47] approximated the rear shear layer effect by assuming that the boundary layers remain attached over the same fraction of a region of adverse pressure gradient as that of the forward boundary layers. However, in view of the complex velocity distribution on the afterbody, it is incorrect to apply the same boundary-layer considerations as were used on the forebody. It is safe to say that the numerical perturbations introduced into the model in attempting to account for the secondary effects of countervorticity may cause more error than would the neglect of the effect altogether. This consideration plus the introduction of the circulation reduction mechanism (yet to be described) obviate the need for the separate accounting of the effect of the rear shear layers.

E. CONVECTION AND REDISCRETIZATION MECHANISM

The vortices emanating from a separation point may be convected in a number of ways. Three most promising schemes are those given by the following expressions:

$$z(t+\Delta t) = z(t-\Delta t) + 2q(t)\,\Delta t \tag{29a}$$

$$z(t+\Delta t) = z(t) + \frac{1}{2}[3q(t)-q(t-\Delta t)]\,\Delta t \tag{29b}$$

$$z(t+\Delta t) = z(t) + q(t)\,\Delta t \tag{29c}$$

where $q(t)$ is the complex velocity of the vortex evaluated at the positions and times indicated. These schemes yield more or less the same accuracy and the use of one in lieu of the others is primarily governed by the simplicity of the method and computation time considerations. In the present analysis the simple Eulerian scheme given by Eq. (29c) is used because of its simplicity and because the use of relatively small time intervals ($\Delta t = 0.125$) make the method sufficiently accurate. Clearly, the results obtained with the three schemes cited above, or with others, cannot be compared without taking into consideration the effect of the time intervals used and the discretization process (if one is employed). All such convection schemes must assure, within the overall limitation of the model, that the vortex paths in regions of very small radius of curvature do not significantly deviate from those calculated with much smaller time intervals.

It has been explained in connection with the discussion of the historical development of the DVM that all investigators, with the exception of Fink and Soh [46], let the vortices move in the form of vortex clouds and took special measures to eliminate the difficulties arising from vortex-vortex and vortex-cylinder proximity effects. Not to be entirely critical, the use of vortex clouds can yield force-transfer coefficients nearly identical to those obtained with the use of rediscretized sheets. However, one drawback of the vortex clouds is that it does not allow the formation of spiralling vortex sheets as often observed experimentally. There are other features of the rediscretization which will become clear later. The vortex clouds stem partly from the accumulation of the logarithmic errors and do not in any way represent a turbulent vortex. In the early stages of the present investigation the vortex clouds were used to obtain some idea about the gross features of the asymmetric wake. Figure 10 is a sample computer plot of vortex clusters. It is not possible to identify

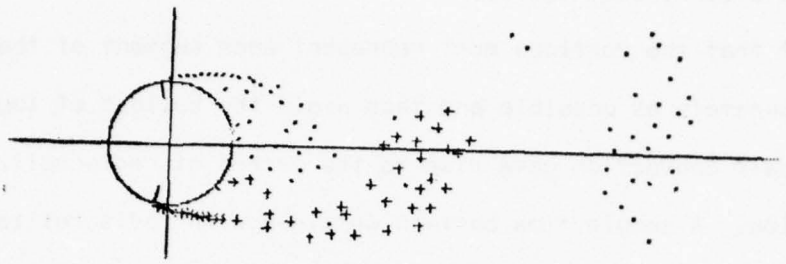

Fig. 10. Flow configuration without rediscretization.

Fig. 11. Flow configuration with rediscretization.

a spiralling sheet in Fig. 10, but the shedding of the vortices and the thinning of the connecting vortex sheets between two adjacent vortex clusters are clearly observable.

The fact that the vortices must represent each segment of the shear layer as accurately as possible and thus avoid the buildup of logarithmic errors in their convection gave rise to the method of rediscretization or redistribution. A sample flow pattern obtained with rediscretization is shown in Fig. 11 where the point vortices are connected by line segments to denote the position of the sheet. The mathematical foundations of the concept have already been introduced. In the following, the details of the mechanism where the rediscretization is affected are described.

Consider a segment of the vortex sheet at an instant t and assume that the vortices are connected by straight line segments (see Fig. 12). The distance between any two vortices is given by

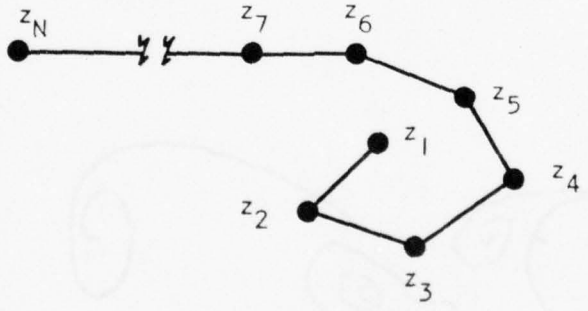

Fig. 12. Vortex sheet before rediscretization.

$$\delta s_n = |z_n - z_{n-1}| \tag{30}$$

The length of the sheet from the position z_1 (core of the spiral) to the n-th vortex is given by

$$s_n = \sum_{j=2}^{n} \delta s_j = \sum_{j=2}^{n} |z_j - z_{j-1}| \tag{31}$$

The total length of the sheet for N number of vortices becomes

$$s_N = \sum_{j=2}^{N} \delta s_j \tag{32}$$

The vorticity per unit length of the sheet at each z_n is given by

$$\gamma_n = \frac{\Gamma_n}{(\delta s_{n+1} - \delta s_{n-1})/2} \qquad N < n < 1$$

$$\gamma_N = \Gamma_N / \delta s_N \tag{33}$$

$$\gamma_1 = \Gamma_1 / \delta s_2$$

The circulation per unit length, γ_n, may be tabulated as a function of s_n through the use of Eqs. (31) and (33). This tabulation is then used as a piecewise continuous function denoted by $\gamma = \gamma(s)$. The function $\gamma(s)$ uses a linear interpolation of the tabulated values, i.e.

$$\gamma(s) = \gamma_{n-1} + (s - s_{n-1}) \frac{\gamma_n - \gamma_{n-1}}{s_n - s_{n-1}} \qquad s_{n-1} \leq s \leq s_n \tag{34}$$

$\gamma(s)$ represents circulation per unit length and is an invariant at a given time of the rediscretization process.

The next step in the analysis is the replacement of the existing unevenly spaced N vortices with $\hat{N}$ evenly spaced new vortices. In general $\hat{N}$ may be different from N. Replacement of $\hat{N}$ vortices is accomplished by starting at the core of the spiral, z_1, and placing vortices at intervals of δs measured along the straightline segments connecting the original

vortex positions (see Fig. 13). It should be noted that when the method is applied to the example depicted in Fig. 13, $\hat{z}_2$ and $\hat{z}_3$ are positioned such that $|\hat{z}_2 - \hat{z}_1| = \delta\hat{s}$ and $|\hat{z}_3 - z_2| + |z_2 - \hat{z}_2| = \delta\hat{s}$. In other words, distances are measured along the straightline segments of the existing sheet.

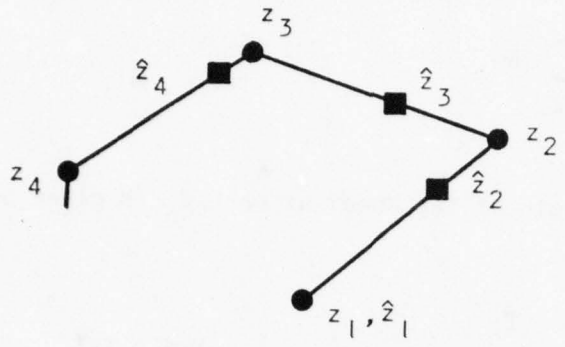

Fig. 13. Vortex sheet after rediscretization.

The strengths of the new vortices are calculated through the use of the distribution function $\gamma(s)$ such that the circulation per unit length at a new position, $\hat{z}_n$, is the same as for the original sheet at the said position, i.e.,

$$\hat{\Gamma}_1 = \gamma(o)\ \delta\hat{s}_2$$

$$\hat{\Gamma}_n = \gamma(s^*)\ \frac{\delta s_{n+1} + \delta s_{n-1}}{2} \qquad 1 < n < \hat{N} \qquad (35)$$

$$\hat{\Gamma}_N = \gamma(s_N)\ \delta\hat{s}$$

where

$$s^* = (n-1)\ \delta\hat{s}$$

The final step in the basic procedure is to insure that there has been no net gain or loss of circulation during the rediscretization process. The

circulation deficit is computed as

$$\Delta\Gamma = \sum_{n=1}^{N} \Gamma_n - \sum_{n=1}^{\hat{N}} \hat{\Gamma}_n \tag{36}$$

and an equal portion of the difference is added algebraically to each vortex, i.e.,

$$\hat{\Gamma}_n = \hat{\Gamma}_n + \frac{\Delta\Gamma}{\hat{N}} \tag{37}$$

Two parameters yet to be specified are $\delta\hat{s}$ and $\hat{N}$. The present model does not change the number of vortices during rediscretization and thus $\hat{N} = N$. $\delta\hat{s}$ and $\hat{N}$ are related by

$$\delta\hat{s} = s_N/(\hat{N} - 1) \tag{38}$$

It is important to note that N is the total number of vortices in a detached sheet (The definition of a detached sheet is introduced later.) and the rediscretization process does not change the position of either the first or the N-th vortex. For the vortex sheets attached to a nascent vortex, however, N represents the number of vortices excluding the nascent vortex. The reason for this is that the conditions (strength and location of the nascent vortex) prevailing at or near the separation point should not be altered by any process once the nascent vortex has been placed in the flow in accordance with the no-slip condition. Thus, for an attached sheet the rediscretization process stops at the vortex immediately adjacent to the nascent vortex.

It is appropriate at this time to give some idea about the actual magnitude of some of the parameters mentioned above:

(i) the strength of a nascent vortex ≈ 0.05 to 0.15

(ii) N = 3 to 80 depending on the length of the sheet

(iii) $\delta\hat{s} \approx 0.1$

The above numbers are representative of those encountered for a stationary cylinder with a time step, $\Delta t = 0.125$.

F. VORTEX SHEDDING AND CIRCULATION REDUCTION

1. Vortex Shedding

One of the least understood of the wake formation processes is vortex shedding where the sheet connecting the spiralling vortex to the separation point is cut. That portion of the sheet which remains attached to the cylinder begins to roll up into a new vortex spiral while the detached portion moves downstream to become part of the vortex street. The shedding process is accompanied by a number of interactive phenomena such as the motion of the shed vortices, adjustment of the longitudinal and lateral spacing of the vortex cores, and the reduction of circulation through the exchange of oppositely signed vorticity. These phenomena are so interlocked that attempts to explain the reasons for the occurrence of one become in turn questions to be explained. Evidently one possible way to resolve this dilemma is to have an exact solution of the problem. Numerical models such as the finite difference technique, having failed to elucidate the interactive mechanisms, left researchers with the need to develop techniques which could be used in more phenomonological models such as the DVM. It is absolutely essential that one begin the analysis with a model and then examine its validity through its predictions.

Inspired by flow visualization and wake measurements, Gerrard [63] proposed that the growing vortex spiral draws the opposite shear layer across the wake when it becomes sufficiently strong. The approach of

oppositely signed vorticity cuts off further supply of circulation to the vortex. The approximate time of the cutting of the sheet is then considered as the beginning of the shedding process. This mechanism is sketched in Fig. 14.

The wake comprised of such shed vortices continuously adjusts itself in both lateral and transverse spacing. In general it is agreed that the wake may be divided into three parts. The first is the so called formation region ($\ell_{fr} \simeq 5$); the second, the stable region where the vortices exhibit the characteristics of a fairly uniform vortex street ($5 \leq \ell_{sr} \leq 12$); and the third, the unstable region extending beyond x larger than about 12 [64].

The lateral spacing of the vortex cores gradually increases within the stable region and, like the longitudinal spacing, depends on the Reynolds number.

Even though considerable experiments have been conducted (particularly at low Reynolds numbers) to delineate the basic features of the wake, very few attempts have been made to measure directly the strength of the vortices as a function of x at a given Reynolds number. Admittedly, this is an extremely difficult undertaking. Several investigators (Schaefer and Eskinazi [64], Griffin [65], and Davies [66]) measured the longitudinal and transverse spacing of the vortices in the stable region and calculated indirectly the strength of the vortices (assumed to be identical) through the use of von Karman's vortex street model. Consequently, the vortex strengths are approximate and highly dependent on the initial inputs. The most important conclusion resulting from such investigations is that the strength of the vortices decreases with increasing distance downstream. The question concerning how much of the circulation generated remains in a vortex has been the subject of discussion since the time of Prandtl. As

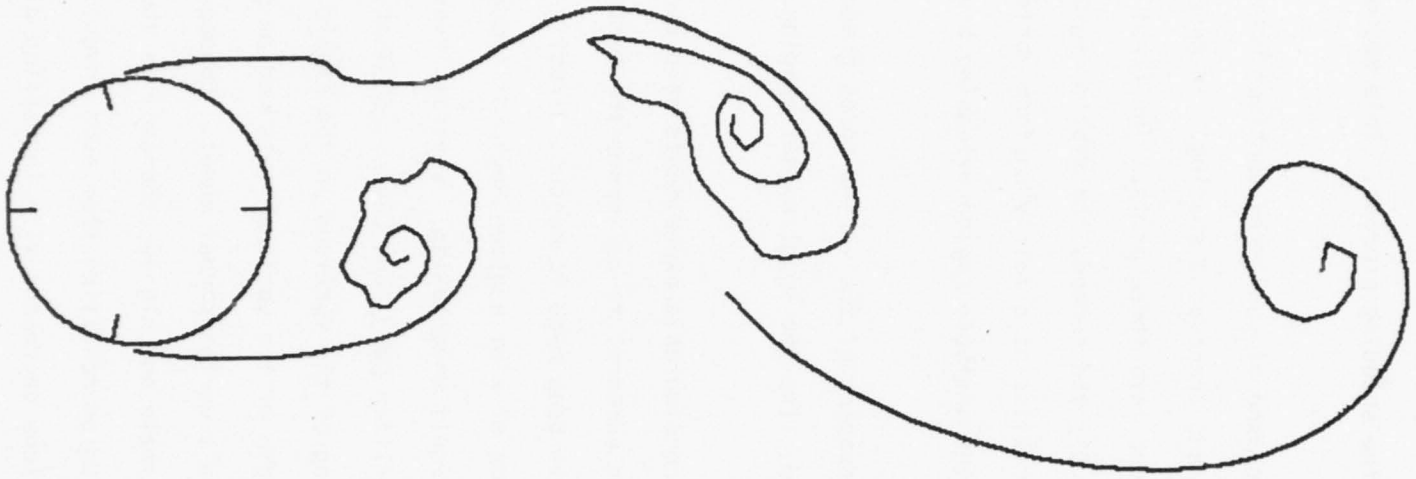

Fig. 14 Initiation of vortex-shedding sequence

noted earlier Prandtl suggested that the net circulation remaining in a vortex is about 50 percent of that generated. Discrete vortex models used by Clements [67] and Sarpkaya [68] give a reduction of about 15 percent. This value is significantly smaller than the estimates of 40 percent reduction (Fage and Johansen [10]), 57 percent (Roshko [11]) and 70 percent (Bloor and Gerrard [69]). It should not be inferred from the foregoing that the vortices once having acquired a net circulation of about 40 percent continue to retain that circulation forever. The understanding of the physics of circulation reduction is of major importance in the development of any phenomonological model and is discussed in greater detail in the following section.

2. Circulation Reduction

All investigators using the DVM have recognized that greater attention must be paid to the circulation reduction if the DVM is to produce results comparable to those obtained experimentally. In the early stages of the evolution of the present model the need for a circulation reduction mechanism was quickly reaffirmed from the magnitudes of the lift and drag forces.

Before undertaking a detailed discussion of possible circulation reduction mechanisms, it is advantageous to discuss the results obtained through the measurement of the vortex strengths. Schmidt and Tilmann [70], through the use of an ingenious ultrasonic sound beam technique, measured the variations of the circulations of vortices without inserting a probe. Their measurements were made at various Reynolds numbers by changing both the velocity of flow and the diameter of the cylinder. Figure 15 shows Γ as a function of x and is representative of the results obtained by Schmidt and Tilmann. In their experiments the Strouhal number was about 0.21 and the mean velocity at the point of separation may be taken as $U_s \simeq 1.5\ U_\infty$

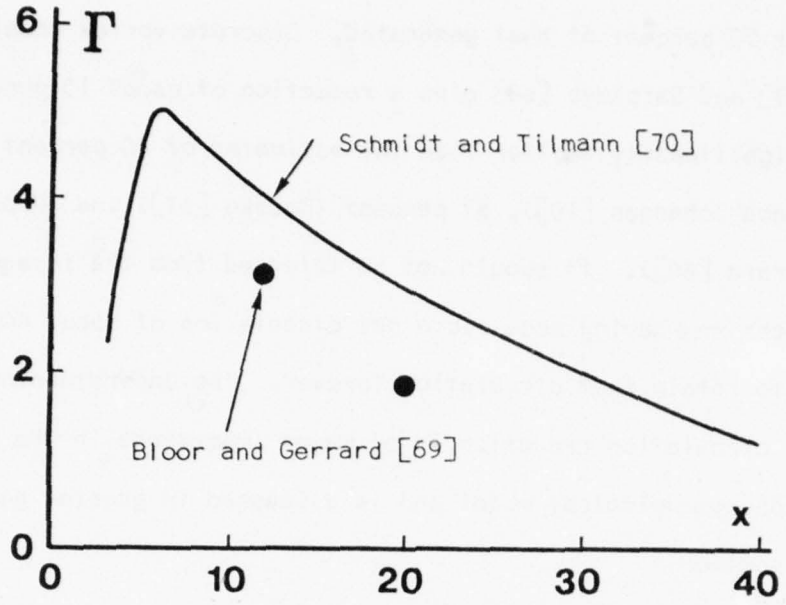

Fig. 15. Vortex strength versus distance [69, 70].

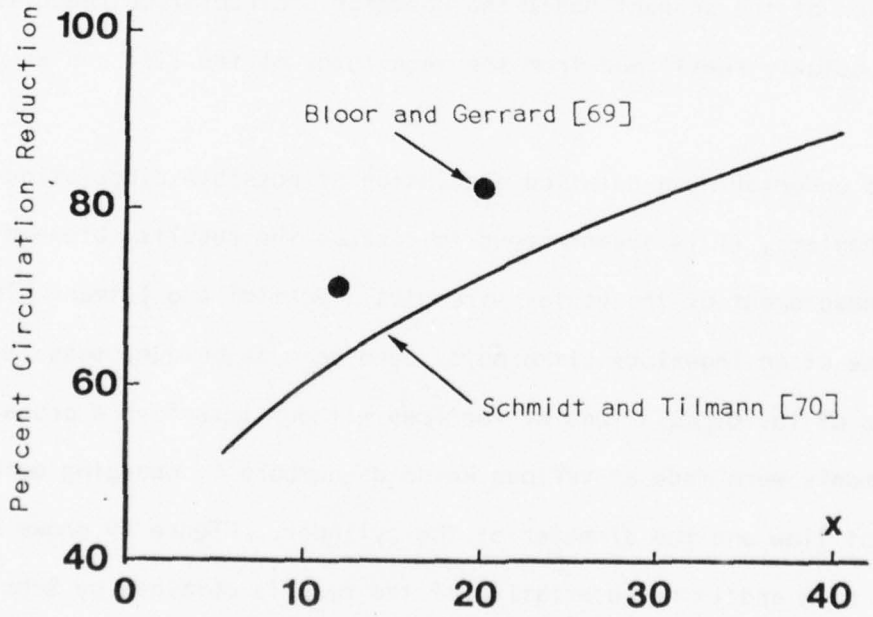

Fig. 16. Percent of circulation reduction versus distance [69, 70].

Thus, the total circulation generated during the period T = 1/f is approximated by

$$\Gamma = \frac{1}{2} U_s^2 \frac{D}{U_o St} = 10.7$$

In the observed formation region, $1 < x < 6$, the vortices grow rapidly and at the same time lose some of their strength due to various circulation reduction mechanisms. One can think of a net circulation reduction only for vortices which are in the stable and unstable regions. It must be noted that the ultrasonic technique used in Schmidt and Tilmann's experiments cannot yield accurate vortex strengths in the formation region because the path of the sound beam crosses over two oppositely signed vortices. In the stable region, however, only one vortex crosses the path of the sound beam at a given time. For the reasons cited above, part of the curve extending from $x \simeq 10$ to its experimentally reported maximum value of 40 is used to calculate the circulation reduction by dividing the circulation values by 10.7. The result is shown in Fig. 16. Also shown in Fig. 16 are two reduction ratios computed similarly from Bloor and Gerrard's [69] reported vortex strengths at x values of 12 and 20. The circulation reduction shown in Fig. 16 should be interpreted only as a reflection of the change of circulation with distance rather than as definitive values since such values depend on the Reynolds number, three-dimensionality effects, and the methods of their evaluation.

One or more physical mechanisms are needed to explain and to model the observed circulation reduction. Circulation may be reduced only by oppositely signed circulation. This hypothesis is somewhat mechanistic but is easily adaptable to numerical modelling. There is no question that in reality the entire mechanism may be related to the action of viscosity.

Leaving aside momentarily the complex relationship between the action of viscosity and circulation reduction, attention is concentrated on three sources of circulation exchange. It has been noted by the users of the DVM that the circulation may be reduced by the oppositely-signed circulation generated on the afterbody (countervorticity). In accordance with this assumption, the discrete vortices which come closer than a preassigned distance to the cylinder and the real vortices which cross the cylinder boundary are annihilated. Experiments by Fage and Johansen [10] have shown that only about a 10 percent reduction is brought about by the entrainment of fluid bearing circulation of opposite sign from the flow aft of the separation points. Numerical experiments to be discussed in another section of this work, as well as those done by others, show that the circulation generated on the downstream face of the cylinder can account for no more than about 1/5-th of the total reduction in circulation. This fact calls for other mechanisms which account for the remainder of the circulation loss. The second mechanism postulated for the exchange of oppositely-signed circulation is an integral part of the shedding mechanism. As proposed by Gerrard [63], when the growing vortex acquires a sufficiently large strength, it draws the feeding shear layer of the other growing vortex across the wake, thereby inhibiting further growth of the vortex. The tail of the cut sheet is then absorbed by the still attached vortex on the opposite side of the wake. This mechanism, quite distinct from the effect of the boundary layer on the rear of the cylinder, further reduces the strength of a given vortex. However, numerical experiments again show that the reduction due to this mechanism alone is far from sufficient to bring the circulation down to the observed or measured values. Consequently, a third mechanism must be postulated with which not only the vortices in the formation region but also those further downstream experience

additional circulation reduction. The origins of the third reduction mechanism may be partly in the ingestion or entrainment of fresh fluid into the shear layers, partly in the instabilities in the spiralling vortex sheets, partly in slow viscous reduction, and partly through some other as yet unknown mechanism. Regardless of the true origins of the reduction mechanism, two facts remain undisputed: the circulation of a given vortex does decay with time and the vorticity diffuses through viscous and turbulent action; and, the DVM cannot predict even the most gross features of the real flows (for example, lift and drag coefficients and circulation distributions) without the use of a circulation reduction mechanism.

Lastly, it is necessary to briefly discuss the effect of diffusion of vorticity on the apparent reduction of circulation. Diffusion means that the vorticity is spread over a larger area. This in turn means that larger numbers of suitably distributed point vortices for each segment of the vortex sheet rather than a single elemental vortex represent the corresponding distributed vorticity. Ordinarily, the point vortices (whether on a sheet or concentrated) are assumed to be placed at the center of gravity of the vorticity field.[3] This does not imply that the single vortex at the center of gravity will yield the same velocity at an arbitrary point on the cylinder or at the position of another point vortex as the distributed vorticity. As far as the cylinder is concerned, the said

---

[3]The center of vorticity of M point vortices is computed as

$$z = \frac{\sum_{j=1}^{M} \Gamma_j z_j}{\sum_{j=1}^{M} \Gamma_j}$$

effect becomes relatively small as the distance between the vortex and the cylinder increases. Consequently, the calculations are not noticeably affected by the diffusion of vorticity in the far field. Since diffusion is a matter of time, the vortices in the immediate vicinity of the cylinder do not undergo significant diffusion. The foregoing simply points out the difficulty of accounting for all direct or indirect decay mechanisms and the need for a suitable hypothesis which will account for the circulation decay and yet be compatible with the basic premises of the DVM. As is discussed in greater detail later, the present model accounts for the effect of rear shear layer, circulation cancellation brought about by the shedding mechanism, and finally by the cross-street circulation exchange. The last process is accomplished simply by transferring a certain percentage circulation between oppositely signed vortices at each time step.

IV. DETAILS OF THE NUMERICAL MODEL AND DISCUSSION OF RESULTS

A. SPECIFIC DETAILS OF THE MODEL

1. Typical Sequence of Calculations at an Arbitrary Time

The most straightforward way to describe the particulars of the model is to examine the sequence of events that occur during a typical computational cycle. Figure 17 is a flowchart indicating the order in which the model executes the various phases of the analysis. Each of the events that occur during every computation cycle are described in the order of their occurrence. The asymmetry introduction and vortex shedding processes occur only under certain flow conditions and are addressed separately.

At the beginning of each computation cycle the velocity distribution on the forebody of the cylinder is calculated at one degree intervals from the most recent position of the forward stagnation point. The positions of the upper and lower separation points are then determined through the use of Pohlhausen's method as described earlier. This allows the strength and positions of the two nascent vortices to be determined according to the no-slip condition.

The next step is the convection of each of the vortices by a simple Eulerian method where the velocity of each vortex is computed at its present location. The velocities of the nascent vortices are computed at the point of their introduction prior to their actual placement into the flow. This insures that a nascent vortex is convected with the velocity prevailing at the time and place of its creation. Subsequently, the lift and drag coefficients are determined through the use of Eq. (15).

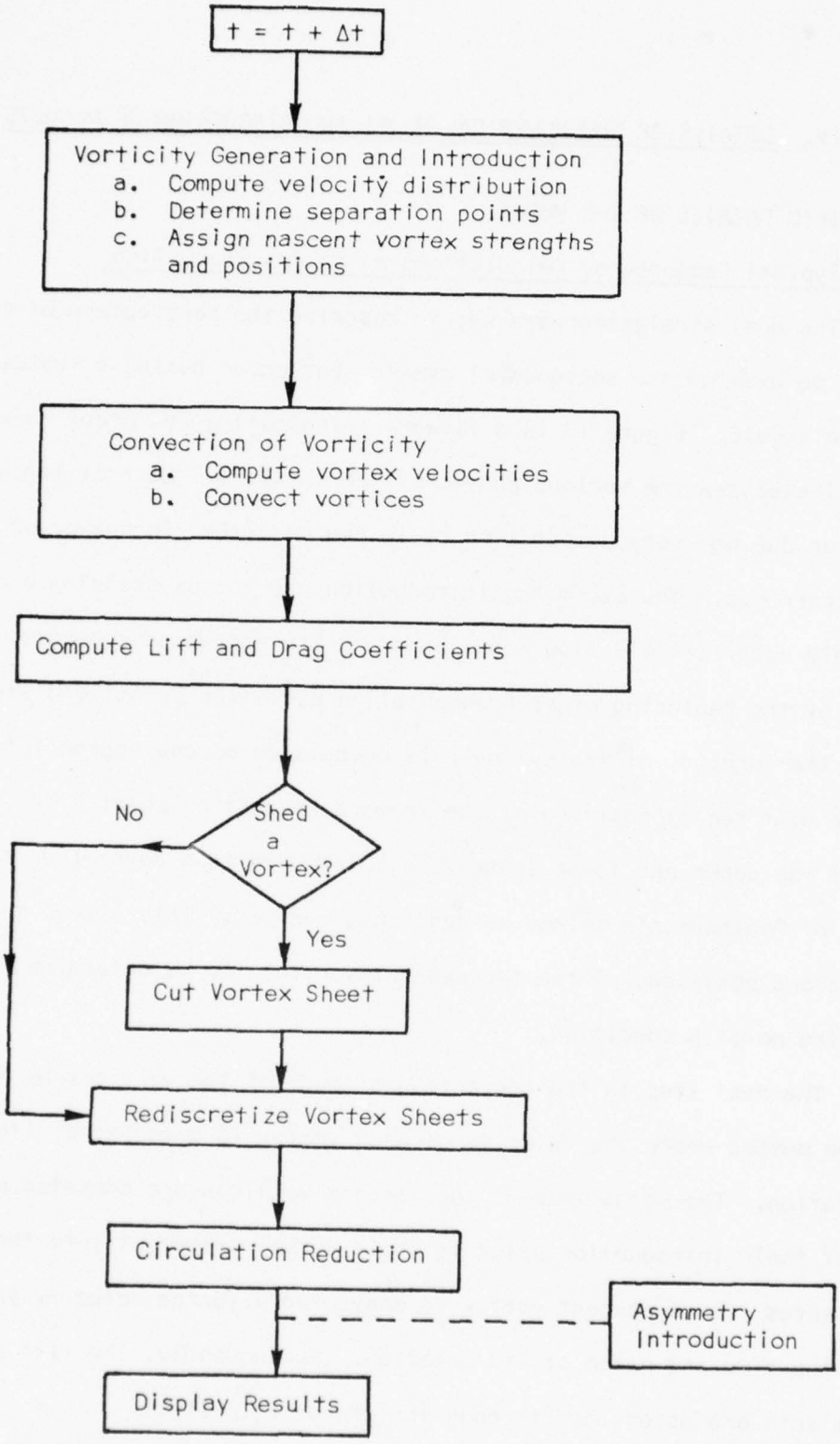

Fig. 17. Flowchart of computation sequence.

The normal sequence of the calculations requires a test for the conditions to determine whether the vortex sheet should be cut and the attached vortex spiral be shed. Because of its importance and the need for special handling, it is discussed separately.

In discussing the problems associated with the use of discrete vortices, it has been pointed out that the elemental vortices must be placed at the center of the sheet segment which they are supposed to represent. This led to the method of rediscretization. Thus, following the test for vortex shedding and if necessary, after the cutting of the vortex sheet, all attached and detached sheets are rediscretized. In doing so, each sheet is separately rediscretized (see Fig. 18). The discretization of the detached sheets is handled in accordance with the steps described in Chapter II, Section E. The only exception to the said process is in the treatment of the attached sheets near the nascent vortex. It has been repeatedly pointed out that the conditions near the separation point must be disturbed as little as possible by rediscretization or any other flow of events. In accordance with this principle, the nascent vortex and its immediate neighbor are not allowed to change their strengths or positions.

The next step in the sequence of calculations calls for circulation reduction and coalescence. It is simply hypothesized that every vortex in the flow field loses its strength in an amount proportional to its current strength. This hypothesis is based on heuristic reasoning, observations, and numerous calculations. Further justification of the hypothesis is made later. Here only the actual process incorporated into the computer code is described.

During each computation cycle for $t > 5$, the strength of every vortex, except the nascent vortices, is reduced according to the following

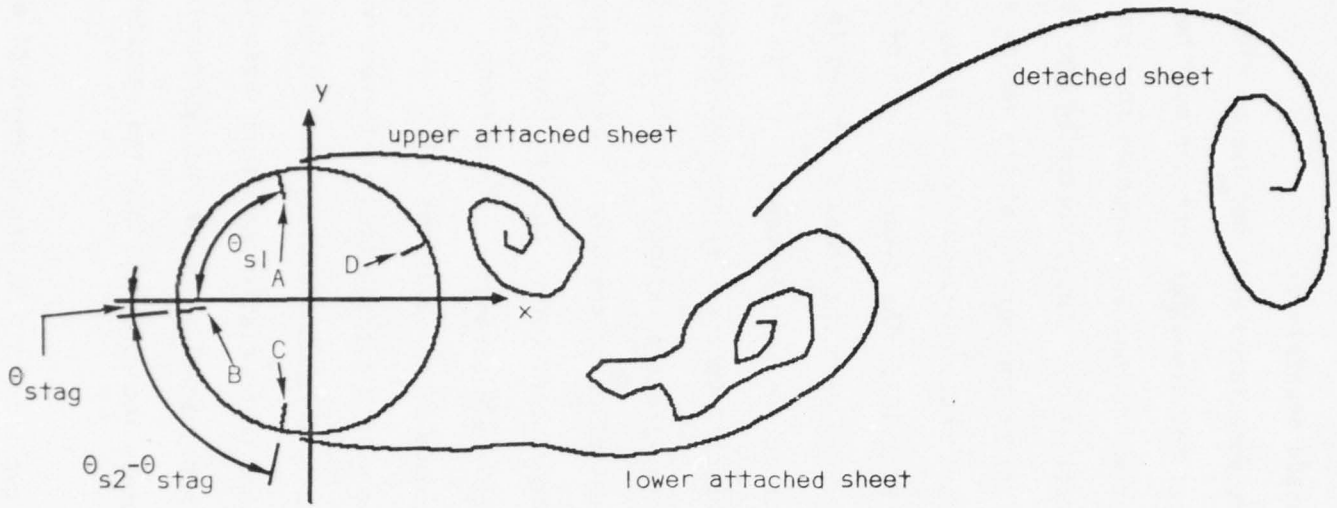

A : upper separation point
B : forward stagnation point
C : lower separation point
D : direction of resultant force

Fig. 18. A sample wake configuration.

expression

$$\Gamma_n(\text{new value}) = (1-p/100)\,\Gamma_n(\text{old value}) \qquad (39)$$

where p depends on the location $x_n = \mathrm{Re}\{z_n\}$ as depicted in Fig. 19. For $t < 5$, p is varied linearly from zero to its final value of unity.

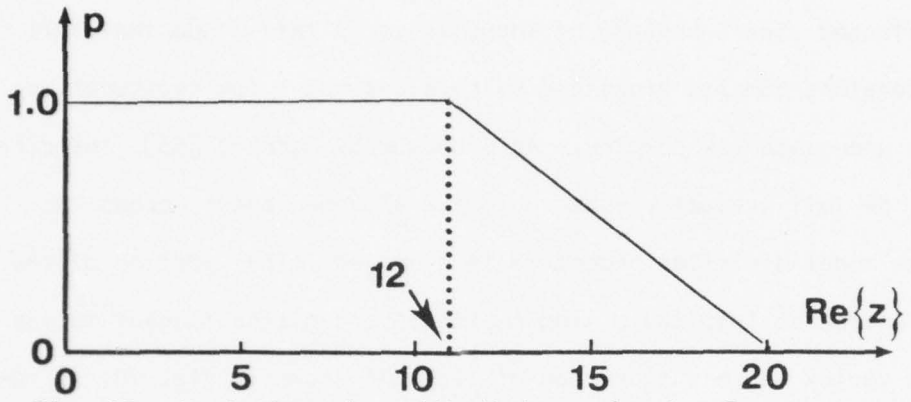

Fig. 19. Variation of p with distance for $t > 5$.

As discussed in connection with various circulation reduction mechanisms, there are two other processes whereby the circulation is reduced. The first is the reduction resulting from the proximity of vortices to the cylinder. Whenever a point vortex comes closer to the cylinder than a radial distance smaller than $\Delta r = 0.04$, that point vortex is assumed to be annihilated and removed from the flow field. The part of the sheet connected to the nascent vortex is excluded from this process. The annihilation of circulation in this manner results only in a small reduction in the total circulation and cannot account for a 40 to 50 percent reduction in the strength of the vortices in the stable region. The previous applications of the DVM which considered this annihilation mechanism together with that resulting from the occasional proximity of oppositely-signed vortices (rediscretization not used) obtained only a mere 15 percent reduction in circulation [67, 68]. This fact was the first indication of the need for an additional circulation reduction mechanism.

The second of the two mechanisms concerns the entrainment of the tail of the detached sheet into the vortices across the wake. For the sake of discussion, assume that an attached vortex sheet is severed at a suitable point. The details of how the cutting is accomplished is discussed later. The tail of the detached vortex sheet is drawn into the region between two attached sheets because of induction. If left alone that tail eventually develops complex kinks and spirals and makes the rediscretization process unnecessarily complex. As proposed by Gerrard [63], the circulation in the tail gradually ends up in the attached sheet across the wake. In the model a similar procedure is employed. That portion of the tail which penetrates into the mixing region beyond a line tangent to the two attached vortex spirals (upstream of line AA' shown in Fig. 20) is removed from the flow field, and its circulation is uniformly subtracted from that of the sheet across the wake. Calculations which keep track of this cross-wake circulation reduction show that approximately *five percent* of the circulation of the detached sheet is transferred across the wake by this mechanism. It should also be noted that the position of the line severing the tail of the detached sheet is not of particular significance. One may have used other suitable and defensible procedures to accomplish the same purpose.

2. Initiation of Asymmetry and the Vortex Shedding Processes

The first of these two events occurs only once and the second every time period a vortex is shed. As such, they constitute special events in the computational sequence and are discussed separately.

a. Asymmetry Introduction

In nature the inception of asymmetry and the shedding of vortices are intrinsic characteristics of flow about bluff bodies. The causes of asymmetry and the subsequent vortex shedding are closely linked to the

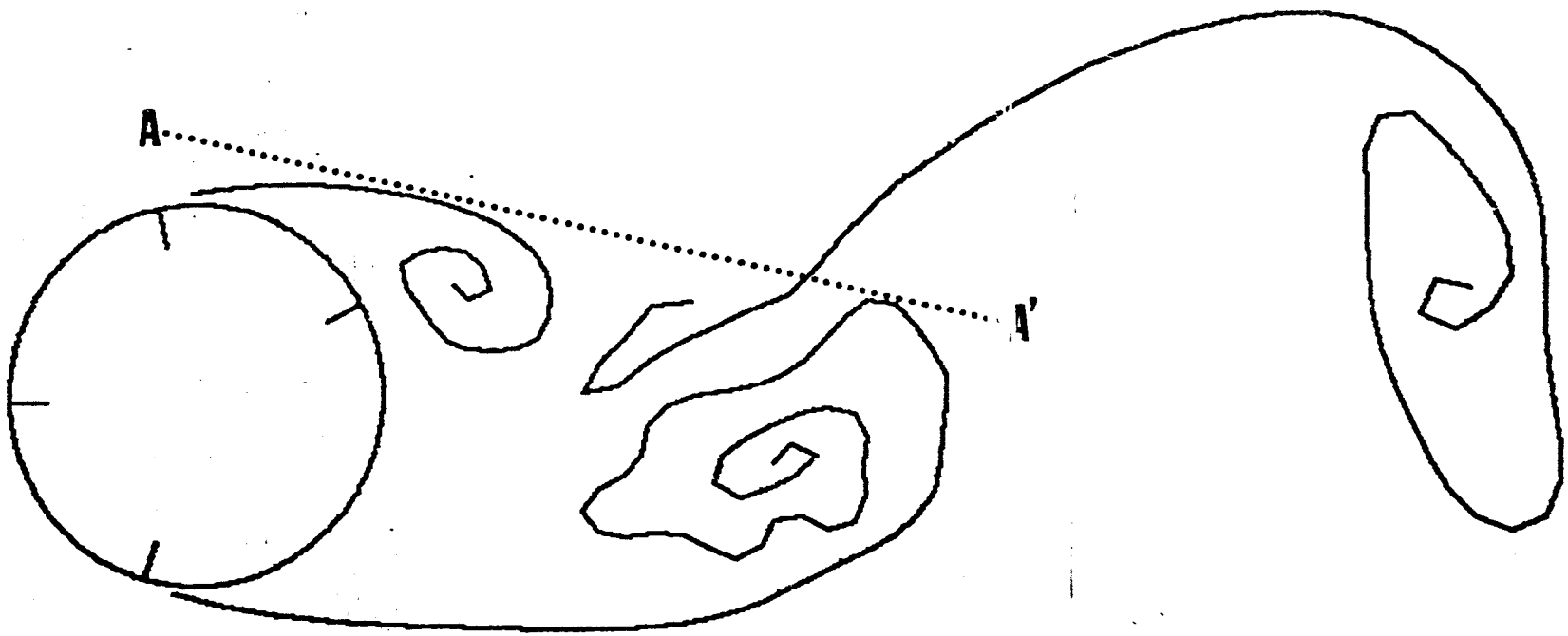

Fig. 20. Circulation reduction associated with vortex shedding process.

instabilities in the shear layers. These instabilities may be brought about by the slight nonuniformities in the ambient flow, randomly distributed turbulence, asymmetry of the body, etc. It appears that the symmetric state of separated flow is not its most stable state.

Whether the flow analysis is by the DVM, finite difference, finite element or whatever, asymmetry must be artificially introduced. Otherwise, the flow field remains forever perfectly symmetric and the vortex shedding process never begins. Figure 21 illustrates the results of the present model when asymmetry is never forced to develop.

Although the onset of asymmetry and the subsequent evolution of the wake have been observed and recorded by many researchers, little is understood about the controlling mechanism. The question of whether the asymmetry begins in the wake and is fed back to the boundary layer, or vice versa, is unknown. Perhaps both occur simultaneously. Regardless, the process is not well enough understood to suggest any preferable way to artificially initiate its occurrence. Consequently, the method utilized in the present model is a result of heuristic reasoning based on well known experimental observations and numerous numerical experiments with the model. Before describing the details and results of the various attempts, it is worthwhile at this point to relate some of the general observations, or lessons learned, from the investigation. Firstly, whatever method of asymmetry introduction is chosen, the steady state results of the model are identical; i.e., the model has no memory of the conditions which initiated the shedding of the first vortex. Secondly, as stated earlier, asymmetry need be introduced only for the shedding of the first vortex. Following the shedding of the first vortex, the shedding process continues under its own impetus. Thirdly, every asymmetry mechanism involves a trade-off between the intensity and the duration of the perturbation

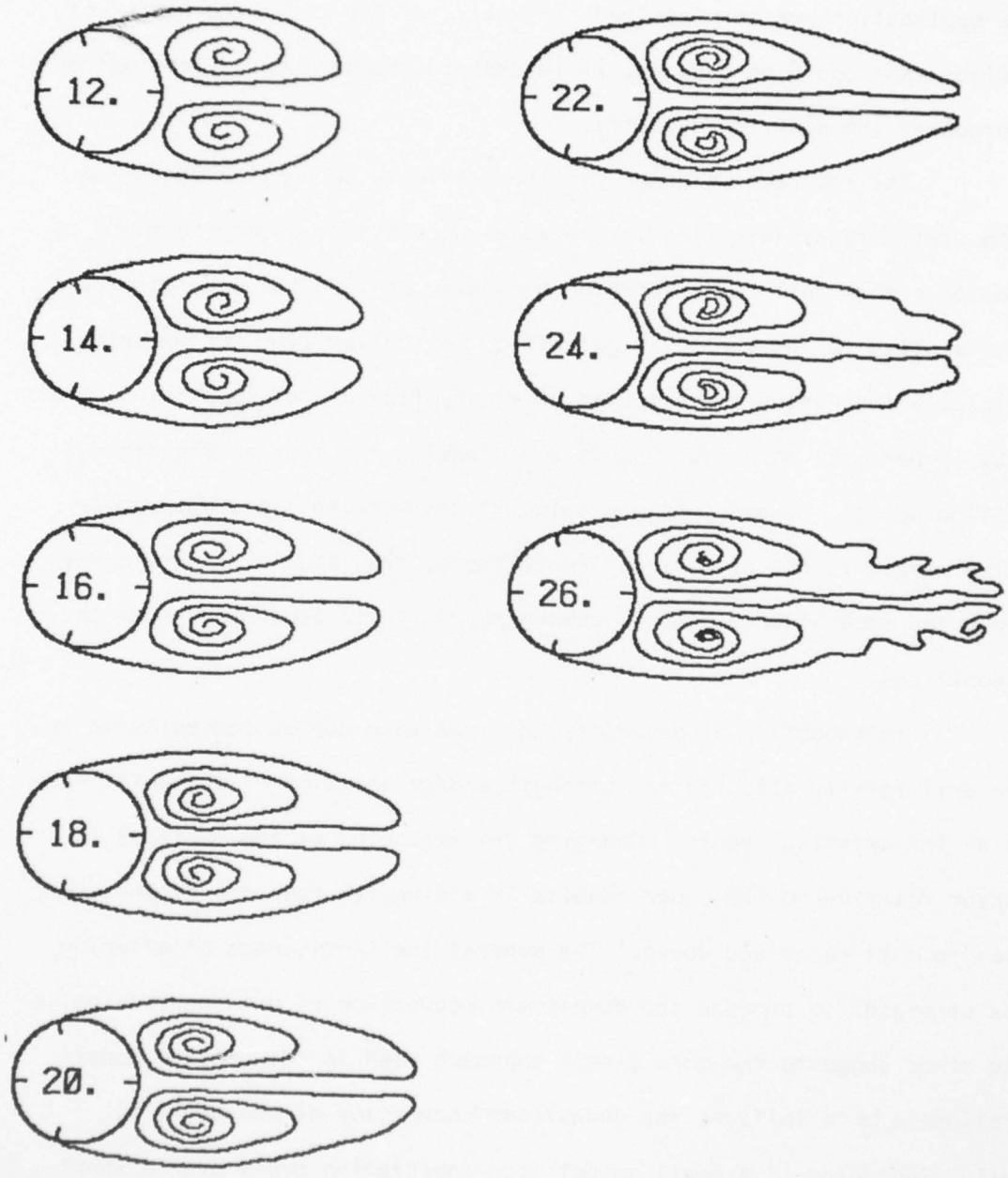

Fig. 21. Evolution of flow without asymmetry introduction.

applied. Associated with the question of duration is the decision of when to initiate the mechanism. Fourthly, there is an optimum time during which the symmetric flow is most susceptible to the onset of asymmetry. If asymmetry is introduced during this period, the intensity and duration of its application can be minimized. Finally, of the unlimited number of mechanisms that could be devised, it is best to choose the simplest method that produces the desired asymmetry.

The interactive nature of the vorticity generation mechanism and the vorticity distribution in the wake suggest that asymmetry might be introduced either into the generation mechanism or into the wake itself. Methods applied to the vorticity generation method involve, for example, artificially increasing the computed vorticity flux at one separation point (say by 10 percent) and simultaneously decreasing the flux at the other separation point. However, sample calculations with this procedure show that the method is not effective. Furthermore, the large asymmetry causes the computed separation angles to undergo unrealistic excursions from their mean positions.

Introduction of asymmetry into the wake can be accomplished by either artificially altering the strength and/or position of the point vortices on the existing sheets. Changing the strengths of the vortices in one sheet relative to the other results in a sluggish response of the wake similar to that described above. The general ineffectiveness of altering vortex strengths to produce the downstream convection of one sheet relative to the other suggests the more direct approach used in the present model. The rationale is to initiate the downstream convection of one sheet by actually displacing it a small amount each computation cycle over a short period of time so that when the mechanism is discontinued the sheet continues to move without external influence.

Numerous numerical experiments have shown that a gradual application and buildup of the displacement increment serves to provide a smooth transition from symmetric to asymmetric conditions. The initiation time and duration of application are based primarily on two considerations. Firstly, this time interval should correspond to the period during which the flow is most susceptible to asymmetry. Secondly, the initiation of the mechanism should begin after the initial peak in the drag curve. Since the cause of this drag overshoot is the symmetric growth of the vortices, the asymmetry mechanism should not be allowed to influence this symmetric development.

In the following the specifics of the asymmetry introduction method are presented. During each computation cycle within the interval $5.0 \leq t \leq 9.0$ the vortices of the upper attached sheet are displaced downstream an amount given by (see Fig. 22)

$$\Delta x = 0.02 \{1.0 - \cos[\pi(t-5)/4]\} \tag{40}$$

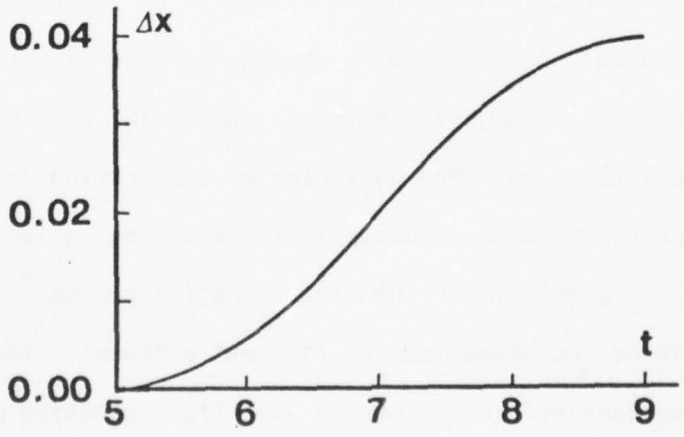

Fig. 22. Variation of the asymmetry perturbation Δx with time.

Several points are worthy of discussion. Firstly, the displacement given by Eq. (40) is not unique and any other form of displacement function could have accomplished the same purpose. The particular choice, depicted by Fig. 22, introduces the disturbances gradually and continuously without shocking the flow field. Lastly, the total displacement applied to the sheet during the time interval $5 \leq t \leq 9$ is only 8 percent of the radius of the cylinder.

b. Vortex Shedding Process

Vortex shedding is understood as the mechanism whereby the feeding layer is cut. The specific details of the conditions which dictate the separation of a spiralling sheet from its feeding layer are not known and have yet to be determined experimentally. The numerical model is not in need of such a cut were it not due to the limitations of computation time. If the flow field is allowed to evolve asymmetrically, the flow pattern shown in Fig. 23 results. This figure shows not only the evolution of the doubly-connected vortex sheets but also the drawing-in of the tail of the shedding vortex into the mixing region. The continuation of the calculations in this manner are prohibitive even with the largest computers. However, it is instructive in two ways to examine the evolution of the wake in this manner. Firstly, the uncut sheet begins to change the sign of its curvature as the lift force goes through its extremal (see point A of Fig. 23). The change of curvature is in fact the beginning of the drawing-in process of the shear layer across the wake. Subsequently, a strong inflection and kink develop drawing the sheet closer into the formation region. Simultaneously, the lift force increases towards its next extremal. The gradual nature of this process does not permit one to identify a specific moment at which the shedding should commence. Thus, the examination of other flow features exhibiting stronger reaction to the precise moment of shedding are

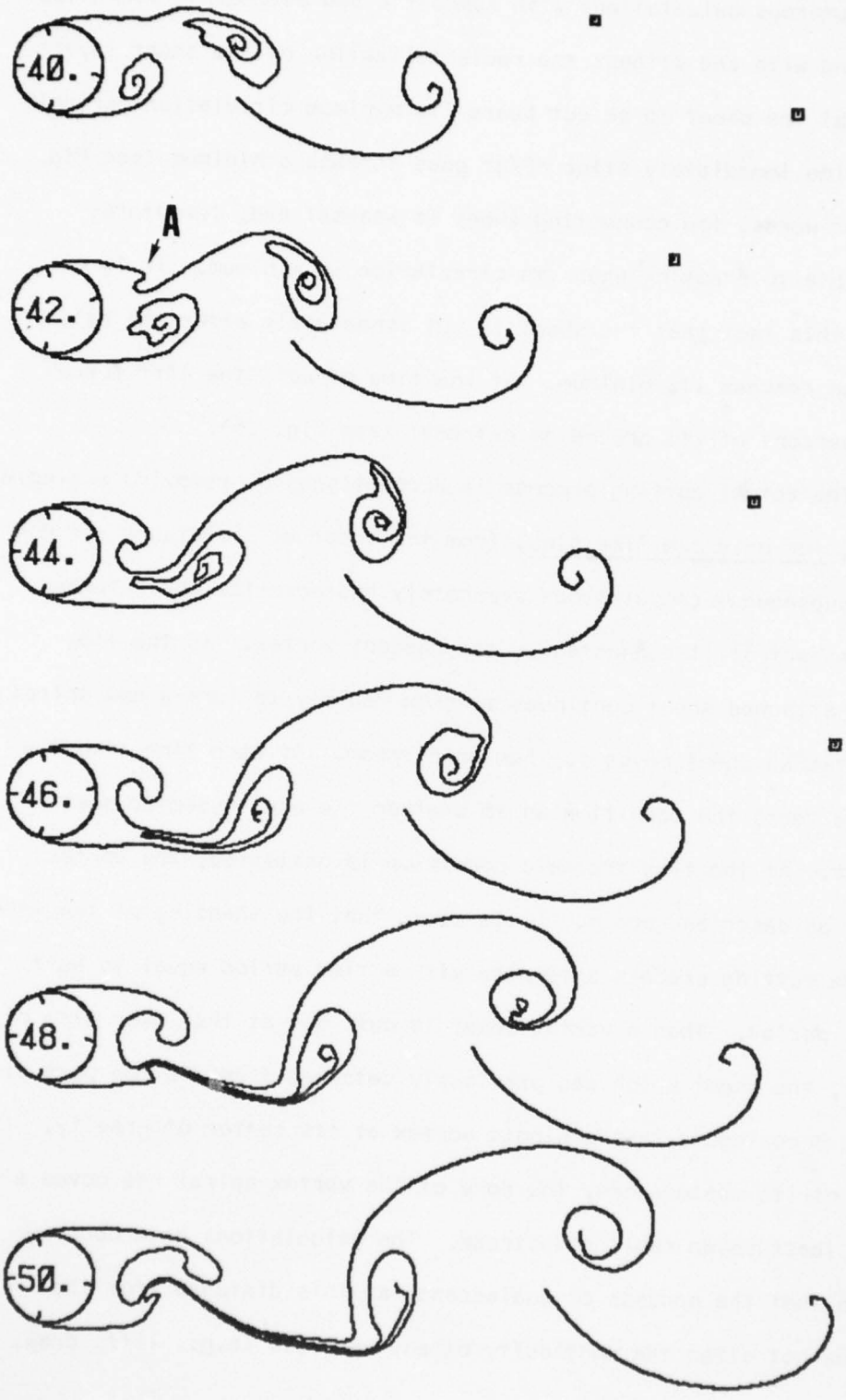

Fig. 23. Evolution of flow without cutting the vortex sheet.

necessary. Numerous calculations with symmetric and asymmetric evolution of the wake and with and without the rediscretization of the shear layers have shown that the sheet to be cut bears its minimum circulation per unit length at a time immediately after $d\Gamma/dt$ goes through a minimum (see Fig. 24). In other words, the connecting sheet is weakest and, therefore, most susceptible to breaking when its circulation is minimum. It is on the basis of this fact that the sheet is cut immediately after the rate of circulation reaches its minimum. At the time of cut, the lift force is about 50 percent of its preceding extremal (see Fig. 25).

The actual cutting process is accomplished by removing a single point vortex, for only one time step, from the sheet at a distance $s = 0.4$ (Fig. 26). Subsequent calculations separately rediscretize the detached sheet and the part still connected to the nascent vortex. As the flow evolves, the attached sheet continues to grow rapidly to form a new spiral while the detached sheet moves further downstream. At each time step the computer code tests the condition as to whether the new connected sheet should be cut. At the time the said condition is satisfied, the vortex sheet is cut as described above. It is clear that the shedding of the vortices and the cutting process alternate with a time period equal to half the Strouhal period. When a vortex sheet is cut, say at the lower side of the cylinder, the sheet which was previously detached from the top part of the cylinder is coalesced into a single vortex at its center of gravity. At the time of its coalescence, the core of the vortex spiral has moved a distance at least seven radii downstream. The calculations have conclusively shown that the process of coalescence at this distance from the cylinder does not alter the continuity of any variable (e.g., lift, drag, circulation, etc.).

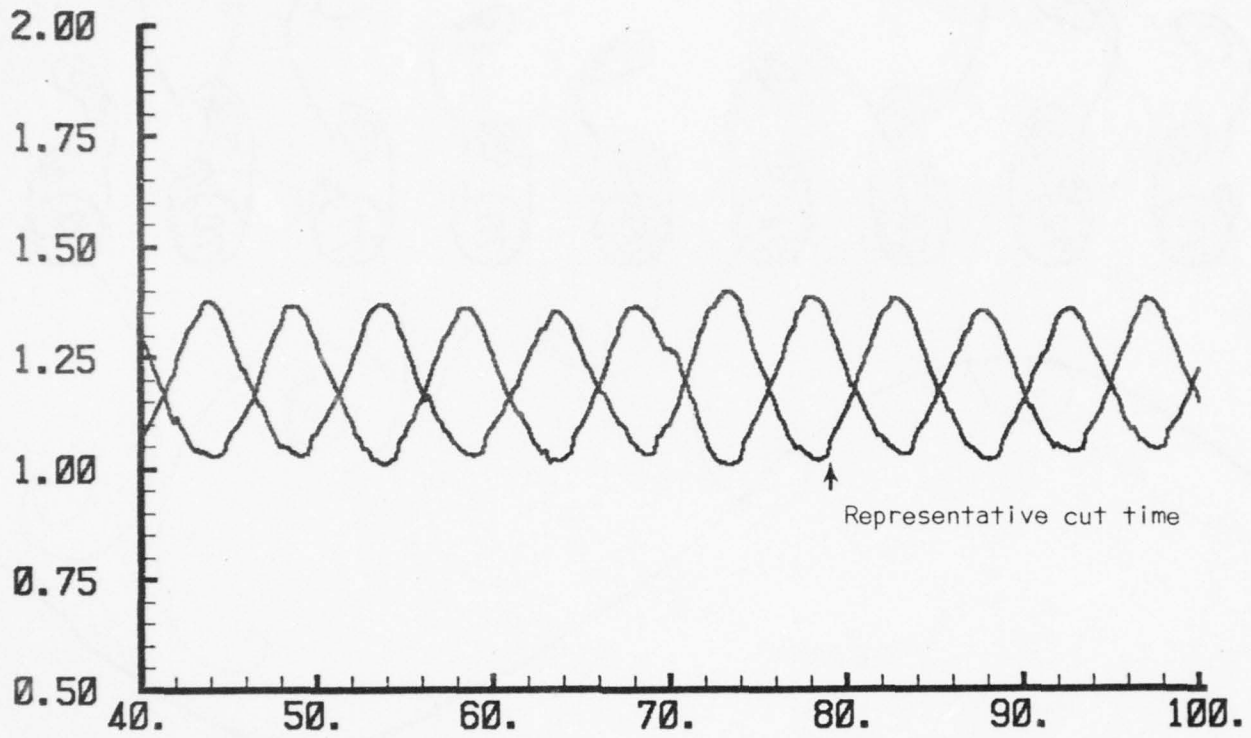

Fig. 24. $d\Gamma/dt$ prior to and after the cutting of the sheet.

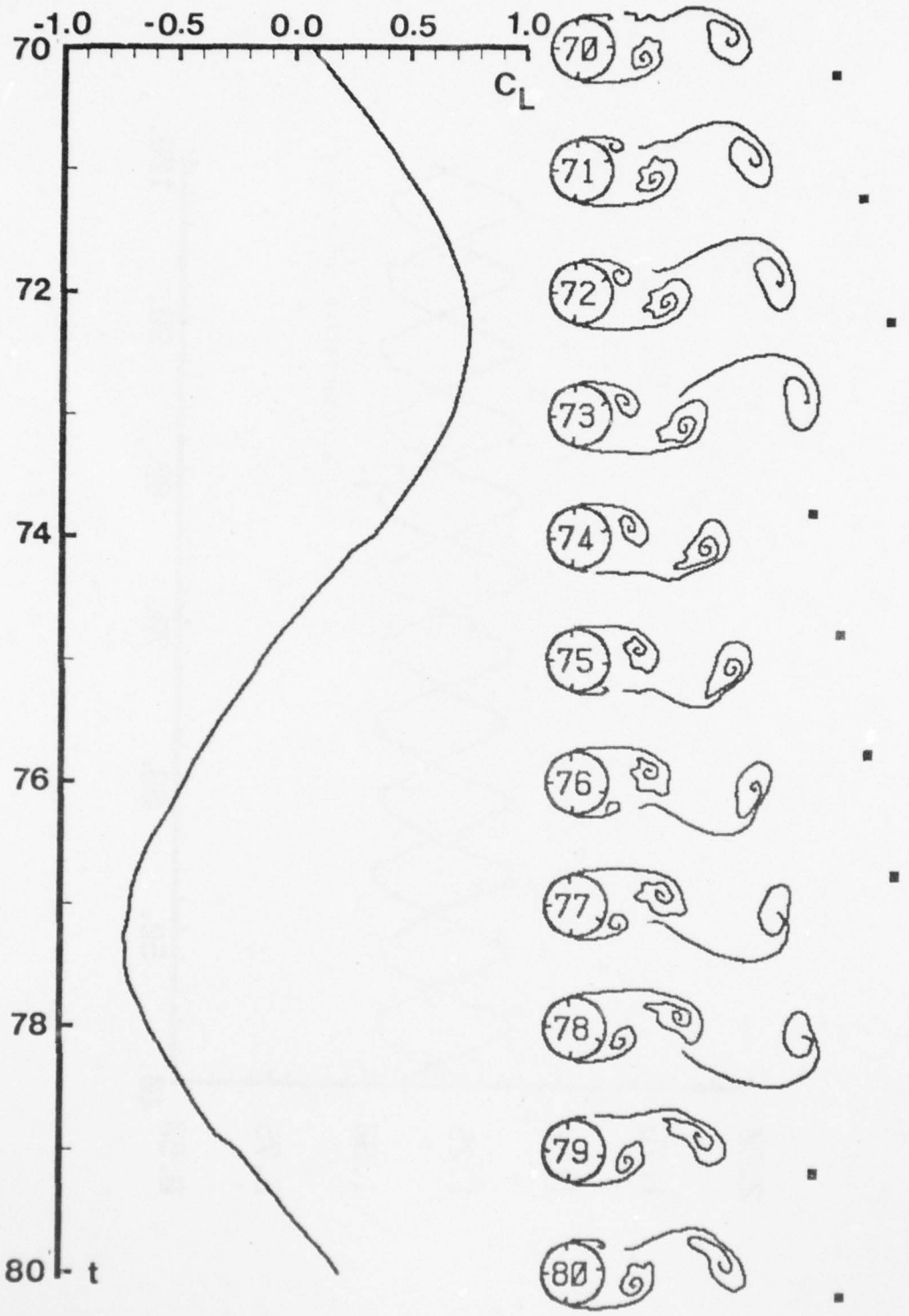

Fig. 25. Variation of lift during a cutting cycle.

Fig. 26. Cutting of a vortex sheet.

B. DISCUSSION OF RESULTS AND SENSITIVITY ANALYSIS

In the following, the results obtained with the numerical model (referred to hereafter as the standard run) are presented. Following this, the variation of some of the important kinematic and dynamic parameters to the variation in others is discussed. The purpose of these discussions is to partly establish the stability of the results, partly to relax the range of variability of the nondisposable parameters, and partly to establish the cause and effect relationships. At this time, no distinction is offered concerning the choice of parameters in the model and the calculated results. Furthermore, no distinction is made between prediction and inspired hindsight.

1. Results Obtained with the Standard Run

The standard run is computed using $\Delta t = 0.125$, $p = 1.0$ (see Fig. 19) and with the asymmetry introduction and the shedding mechanisms previously described.

The evolution of the wake over one arbitrarily chosen cycle is shown in Figs. 27 and 28. Figure 27 depicts the near wake region and Fig. 28 shows the far wake vortex street.

The variations of the lift and drag coefficients with t are shown in Figs. 29 and 30. The drag coefficient reaches a maximum at $t \simeq 4.2$ and then rapidly decreases to its ultimate mean value of about 1.2. The fluctuations of C_D have a frequency twice the vortex shedding frequency and an amplitude of about 0.06. The overshoot of the drag coefficient is a direct consequence of the rapid accumulation of vorticity in the symmetrically growing vortex spirals. Following the shedding of the first vortex, C_D drops sharply and the lift coefficient increases, ultimately reaching a mean amplitude of about 0.65. The slight variations in the oscillations of C_D and C_L come from various sources. The vortices absorbed during the cross-

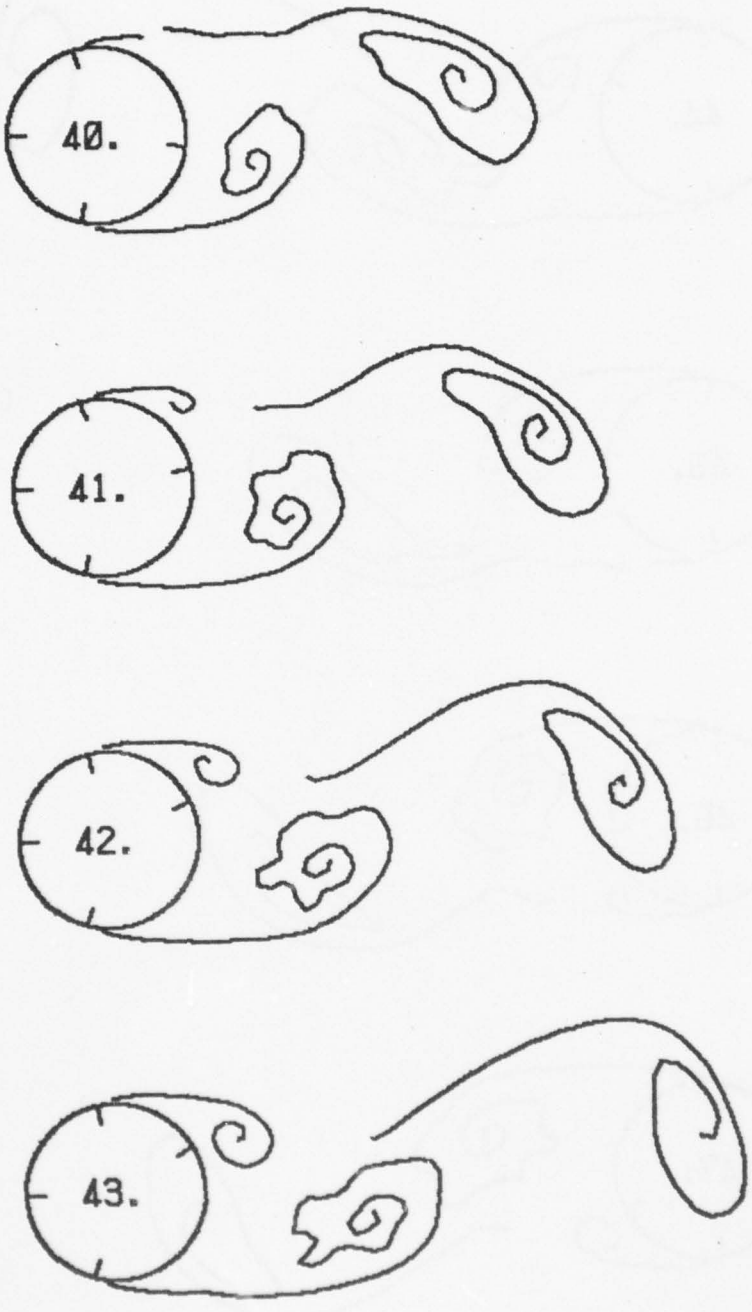

Fig. 27. Evolution of flow in the near wake.

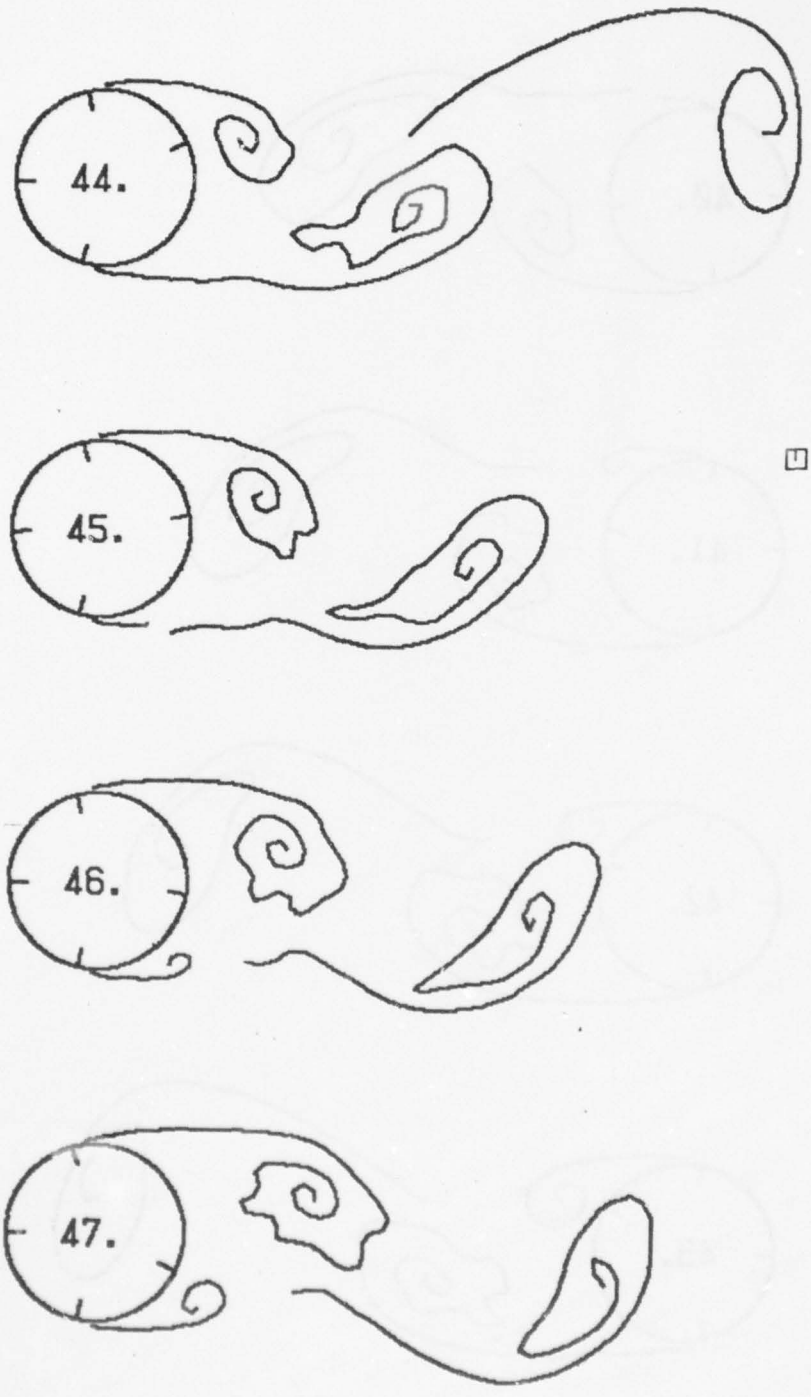

Fig. 27 (con't). Evolution of flow in the near wake.

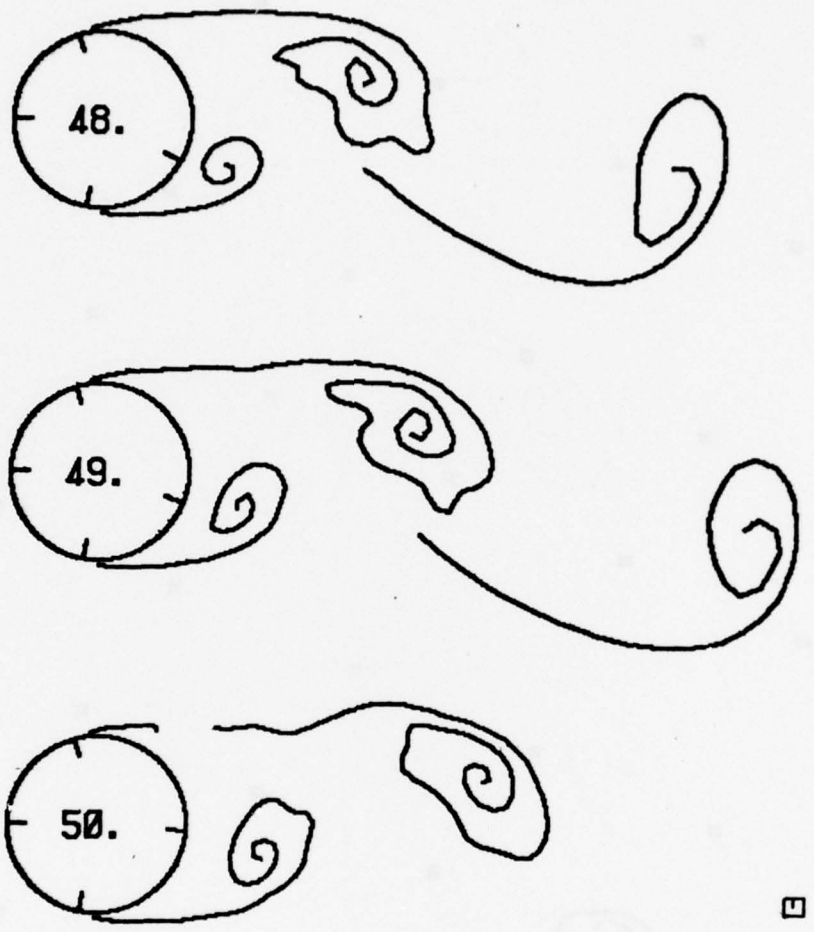

Fig. 27 (con't). Evolution of flow in the near wake.

Fig. 28. Evolution of flow in the far wake and the vortex street.

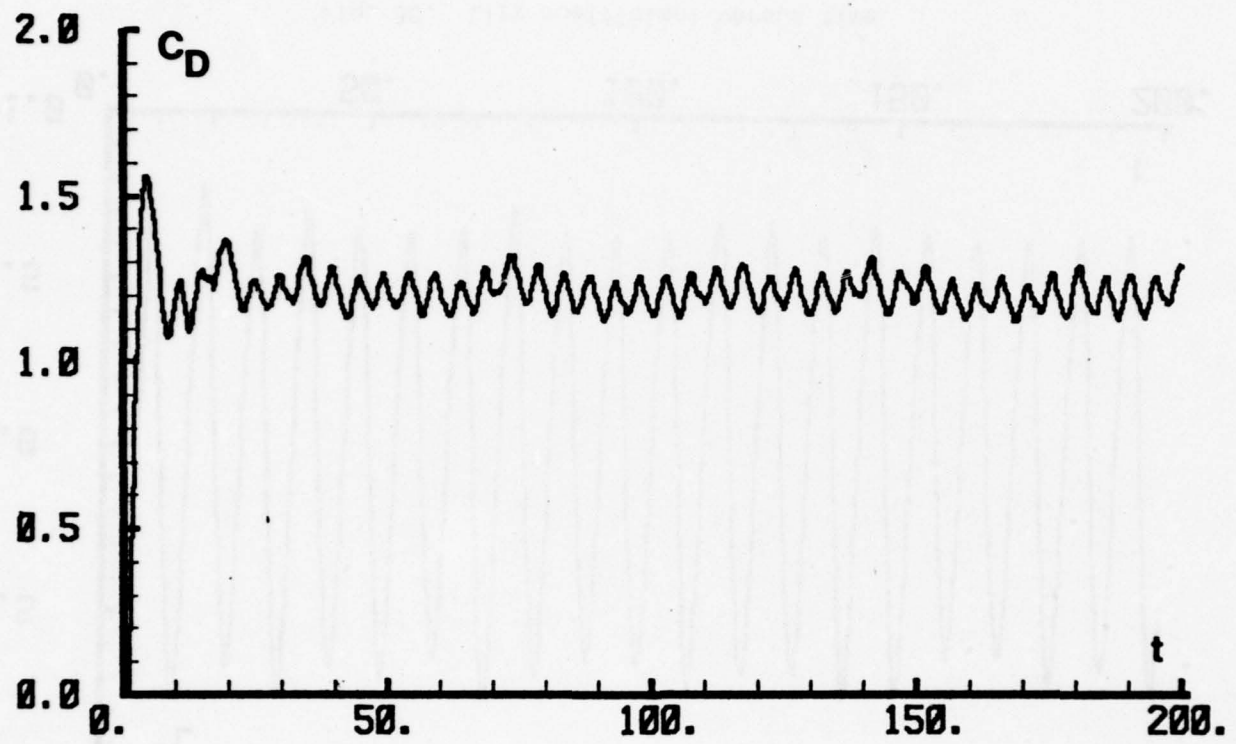

Fig. 29. Drag coefficient versus time.

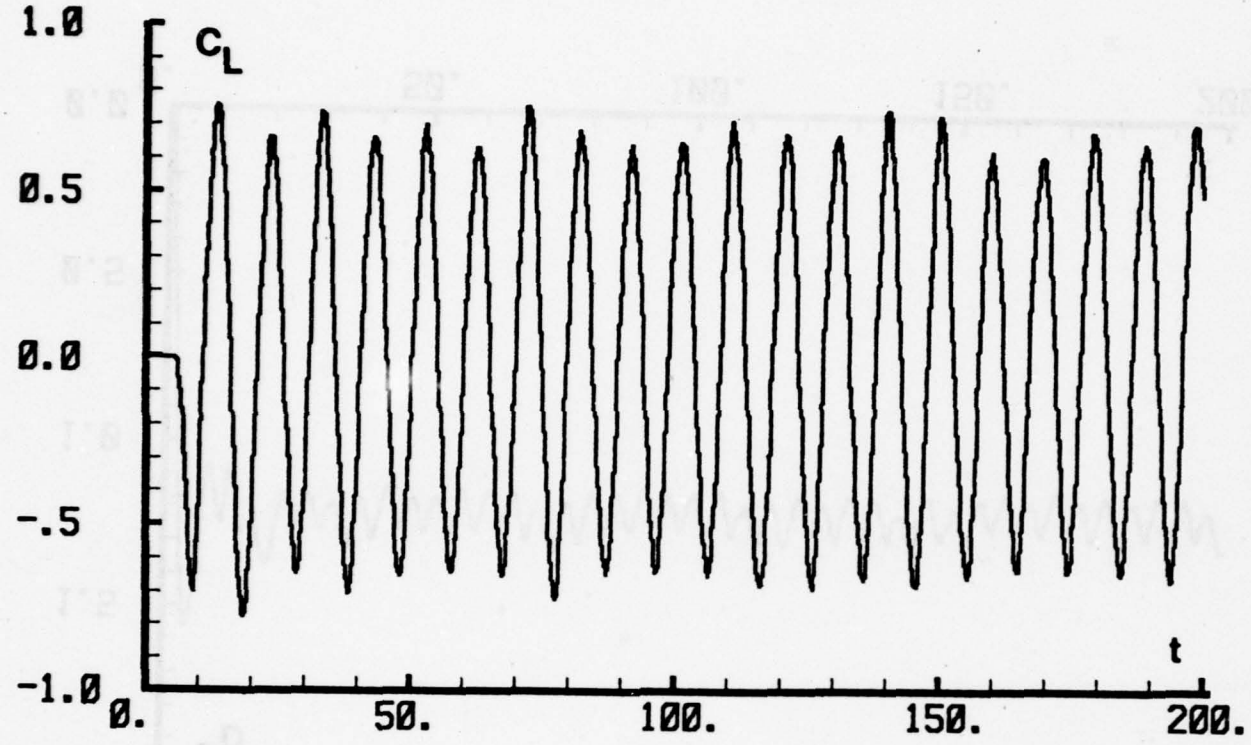

Fig. 30. Lift coefficient versus time.

wake cancellation mechanism may be one more or one less during two different cycles. The increase of the otherwise finite length of the wake does not permit the vortex sheets to follow exactly identical paths from one cycle to another. Regardless, the said perturbations in C_D and C_L are quite small and well within the accuracy of the numerical model.

The amplitude of the lift coefficient is certainly within the range of lift coefficients reported in the literature. However, it is not possible to find a truly two-dimensional laboratory experiment to compare the calculated results with greater definitiveness. More is said later about the dependence of the amplitude of C_L on other parameters, in particular on the circulation reduction mechanism.

Figure 31 shows a comparison of the calculated and measured drag coefficients. The results are strikingly similar and may be taken as a first indication of the workings of the model.

The oscillations of the separation points in terms of the angles measured from $\theta = 0$ (not necessarily the instantaneous position of the stagnation point) are shown in Fig. 32. The separation angle for a given separation point oscillates nearly sinusoidally with an amplitude of $\Delta\theta = 3$ degrees about a mean value of $\bar{\theta}_s \simeq 77$ degrees. The frequency of oscillation of θ_s is identical to that of the shedding of vortices.

The stagnation point does not remain at $\theta = 0$ even in steady flow about a stationary cylinder. Figure 33 shows the oscillation of the stagnation point. Similar oscillations have been reported by Dwyer and McCroskey [71]. The separation angles relative to the instantaneous position of the stagnation point are shown in Fig. 34. A comparison of Figs. 32 and 33 show that the oscillations of the separation and stagnation points are 180 degrees out of phase. In other words, if the stagnation point moves up, say to $\theta = 2$, the separation point at the upper half of the cylinder moves

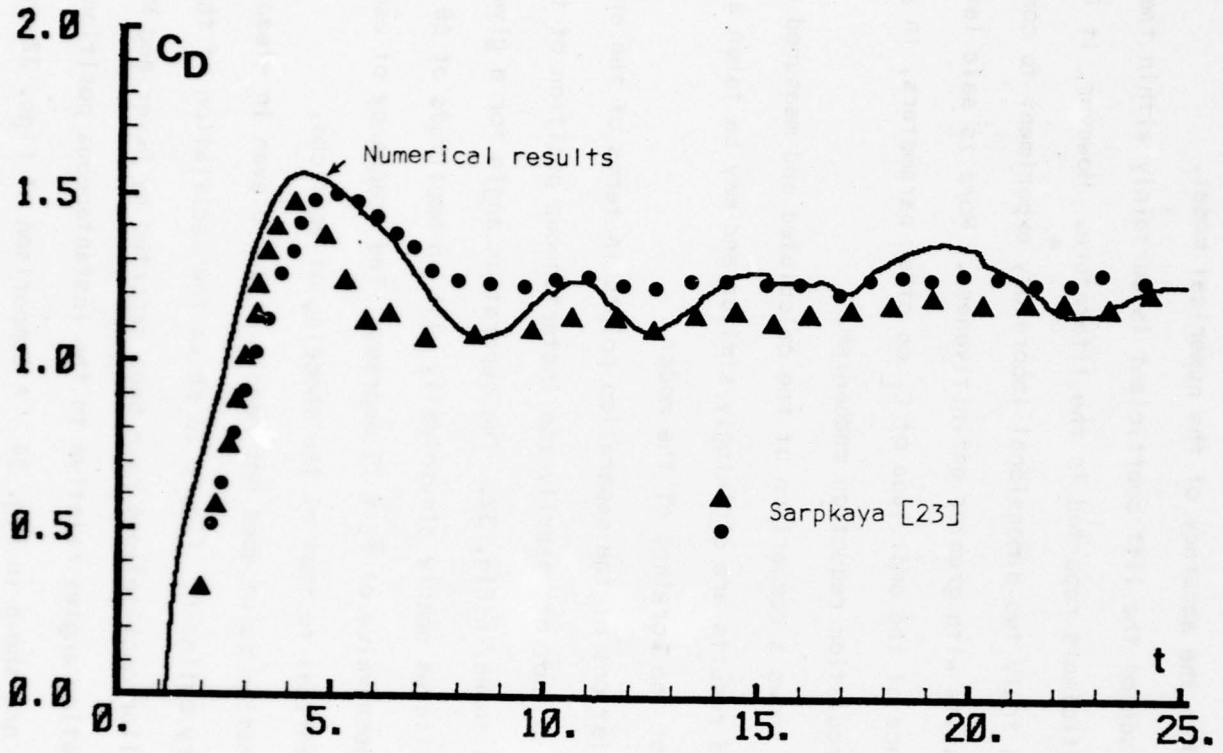

Fig. 31. Comparison of predicted and measured drag coefficients versus time.

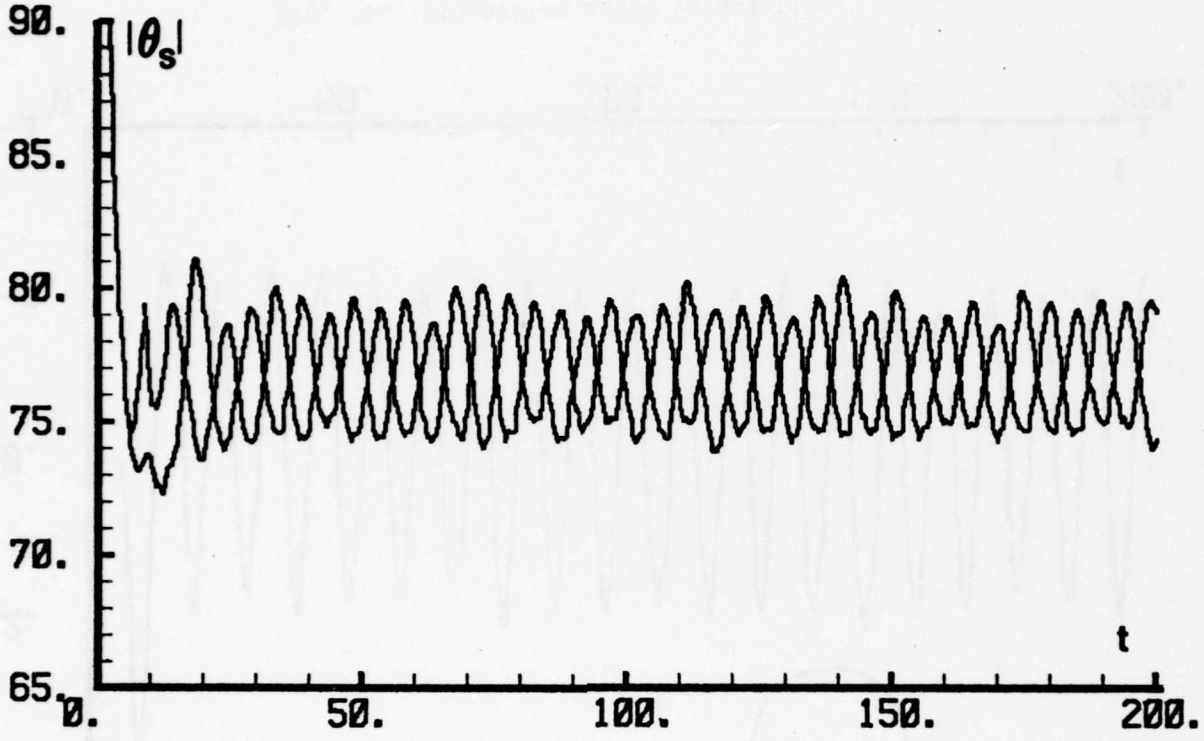

Fig. 32. Separation angle versus time.

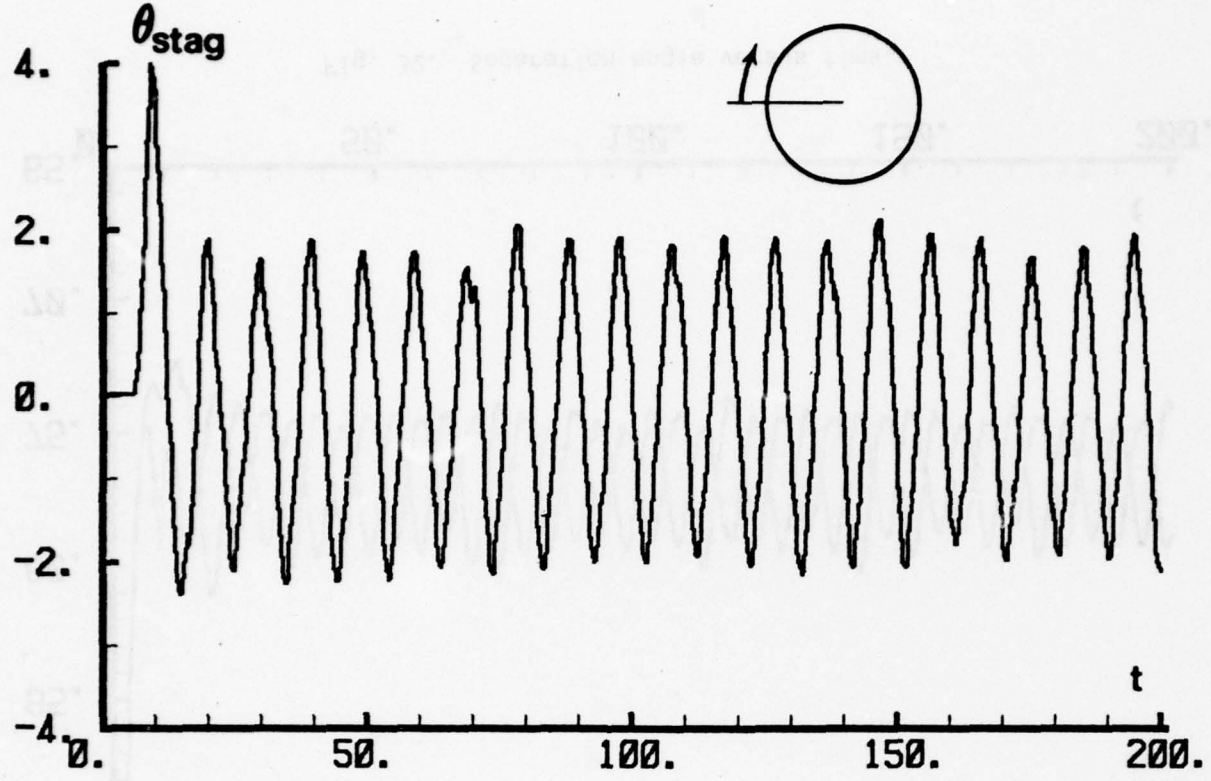

Fig. 33. Stagnation angle versus time.

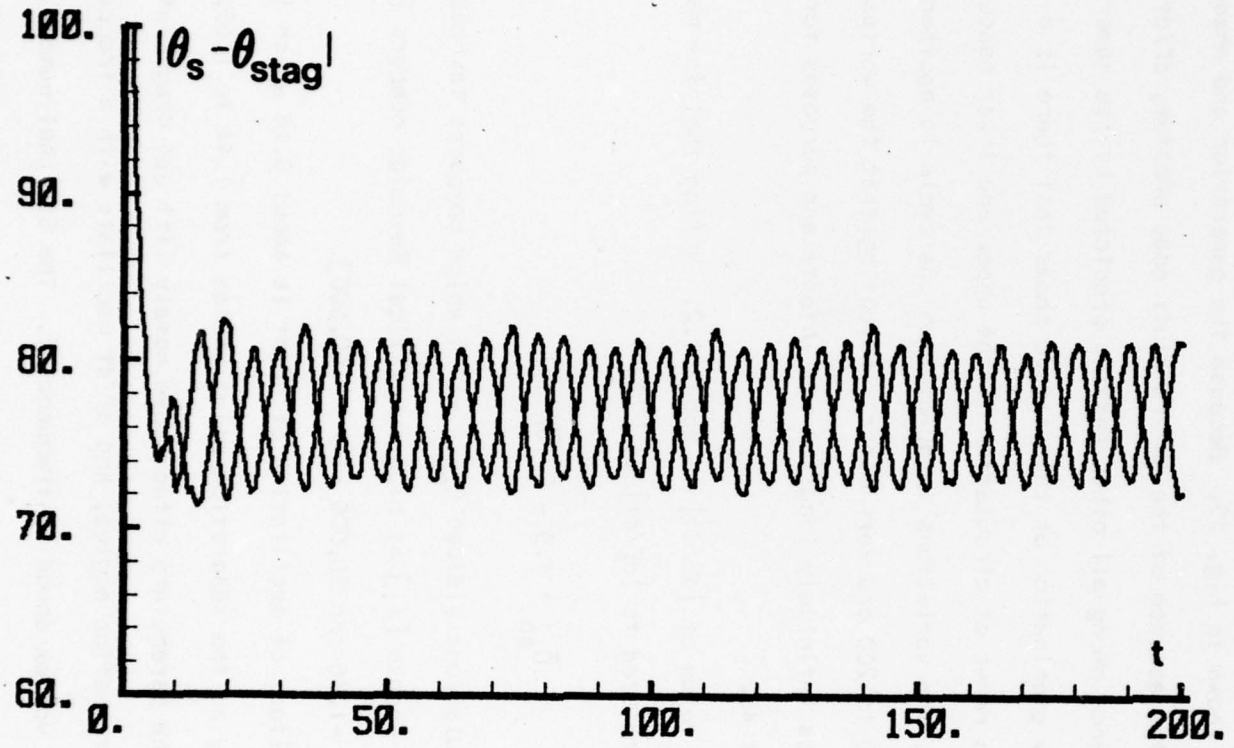

Fig. 34. Separation distance versus time.

backwards from a mean position $\theta_s = 77$ to $\theta_s = 74$ degrees. This fact is also in conformity with previously reported results [71].

The rate of change of circulation at both the upper and lower separation points is shown in Fig. 35. Because the generation and shedding of circulation are the essence of the entire bluff body problem, $d\Gamma/dt$ has a special significance among all other results predicted by the numerical model. A cursory examination of this figure shows that there is a perfect similarity of the rates of circulation of the upper and lower nascent vortices. Secondly, the variations in $d\Gamma/dt$ from one cycle to another as t increases from 40 to 200 are very minor, indicating that the vortex street may be regarded as infinitely long for all intents and purposes for t larger than about 40.

The mean value of $|d\Gamma/dt|$ is about 1.2. Noting that the mean base pressure $\bar{C}_{pb}$ is related to $|d\Gamma/dt|$ by [72]

$$\bar{C}_{pb} = 1.0 - 2\,|\overline{d\Gamma/dt}| \qquad (41)$$

The present calculations yielded $C_{pb} = -1.35$ which compares favorably with that reported by Roshko [11] at high subcritical Reynolds numbers [C_{pb} (experimental) = -1.36 for $20{,}000 < Re < 100{,}000$].

The amplitude of oscillation of $d\Gamma/dt$ is about 0.18 which indicates that the velocity at the separation point varies from 1.41 to 1.65.

All of the parameters cited above, namely lift and drag coefficients, separation and stagnation angles, and $d\Gamma/dt$ oscillate with a frequency identical to the vortex shedding frequency f. The Strouhal number, $St = f_v D/U$ is found to be $St = 0.205$. The experimental values of the Strouhal number are reported to lie between 0.195 and 0.210 for the Reynolds number range from 2,000 to 400,000 (see Fig. 36). Thus, the predictions of the model are in conformity with the measurements in the range of Reynolds

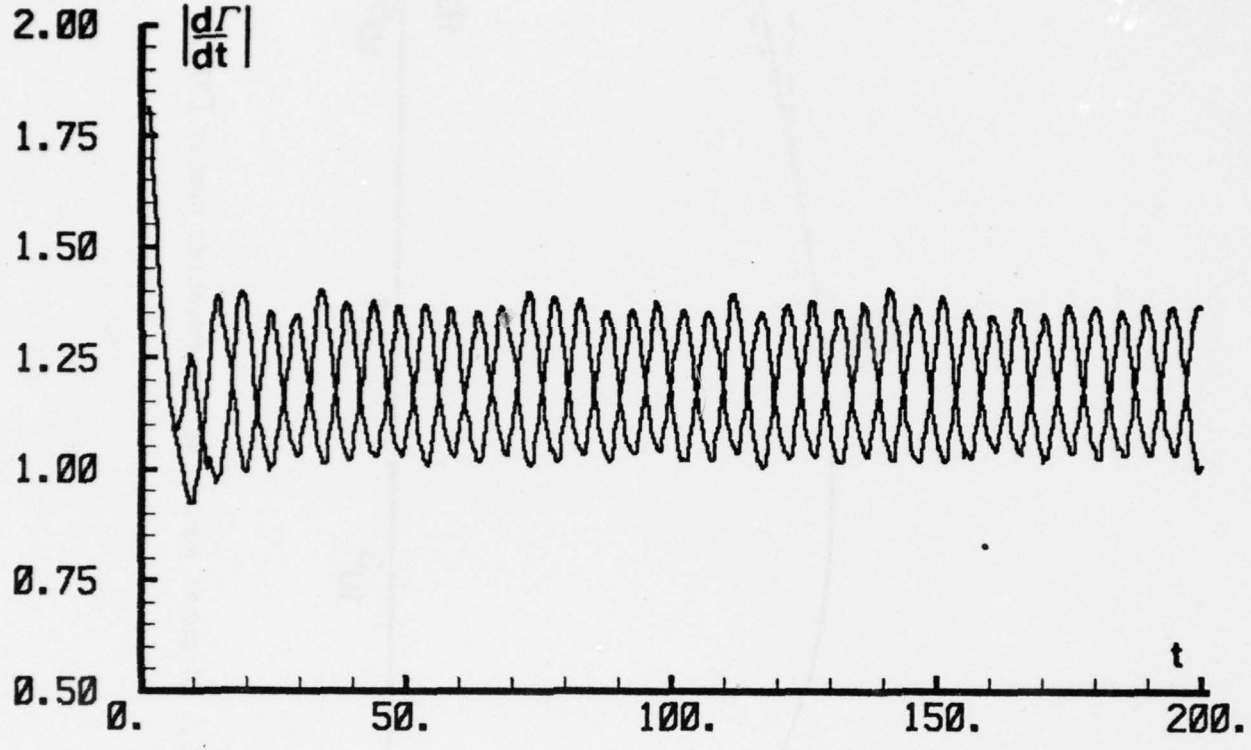

Fig. 35. Rate of circulation generation versus time.

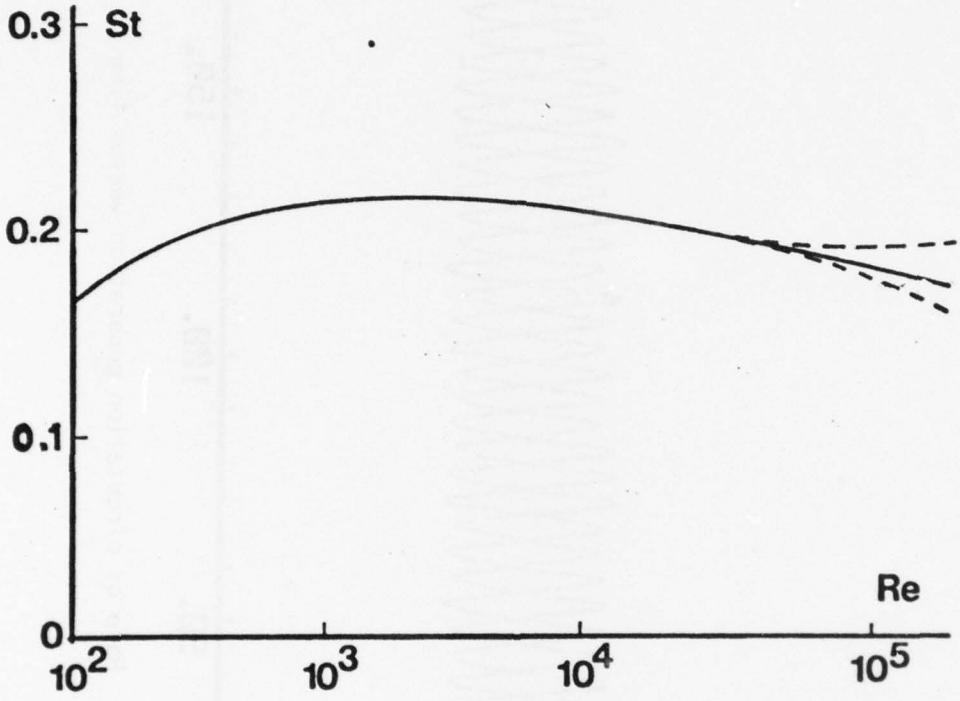

Fig. 36. Strouhal number versus Reynolds number [73].

numbers where the DVM is applicable. As is noted later, the Strouhal number is the least sensitive of all the parameters to the variations of the non-disposable parameters.

One of the often discussed characteristics of the vortex street, particularly in the stable region, is the relative spacing of the vortices. Von Karman's classic stability analysis gave $h_v/\ell_v = 0.281$ (see Fig. 37). Since von Karman, the said ratio has been determined experimentally by a great number of investigators and it has been found that h_v/ℓ_v varies from about 0.19 to 0.3.

The lateral and transverse vortex spacings obtained with the standard run are shown in Fig. 37. The asymptotic values of ℓ_v and h_v are well within the experimentally determined values [74]. In the stable region of the street, the lateral spacing decreases somewhat and the transverse spacing gradually increases from about 0.63 to its asymptotic value of about 1.05. The ratio h_v/ℓ_v in the asymptotic range is seen to be 0.23, a value which compares well with those reported experimentally [74]. Evidently, it is not meaningful to think of vortex spacings within the formation region.

All discrete vortex models of separated flow about bluff bodies indicate the need for greater loss of circulation in the wake in order to bring a closer correspondence between the calculated and measured separation points, lift and drag coefficients, $d\Gamma/dt$, etc. For example, Deffenbaugh and Marshall [47] obtained a mean separation angle of 67 degrees and a mean drag coefficient of 0.9 even though the smaller separation angle should have yielded larger drag than that found experimentally due to the increased wake size. In the present model all conceivable circulation reduction mechanisms have been taken into consideration. Their variations with x or t may not be unique or in conformity with those obtained

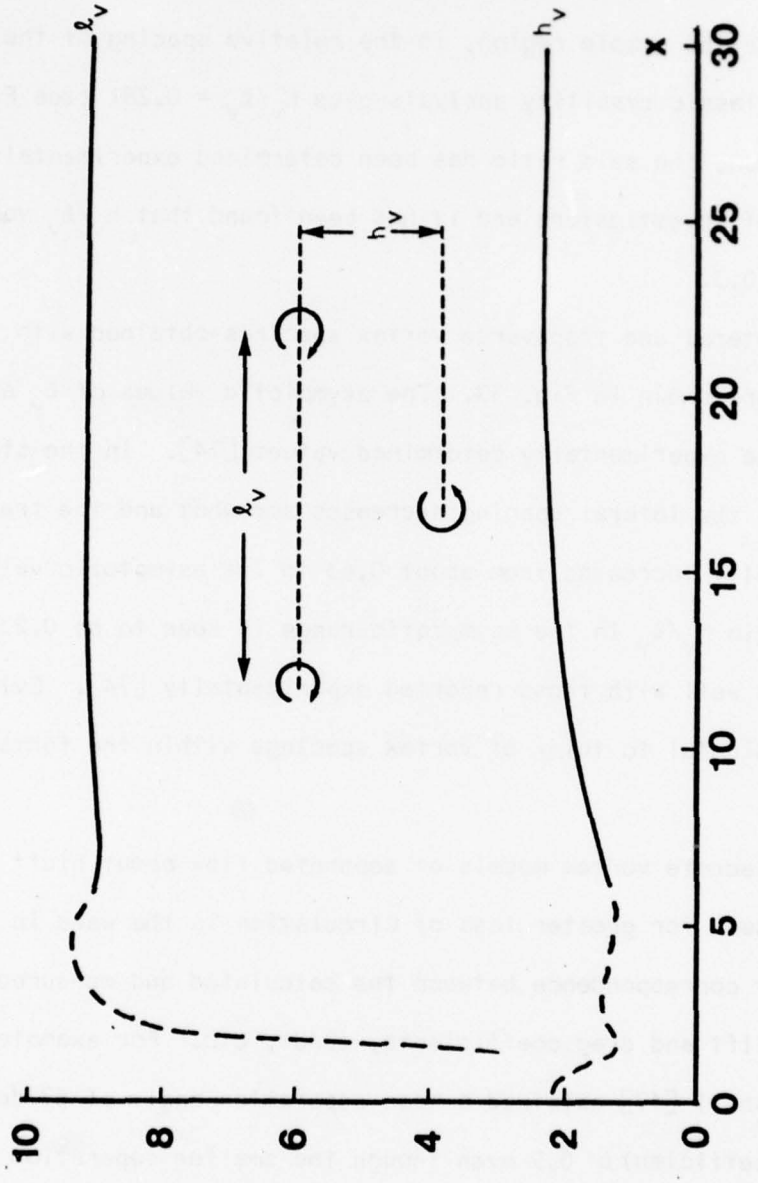

Fig. 37. Longitudinal and transverse vortex spacings.

experimentally but their characteristics follow all vortex shedding mechanisms so far advanced. Figure 38 shows the circulation retained by a vortex sheet from its inception to its subsequent coalescence and convection into the far wake. Also shown in this figure are the two experimental points reported by Bloor and Gerrard [69] and the mean curve drawn through the data reported by Schmidt and Tilmann [70] (see Fig. 15). The comparison of all the results is better than expected in view of the fact that the experimental determination of circulation through direct or indirect methods is an extremely difficult and approximate task. In particular, the ultrasonic sound beam technique used by Schmidt and Tilmann yields the vortex strengths only approximately in the stable and unstable region of the vortex street. There are no measurements of the vortex strengths in the formation region. The foregoing does not imply that the particular variation assigned to the circulation loss mechanism (see Fig. 19) is unique. In fact, the only major nondisposable parameter in the entire numerical model is the form assigned to the circulation loss. The need for circulation loss has been amply demonstrated. The form of the particular relationship can only be adjusted with hindsight by comparing all of the predictions of the model with those obtained experimentally. Because of the fact that the differences in measured and calculated circulations are further downstream in the wake, the use of the experimentally suggested p variation does not in any way affect lift, drag, separation angles, $d\Gamma/dt$, and the Strouhal number. This will become more evident in the course of the discussion of the sensitivity of the model. Calculations not reported herein with more exotic forms of p have ascertained the validity of the insignificance of variation of p beyond the stable region.

2. Sensitivity Analysis

This section deals with the effect of the variation of one parameter abouts its value used in the standard run on the remaining major parameters.

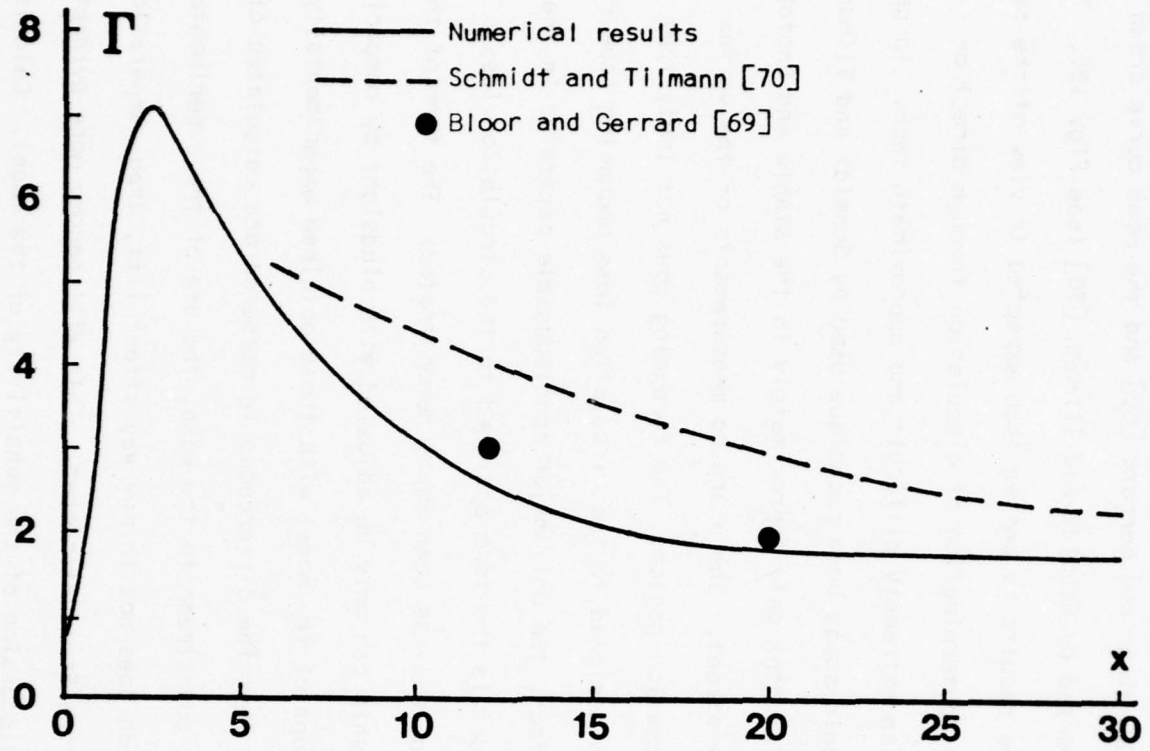

Fig. 38. Vortex strength versus distance [69, 70].

All numerical analyses must use a finite mesh size or time interval. The magnitude of these quantities might affect the results in various ways. In the DVM a large Δt might bring in curvature effects particularly in flow regions where the radius of curvature of the spiral is small. This effect is brought about by the convection of the vortices along straight lines coincident with their instantaneous velocities. Thus Δt should be kept reasonably small to allow the vortices to follow their natural paths. A very small Δt, on the other hand, requires prohibitively large computation times and defeats the purpose of the numerical experiments.

The standard run was made with $\Delta t = 0.125$. Additional runs were made varying Δt from 0.1 to 0.2. The resulting drag and lift coefficients are presented in Figs. 39 and 40. The differences in the two coefficients for all values are negligibly small and certainly within the range of accuracy expected from numerical calculations. Other parameters such as separation and stagnation angles, circulation loss, Strouhal number, etc. remain essentially identical to their corresponding values obtained with $\Delta t = 0.125$.

The role played by the loss of circulation in both laboratory and numerical experiments has already been discussed. Here attention is devoted to the selection of the particular value of p and the effect of its variation on the remainder of the predictions. Several hundred hours of calculations have shown that one can arrive at an approximate value of p by comparing the predicted and measured values of the vortex strengths and the lift and drag coefficients. None of these parameters, however, exhibit the same degree of variation with p at corresponding times and downstream distances. For example, the comparison of the vortex strengths in the stable region, where most of the measurements are made, is not very meaningful

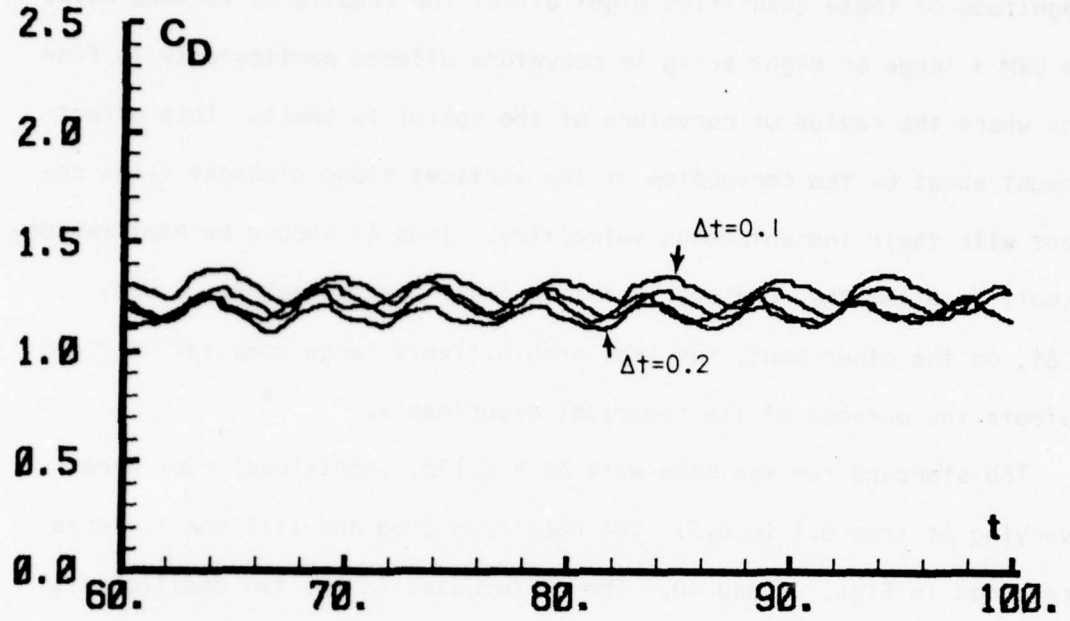

Fig. 39. Drag coefficient versus time for Δt=0.1, 0.125, 0.15 and 0.2.

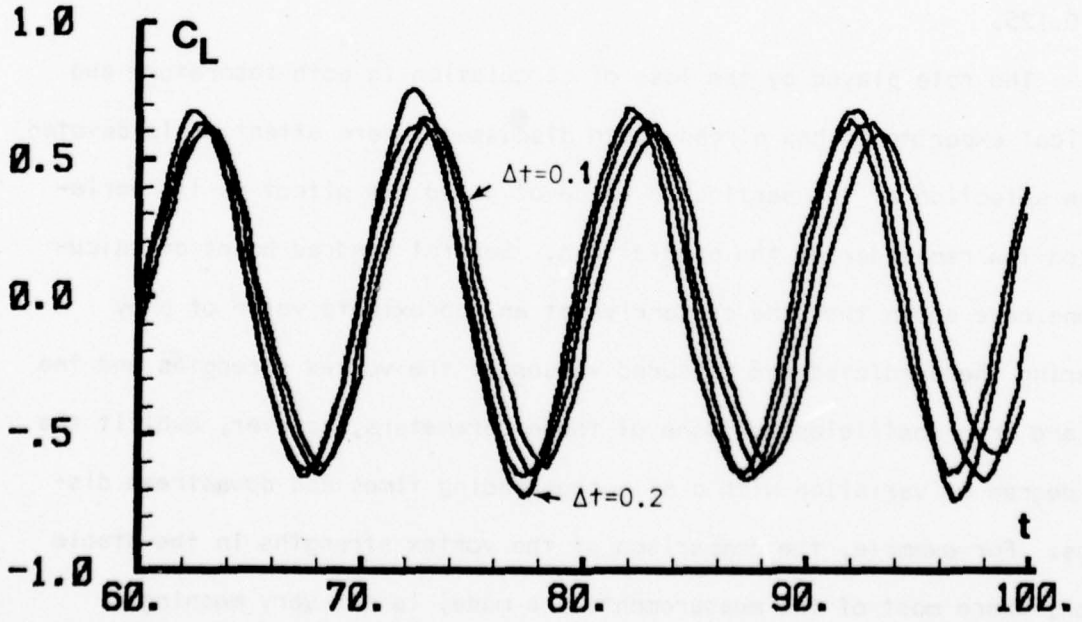

Fig. 40. Lift coefficient versus time for Δt=0.1, 0.125, 0.15 and 0.2.

since the effect of such vortices on the lift and drag coefficients is very small. Thus, it was decided to choose the p value such that the terminal value of the drag coefficient conforms to that measured in the subcritical region. No other experimental data was used in the analysis. Numerical experiments with various values of p have shown that p = 1.0 yields $\bar{C}_D \simeq$ 1.2. Having determined a value of p, it is necessary to examine its variation on all of the predictions of the model.

The drag coefficients obtained with p = 0, p = 0.5, p = 1, and p = 2 are shown in Fig. 41. The insert in Fig. 41 shows the variation of $\bar{C}_D$ with p in the asymptotic range of C_D. Evidently a 100 percent change in p about p = 1 caused only about 10 percent change in C_D. Consequently, the tuning of the model through the use of C_D = 1.2 is not as critical as it may have appeared at first sight. Figure 41 also shows that a circulation loss mechanism is necessary (see curve for p = 0) if the numerical model is to yield results in conformity with the experiments. As noted earlier, the need for circulation loss is also evidenced by the vortex-strength measurements (see Fig. 38). Thus, the important question in the evolution of the model is not whether there should be a circulation loss but rather what should the mechanism and magnitude of this loss be.

The variation of the lift coefficient with p is shown in Fig. 42. It is immediately apparent that the lift coefficient is far more sensitive to p than C_D. Regardless of its sensitivity, however, C_L remains well within the experimentally reported values. One could fine-tune the value of p by matching the measured and calculated values of C_L. Unfortunately, this is not possible since there are no reliable C_L values, particularly in the region of high subcritical Reynolds numbers. Consequently, no attempt is made to slightly increase or decrease p from p = 1 to obtain a specific

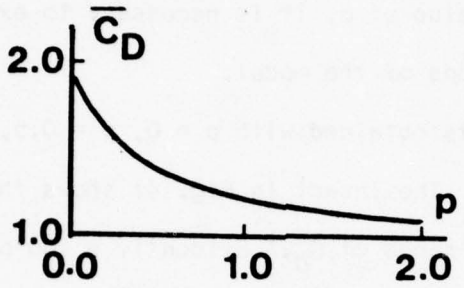

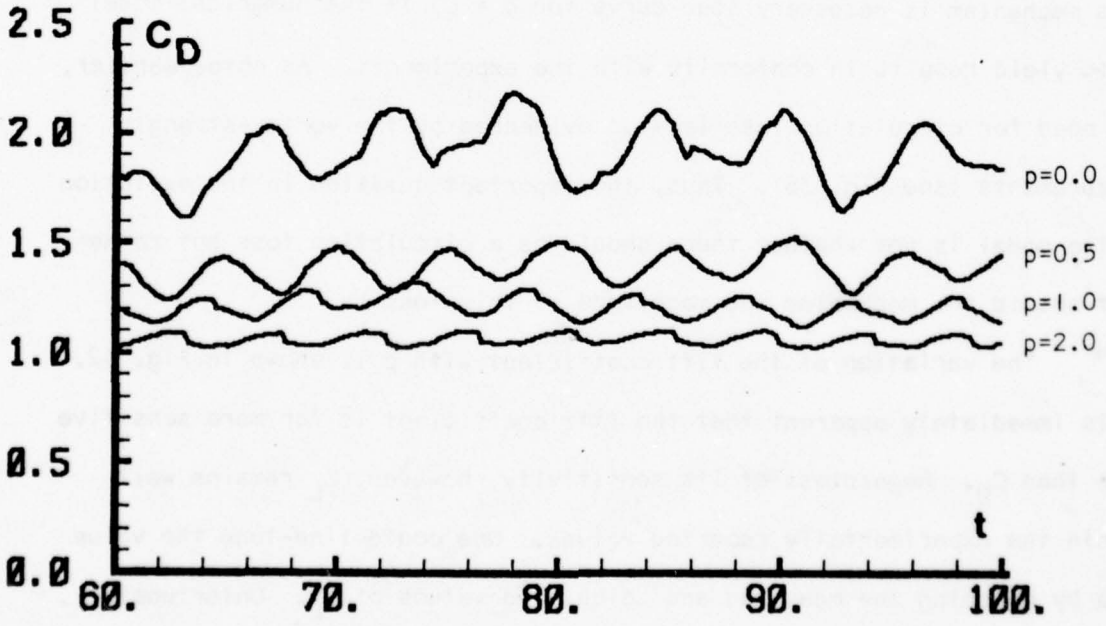

Fig. 41. Drag coefficient versus time for p=0.0, 0.5, 1.0 and 2.0.

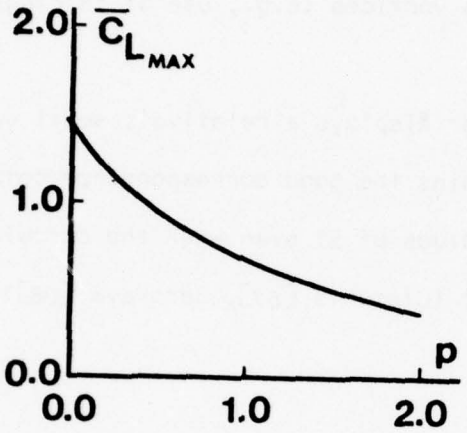

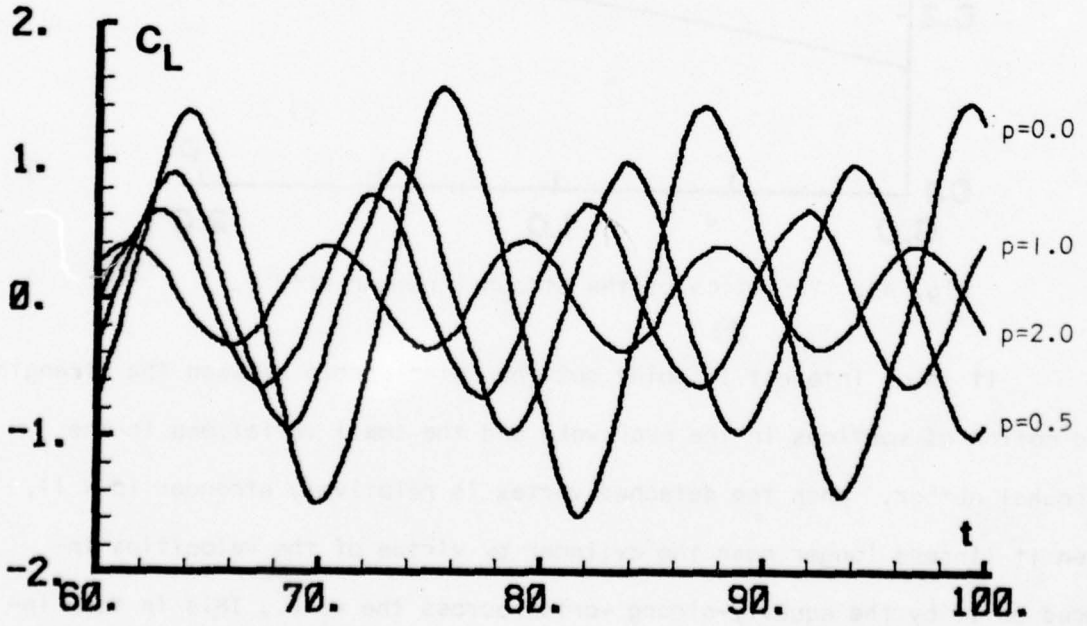

Fig. 42. Lift coefficient versus time for p=0.0, 0.5, 1.0 and 2.0.

C_L value. The importance of Fig. 42, rather, lies in the fact that the numerical model clearly shows the sensitivity of C_L to circulation loss and offers an indirect explanation of the difficulties encountered in the laboratory experiments. The findings of the model can also be taken as a means of reducing the transverse force by artificially increasing the circulation dissipation in vortices (e.g., use of fairings, wire screens, etc.).

The Strouhal number displays a relatively small variation with p (see Fig. 43). This explains the good correspondence obtained between measured and calculated values of St even when the circulation reduction does not exceed 15 percent (Clements [67], Sarpkaya [68]).

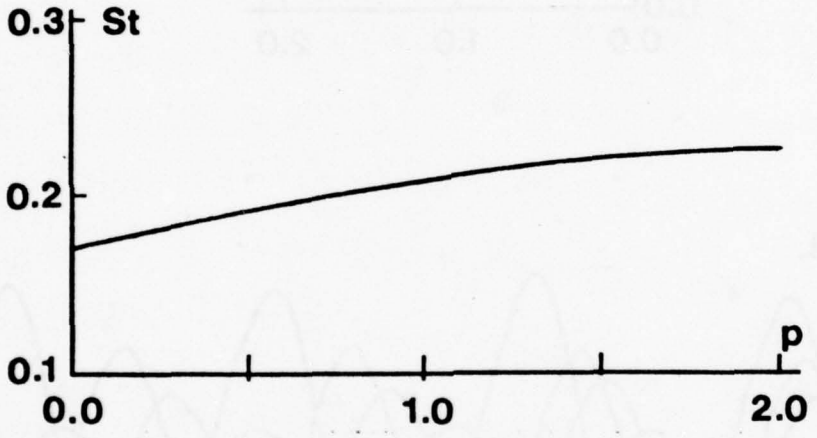

Fig. 43. Variation of the Strouhal number with p.

It is of interest to point out the relationship between the strength and motion of vortices in the near wake and the small variations in the Strouhal number. When the detached vortex is relatively stronger ($p < 1$), then it lingers longer near the cylinder by virtue of the velocities induced on it by the equally-strong vortex across the wake. This in turn increases the period of vortex shedding or decreases the Strouhal number. For weaker vortices ($p > 1$) the inverse is true.

dissipation based on turbulent diffusion and that diffusion could be quantified only by additional measurements which will complement the numerical experiments. As is often the case in many aspects of fluid mechanics, the question seems to have been reduced once again to the understanding of the physics of turbulence.

V. SUMMARY OF THE RESULTS

The numerical model based on the rediscretization of vortex sheets and the mutual interaction between the boundary layers and the wake yielded numerous results which may be summarized as follows:

1. A discrete vortex model of flow past a stationary cylinder may be formulated with only one nondisposable parameter. Experiments and the numerical results show the necessity of circulation reduction but not necessarily the exact mechanism by which it is accomplished.

2. Based on a postulated circulation reduction mechanism, all predictions of the model are in conformity with those obtained experimentally. The fact that all and not only a few of the parameters agree with the experimental measurements adds further credibility to the assumptions made and to the power of prediction of the model.

3. A concerted effort is made to establish a balance between simplicity and accuracy. To this end, simple linear relationships have been preferred in lieu of more complex ones.

4. One of the most important aspects of the numerical model is its flexibility. Practically all parameters have a wide stable range and allow the user to perform numerical experiments to seek a physical understanding of the intricate relationships between two or more parameters.

5. The demonstration of the applicability of the discrete vortex model to the analysis of flow about a bluff body with mobile separation points shows that similar models can be constructed with ease for bodies with fixed separation points. This allows one to study such problems as vortex shedding from ship bilge keels, stall over aircraft, fuel slushing in large

containers, etc., in naval hydrodynamics and aeronautics.

6. The model, as it stands, can be used in the analysis of a great many flow-structure interaction problems. Of particular interest is the analysis of a circular cylinder undergoing forced or self-excited transverse oscillations. Clearly, the numerical experiments with oscillating cylinders can not only shed additional light on the mechanisms which bring about such oscillations but also increase the universality of the model.

VI. APPLICATION OF THE DISCRETE VORTEX MODEL TO SELF-EXCITED TRANSVERSE OSCILLATIONS

A. INTRODUCTION

Numerous experiments have shown that (see Parkinson [75] for an extensive review) when the natural frequency of a bluff body is close to the vortex-shedding frequency, the body may undergo self-excited transverse oscillations. The primary consequences of these oscillations are as follows: (i) The vortex shedding frequency locks on to the natural frequency of the body. (ii) The amplitudes of oscillation and the transverse force increase rapidly up to the point of perfect synchronization where the maximum amplitude is attained. Subsequently, the oscillations decrease either rapidly or abruptly. The abrupt drop in amplitude is a consequence of hysteresis. The reasons leading to the hysteresis are not yet known. (iii) The transverse force leads the displacement by a phase angle which increases gradually at first to about 50 degrees and then rapidly to about 130 degrees. (iv) At the end of the synchronization region, the vortex shedding frequency jumps to that governed by the Strouhal relationship.

The studies concerned with the understanding and prediction of the synchronization phenomenon may be classified in three categories. The first and most extensive category has been the experimental observations and measurements with forced or self-excited oscillations of circular cylinders, cables, and a small group of other bluff bodies. The second category of investigations dealt primarily with the analysis of the structural aspects of the equations governing the vibrations by making

ad hoc assumptions about driving fluid forces. Finally, the third category concentrated on the understanding of the flow field and the nature of the fluid forces. It has not yet been possible to understand the coupled structural and fluid mechanical mechanisms to explain the reasons leading to the self-excited oscillations.

Mathematical models based on the assumption of a nonlinear oscillator have been developed. Among those, the most noteworthy is that proposed by Hartlen and Currie [76]. Their model predicts some of the observed features of the vortex-induced oscillations. However, the model requires a number of nondisposable parameters and gives no clues about the cause and effect relationships. It has been realized, as suggested by Parkinson [75] among others, that if any understanding of the phenomenon is to be achieved, theoretical developments and numerical experiments must be compared with laboratory experiments to guide and complement each other. It is with this suggestion in mind that the discrete vortex model has been applied to the prediction of the characteristics of self-excited oscillations of a circular cylinder. In the following, first the description of the mathematical foundations of the problem, then the specific details of the numerical procedure, and finally the discussion of the results and a summary are presented.

B. FORMULATION OF THE PROBLEM

The equation of motion for an elastically-mounted and linearly-damped cylinder of unit length (see Fig. 44) may be written in dimensional form as

$$m\ddot{y} + 2m\,\omega_n\,\zeta\dot{y} + m\,\omega_n{}^2\,y = \rho_f\,U^2 c\,C_L \qquad (42)$$

where m represents the mass of the cylinder; y, the displacement; ω_n, the natural circular frequency; ζ, the damping ratio; ρ_f, the fluid density; c, the radius of the cylinder; and C_L, the instantaneous value of the lift coefficient. In Eq. (42), $\dot{y}$ and $\ddot{y}$ represent respectively the first and the second derivatives of y with respect to time.

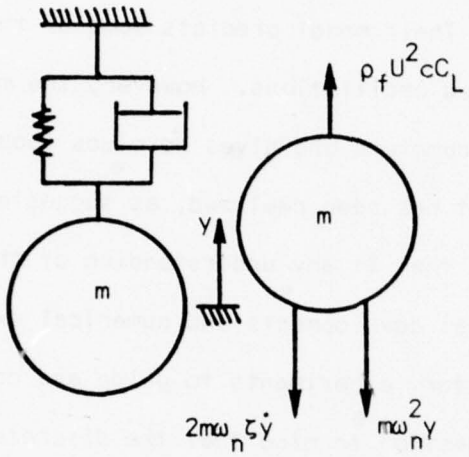

Fig. 44. Elastically-mounted, linearly-damped cylinder.

Defining f_{v_o} as the vortex shedding frequency for the stationary cylinder, S_o as the corresponding Strouhal number, and

$$\eta = y/c\ ,\quad \dot{\eta} = \frac{d(y/c)}{d(Ut/c)}\ ,\quad \ddot{\eta} = \frac{d^2(y/c)}{d(Ut/c)^2}\ ,$$
$$\omega_o = \frac{\omega_{v_o}}{\omega_n} = \frac{f_{v_o}}{f_n}\ ,\quad a_o = \frac{\rho_f c^2}{2\pi^2 m\, S_o^{\,2}}\ ,\quad S_o = \frac{f_{v_o} D}{U} \tag{43}$$

Eq. (42) may be written in normalized form as

$$\ddot{\eta} + \frac{2\pi\zeta S_o}{\omega_o}\dot{\eta} + \left(\frac{\pi S_o}{\omega_o}\right)^2 \eta = 2\pi^2 S_o^{\,2} a_o C_L \tag{44}$$

Because of the need to distinguish the stationary and oscillating vortex shedding frequencies, and hence the Strouhal numbers, the previously and commonly used notation of St for the Strouhal number is modified as denoted above.

The evaluation of Eq. (44) requires the instantaneous value of the lift coefficient. In the present model it is evaluated through the use of the complex velocity potential modified to take into account the motion of the cylinder. Thus, one has

$$w(z) = -\left[(z-z_o)+\frac{1-\dot{z}_o}{z-z_o}\right]+\frac{i}{2\pi}\sum_{n=1}^{N}\Gamma_n\left\{\ell n(z-z_n)-\ell n\left[(z-z_o)-\frac{1}{\overline{z_n-z_o}}\right]\right\} \qquad (45)$$

in which z_o denotes the instantaneous position of the center of the cylinder and $\dot{z}_o$, its velocity (see Fig. 45). The use of Eq. (45) together with the generalized Blasius theorem yields

$$C_D+iC_L = i\sum_{n=1}^{N}\Gamma_n\left[(\dot{z}_n-\dot{z}_o)-\overline{\left(\frac{1}{z_n-z_o}\right)}\cdot\right]-i\dot{z}_o\sum_{n=1}^{N}\Gamma_n-\pi\ddot{z}_o \qquad (46)$$

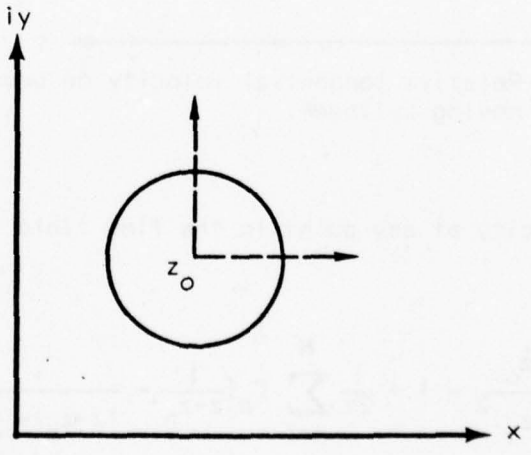

Fig. 45. Coordinate system for oscillating cylinder.

A comparison of Eqs. (46) and (15) shows that z_n is replaced by the relative position $z_n - z_o$ in the latter equation and two new terms are added which account for the forces arising from the velocity and acceleration of the cylinder.

The calculations for the boundary layer and the separation points require the evaluation of the tangential velocities relative to the cylinder. At an arbitrary time t and angle θ (measured as shown in Fig. 46), the tangential velocity is given by

$$u_t = \mathrm{Re}\ \{[q(z_o + e^{i\theta}) - \dot{z}_o]\ e^{-i(\theta-\pi/2)}\} \tag{47}$$

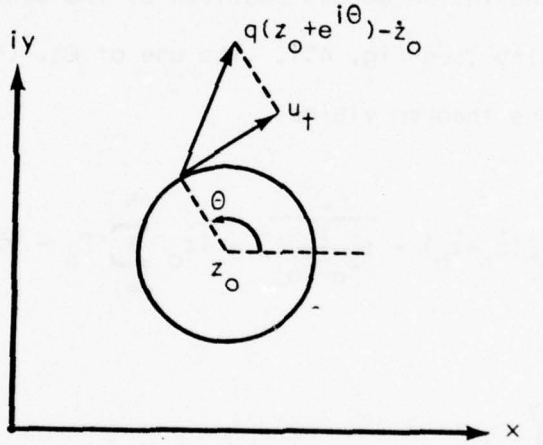

Fig. 46. Relative tangential velocity on boundary of moving cylinder.

As before, the velocity at any point in the flow field is given by

$$-u+iv = \frac{dw}{dz} = \frac{1-\dot{z}_o}{(z-z_o)^2} - 1 + \frac{i}{2\pi}\sum_{n=1}^{N} \Gamma_n \left\{\frac{1}{z-z_n} - \frac{1}{(z-z_o)-\dfrac{1}{\overline{z-z_o}}}\right\} \tag{48}$$

C. NUMERICAL PROCEDURE

It is apparent from the formulation of the problem that the solution of Eq. (44) requires two parameters (ζ and a_o) characterizing the mechanical system and the instantaneous fluid force imparted to the cylinder. The parameter a_o, known as the mass parameter, may be readily calculated for a given cylinder of mass m, radius c, and fluid density ρ_f [see Eq. (43)]. The damping ratio, ζ, is a measure of the relative energy loss within the material due to molecular motion and does not include the so called fluid damping. All fluid forces acting on the cylinder are included in the proper specification of C_L which represents the integrated effect of the surface-pressure loading by the fluid on the vibrating cylinder.

The discrete vortex model developed for the stationary cylinder is used together with Eqs. (46) and (48) to determine the fluid forces acting on the cylinder. Equation (44) is integrated through the use of a fourth order Runge-Kutta method. Otherwise, no additional modifications are introduced into the procedures described in the previous chapter. In fact, the only specification made was the time at which the cylinder was allowed to respond to the fluid forces. Such a decision was necessary to avoid the coupling of two transient states resulting from the impulsive start of the flow and the transient response of the cylinder. This would have made the calculations unnecessarily complex. Instead, it was decided first to establish a flow with a sufficient number of vortices in the wake (e.g., by regarding the cylinder as stationary for $t < 10$) and thereby studying the response of the cylinder through a more or less steady uniform flow. The approximations signified by "more or less" are due to the fact in all numerical calculations the vortex street is finite. In the present calculations, the cylinder is allowed to respond after $t > 10$, which was sufficiently large for all intents and purposes.

Mathematically speaking, there are no particular restrictions on the selection of the numerical values of ζ and a_o other than the fact that they should be physically realizable. From the point of view of actual calculation, however, one must place some restrictions on ζ and a_o to limit the computation time. The smaller the value of ζ, the larger the amplitude of oscillation. The larger the mass of the cylinder or the smaller the parameter a_o (keeping everything else constant), the larger is the transient time during which the cylinder oscillations asymptotically approach their final values. Consequently, a very small value of ζ coupled with a relatively small value of a_o would require many cycles of oscillation before the cylinder reaches its final amplitude. This makes the computation prohibitively expensive and time consuming. The foregoing arguments constituted one of the primary conditions in the selection of ζ and a_o. The second and probably more important reason from a scientific point of view was the focusing of attention on the understanding of the physics of the phenomenon rather than on the solution of specific problems. With the foregoing considerations in mind, the ζ and a_o values shown in Table II were used in the calculations. The role of the new parameter $S_G = \zeta/a_o$ appearing in the table is discussed later.

TABLE II

SET	ζ	a_o	S_G
I	0.02	0.0125	1.6
II	0.04	0.0250	1.6
III	0.08	0.0500	1.6
IV	0.04	0.0125	3.2

D. DISCUSSION OF RESULTS

1. Introduction

The major part of the discussion of the results deals with the phenomenological predictions of the model and their comparison with those observed or measured experimentally. For this purpose only one set of damping ratio and mass parameter is considered. The variations of the lift coefficient, relative amplitude, phase angle between the lift force and the cylinder response, and finally the ratio of the cylinder-oscillation frequency to natural frequency is presented as a function of U_r defined by

$$U_r = \frac{\omega_o}{2\pi S_o} \tag{49}$$

In dimensional terms, $U_r = U/\omega_n D$. The reasons for the choice of this particular parameter are twofold. Firstly, it is commonly referred to in the previous works [75]. Secondly, it is a measure of the velocity of flow past a cylinder of given diameter and natural frequency.

Figure (47) shows the results obtained by Feng [77] with a lightly damped circular cylinder. As noted earlier, when the vortex shedding frequency, f_{v_o}, for a stationary cylinder approaches the natural frequency [$U_r \simeq 0.8$ in Fig. (47)], the vortex shedding frequency becomes nearly identical to the natural frequency of the cylinder. Furthermore, the frequency of oscillation of the cylinder, ω_c, nearly coincides with its natural frequency. As U_r increases towards 1.0, the amplitude of both the oscillation and the transverse force increases rapidly while ω/ω_n and ω_c/ω_n remain nearly constant at a value slightly under unity. As U_r increases further, both amplitudes drop either gradually or abruptly as illustrated in Fig. (47). The abrupt drop is a consequence of hysteresis

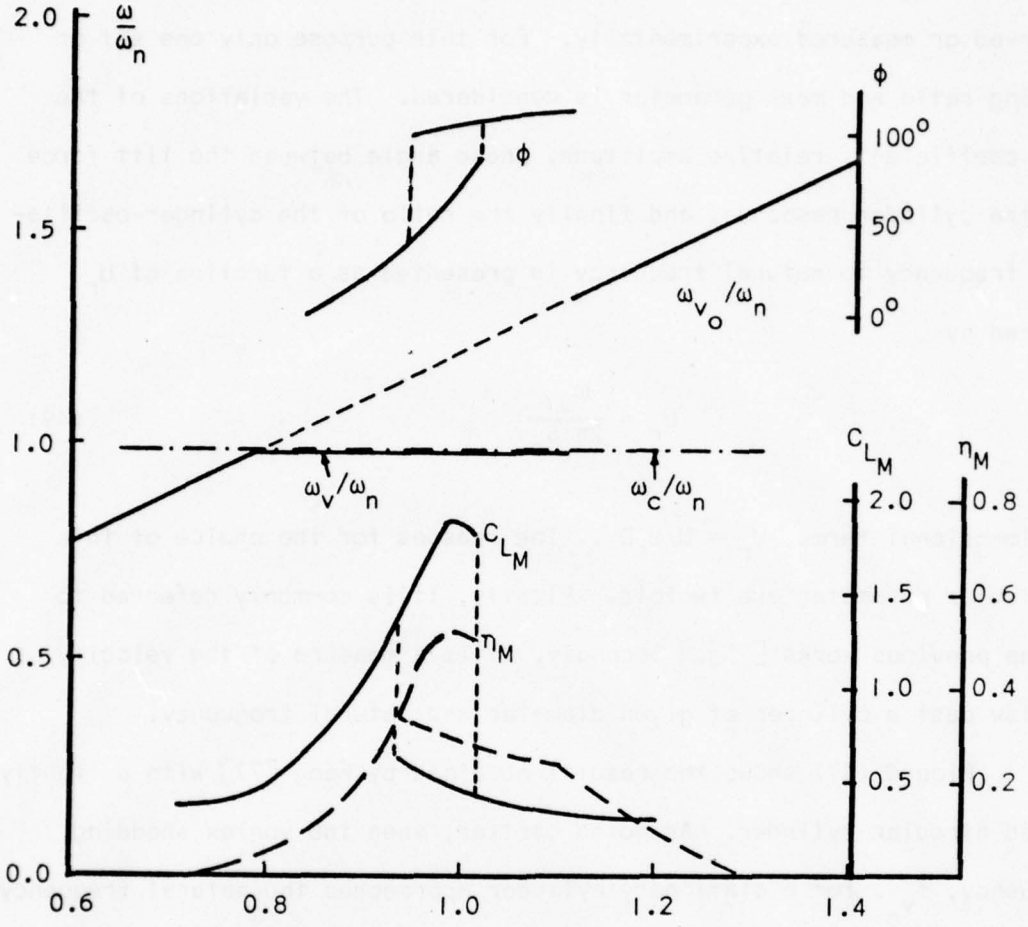

Fig. 47. Experimental results for self-excited transverse oscillations of a cylinder [77].

noted earlier. For $U_r \gtrsim 1.1$ the frequency of vortex shedding, ω_v, jumps to its stationary-cylinder value, i.e., $\omega_v = \omega_{v_o}$. However, the cylinder continues to oscillate at the natural frequency of the cylinder with very small amplitudes. One can, therefore, identify two major regions in the relationship between ω_v, ω_c, and ω_n. For U_r smaller than about 0.8, $\omega_v = \omega_{v_o}$ and $\omega_c \simeq \omega_n$. In the range $0.8 \lesssim U_r \lesssim 1.1$, $\omega_v < \omega_{v_o}$ and $\omega_v \simeq \omega_c \simeq \omega_n$. For $1.1 \lesssim U_r \lesssim 1.3$, $\omega_v = \omega_{v_o}$ and $\omega_c \simeq \omega_n$.

The phase angle between the exciting force and the cylinder response undergoes dramatic changes in the region where $0.8 \lesssim U_r \lesssim 1.1$. The reasons leading to the amplification of the oscillations of the cylinder and the lift force, and the rapid increase of the phase angle from about 20 degrees to 100 degrees have not been understood because of the difficulty of measuring or observing the detailed kinematics of the flow field about the cylinder. Many experiments have essentially confirmed the general features of the results obtained by Feng [77]. Most of the attention has been devoted to the understanding of the locking-on of the vortex shedding frequency to the natural frequency of the cylinder in the range of U_r values $0.8 \lesssim U_r \lesssim 1.1$. In conformity with the previous literature, this region is variously referred to as the synchronization region, locking-on region, capture region, or simply as the resonant region.

The numerical results obtained with $\zeta = 0.02$ and $a_o = 0.0125$ are shown in Fig. (48), again as a function of U_r. It is immediately apparent that the results shown in this figure follow essentially the same trends as those in Fig. (47). Also shown in Fig. (48) are the corresponding values of ω_o and ratios ω_o/ω_o^* or U_r/U_r^* where ω_o^* and U_r^* are the values of ω_o and U_r when η_M reaches its maximum value (point A). This point is referred to as the point of perfect synchronization.

2. Mechanism of Synchronization

Previous investigators [75] have uncovered a number of relatively unrelated facts regarding the kinematic and dynamic behavior of flow about a transversely-oscillating cylinder. The most notable of the observations and measurements may be summarized as follows:

(i) Oscillations increase the spanwise correlation;

(ii) The strength of the vortices increases;

(iii) The mean base pressure decreases and the mean drag coefficient increases;

(iv) Transverse force is amplified relative to its stationary-cylinder value;

(v) The phase angle between lift and cylinder motion increases with U_r;

(vi) The velocity range over which synchronization occurs increases with oscillation amplitude;

(vii) Separation point excursion increases with oscillation;

(viii) Lateral spacing of the vortices decreases with increasing amplitude and is unaffected by changes in frequency of oscillation;

(ix) Wake-formation length decreases systematically with increasing amplitude of vibration for $U_r < U_r^*$ and increases for $U_r > U_r^*$;

(x) The wake contracts for $U_r < U_r^*$ and expands for $U_r > U_r^*$.

The facts summarized above have been distilled from a number of investigations, not all of which have been conducted at identical Reynolds numbers or under similar experimental conditions. Consequently, there are certain features of the flow which have been observed to increase in one investigation and decrease in another. Whenever such conflicts arose, heavier weight was subjectively attached to the observation more frequently

reported. Perhaps the most interesting feature of all these isolated facts is that it has not yet been possible to establish the cause and effect relationship among them through a phenomonologically and mathematically defensible mechanism. In the following, the mechanism suggested by the numerical experiments is described in detail.

Consider an elastically mounted circular cylinder which is at its lowest displacement during a given cycle. Also assume that the stationary cylinder value of the vortex shedding frequency is slightly greater than the natural frequency of the cylinder. As soon as the cylinder begins to move upwards, the lower attached-vortex sheet lags behind the cylinder because of its inertia. In other words, the wake axis passing through the instantaneous center of the cylinder rotates clockwise (see Fig. (49) for t = 189). In the meantime, the velocity relative to the cylinder rotates clockwise an angle dictated by the velocity of the uniform flow and the instantaneous velocity of the cylinder. The rotation of the velocity vector coupled with the rotation of the wake axis moves the upper separation point further downstream and the lower separation point further upstream relative to that which would have existed on a stationary cylinder. The rate of circulation at the upper separation point increases rapidly and decreases at the lower separation point. This gives rise to a larger circulation per unit time than that for the stationary cylinder for the vortex towards which the cylinder is moving. Furthermore, the vortex spiral which is attached to the upper separation point does not move out of the cylinder's way because of its inertia and consequently comes closer to the approaching cylinder. These two facts, namely the increase of circulation and the decrease of the relative distance between the cylinder and the upper vortex spiral, confirm the observation made by

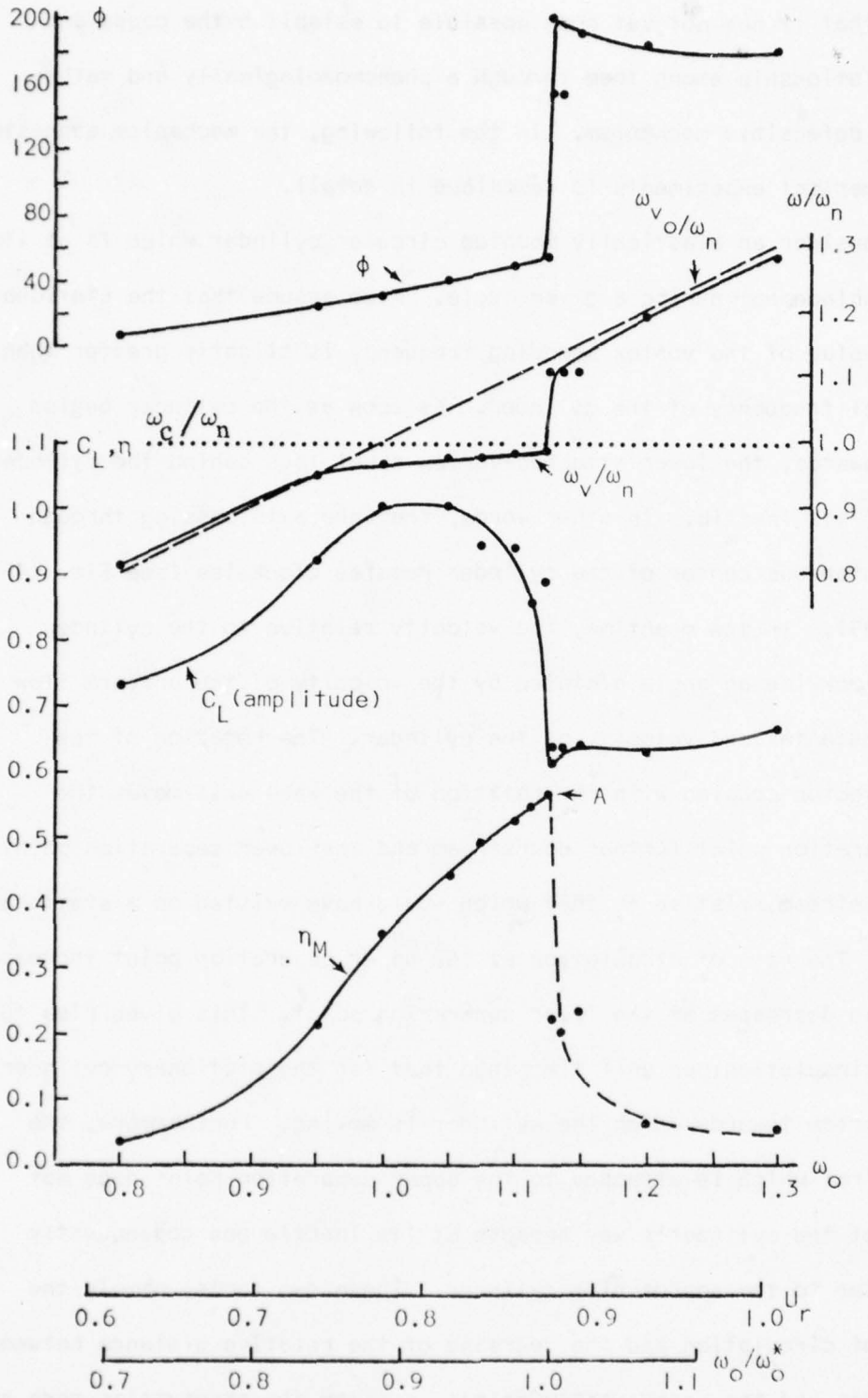

Fig. 48. Numerical results for self-excited transverse oscillations with ζ=0.02 and a_o=0.0125.

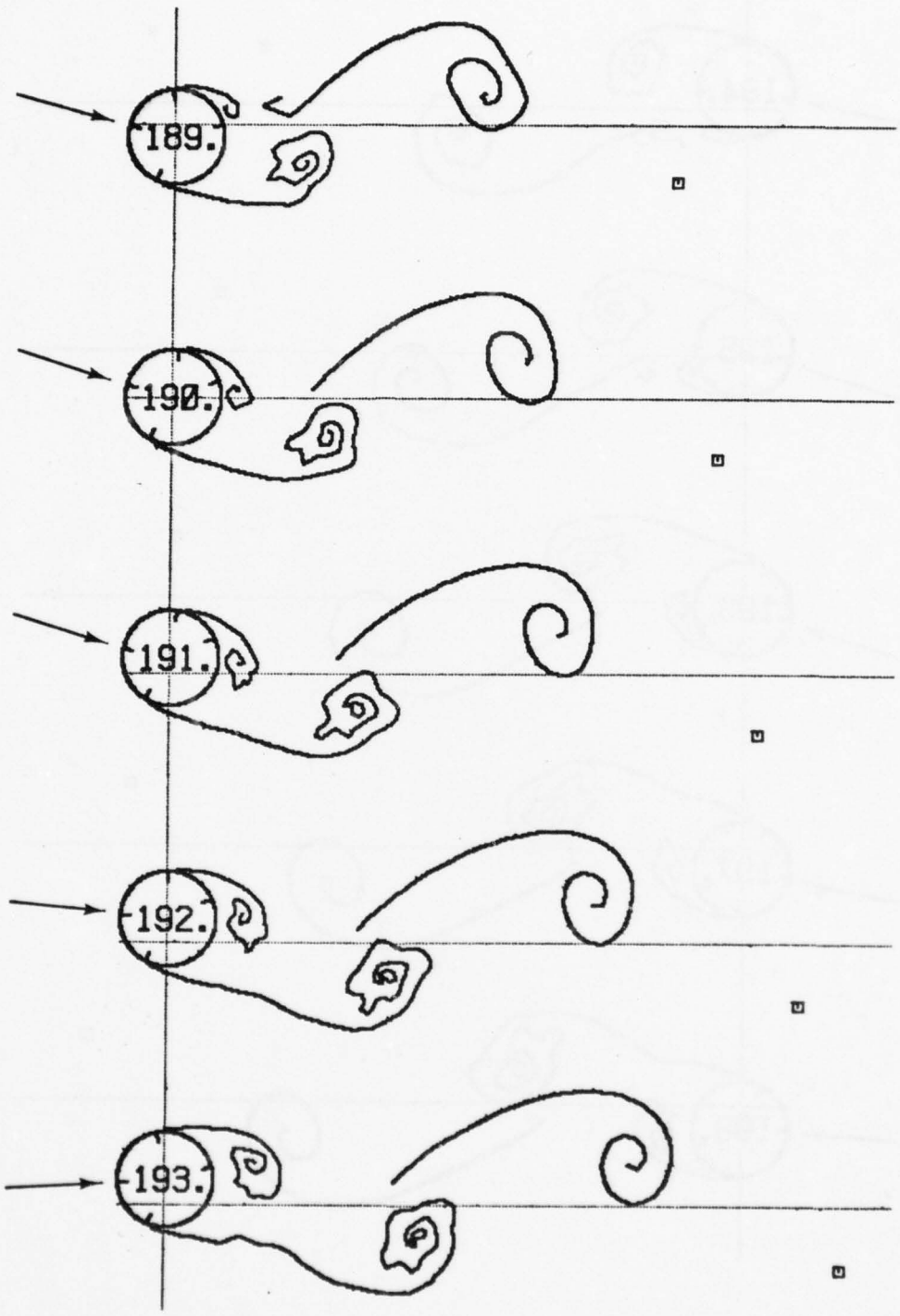

Fig. 49. Wake configuration for self-excited transverse oscillations.

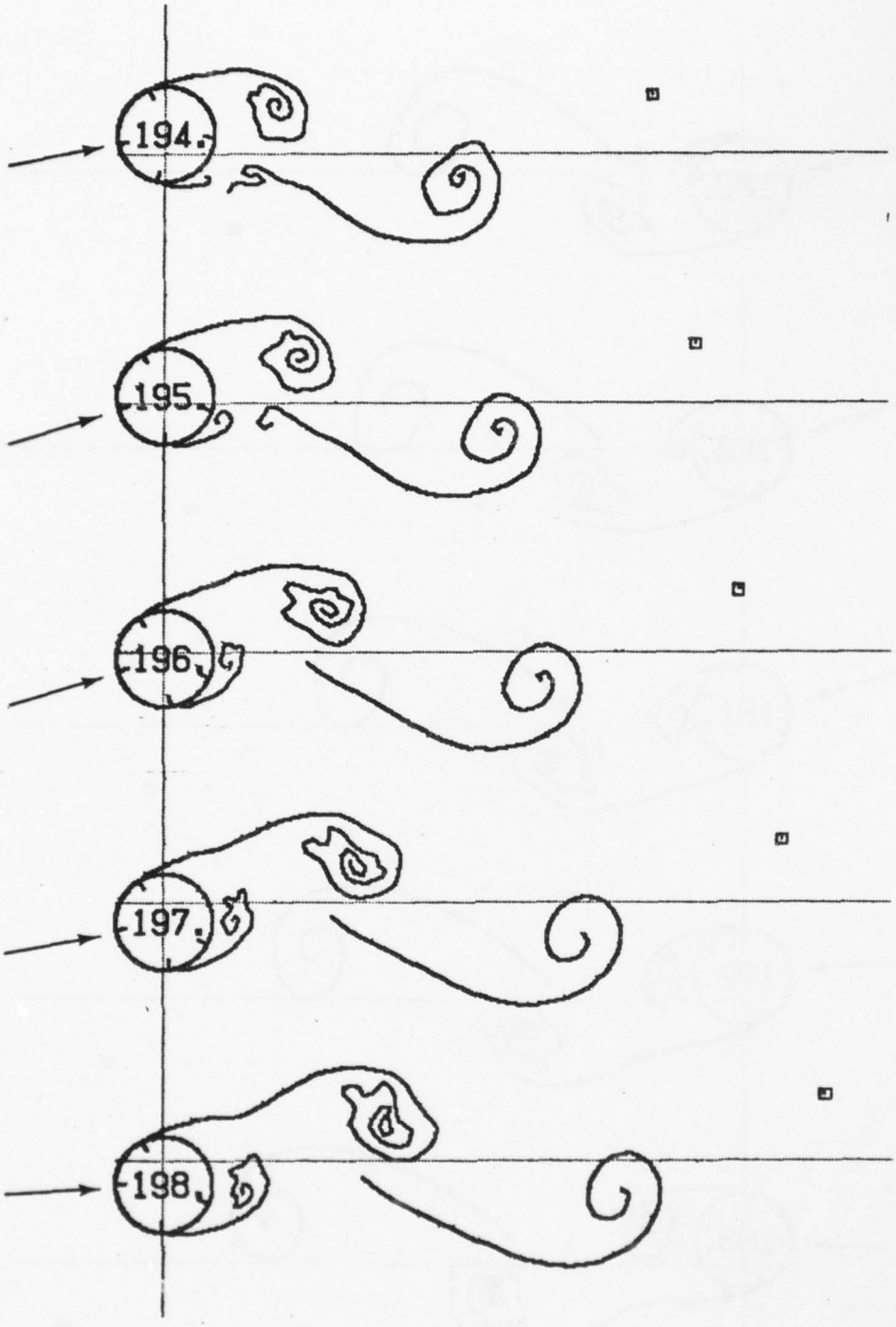

Fig. 49 (con't.). Wake configuration for self-excited transverse oscillations.

Davies [78] that "The growing vortex on vibrating cylinders seems to roll up more quickly and with a strength about 35 percent larger than that for a stationary cylinder." The increase of the vortex strength predicted by the current model will be discussed later. The phenomenon is, however, relatively more involved than the simplified introductory remarks would suggest. There is a third factor which enhances the strengths of the attached vortex sheets. This is directly related to the difference between the period of oscillation of the cylinder, $T_c = 1/f_c \simeq 1/f_n$, and the time required for the shedding of a vortex from a stationary cylinder, i.e., $T_c - T_{v_o}$. Each growing vortex about an oscillating cylinder continues to be fed circulation not only at a higher rate but also for a longer time period. This further reinforces the strength of each growing vortex.

It is now necessary to establish the link between the enhanced vortex strengths and the locking-on of the vortex shedding frequency to the frequency of cylinder oscillation. The results of the stationary cylinder have shown that the larger the strength of the vortices in the near wake the smaller their velocity relative to the cylinder. That is, strong vortices with their equally strong images tend to conserve their moment of circulation. Consequently, the vortices are shed at larger time intervals. This, in turn, leads to smaller Strouhal numbers. The decrease of S, or the increase of T_v, brings T_v closer to T_c. This tendency is reinforced every succeeding cycle until $T_v \cong T_c \simeq T_n$ or until the effects which cause the changes in amplitude, period, lift force, and the phase angle disappear. At such time, a stable periodic state is reached.

The foregoing explanation dealt only with the kinematic aspects of the fluid motion. In the final analysis, it is the balance between

the work done by the fluid on the cylinder and the work done by the dissipative forces (internal friction) which determine the stability of the oscillations. If the net work becomes negative, then the oscillations decay and vice versa. The parameter which establishes the relationship between the friction mechanism and the given state of oscillation is the phase angle between the exciting force and displacement. It is given by [79]

$$\tan \phi = \frac{2\zeta \, \omega/\omega_n}{1-(\omega/\omega_n)^2} \tag{50}$$

As ω/ω_n approaches unity from $\omega/\omega_n < 1$, ϕ increases rapidly, the rate of increase being a strong function of ζ. For a cylinder with very small internal damping, ϕ increases from say 20 degrees to $\phi \simeq 150$ degrees for a very small change in ω/ω_n.

The relationship between the dynamics and the kinematics of the motion for the three states of oscillation and hence the reason for the sustained oscillations in the region of synchronization may be explained as follows. In the case of synchronization (see Fig. 50) the maximum velocity of the cylinder leads the maximum lift and the lift reaches zero at about the time the cylinder reaches its peak amplitude. In other words, the lift force opposes the cylinder motion for a short time period as the amplitude of the cylinder begins to decrease from its maximum displacement. If for any accidental reason the amplitude of the cylinder in one direction were to be increased while the cylinder was undergoing synchronized oscillations, the increased strength of the vortex growing ahead of the cylinder motion increases the period, T_v. This, in turn, decreases the phase angle between the force and the displacement which then <u>increases</u> the phase angle between the force and the velocity.

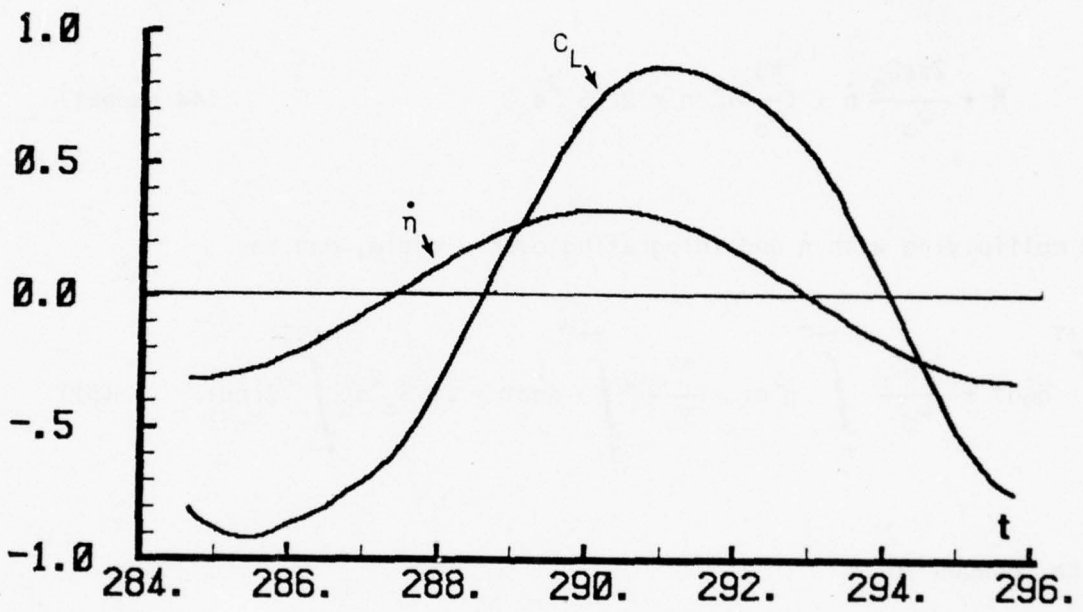

Fig. 50. Lift coefficient and cylinder velocity versus time.

Consequently, the energy transferred from the fluid to the cylinder decreases below that dissipated by the material damping. These sequences of events decrease the amplitude to the level where the energy extracted from the fluid over a cycle is just balanced by that dissipated by internal friction.

The role played by all of the terms of the governing equations of motion and the energy transfer mechanism may be quantified as follows. Re-writing Eq. (44)

$$\ddot{\eta} + \frac{2\pi\zeta S_o}{\omega_o}\dot{\eta} + \left(\frac{\pi S_o}{\omega_o}\right)^2 \eta = 2\pi^2 S_o{}^2 a_o C_L \qquad \text{(44 repeat)}$$

and multiplying with $\dot{\eta}$ and integrating over a cycle, one has

$$\int_t^{t+T} \ddot{\eta}\dot{\eta}dt + \frac{2\pi\zeta S_o}{\omega_o}\int_t^{t+T} \dot{\eta}^2 dt + \left(\frac{\pi S_o}{\omega_o}\right)^2 \int_t^{t+T} \eta\dot{\eta}dt = 2\pi^2 S_o{}^2 a_o \int_t^{t+T} C_L\dot{\eta}dt \qquad (51)$$

which reduces to

$$\frac{2\pi\zeta S_o}{\omega_o}\int_t^{t+T} \dot{\eta}^2 dt = 2\pi^2 S_o{}^2 a_o \int_t^{t+T} C_L\dot{\eta}dt \qquad (52)$$

In the case of a perfect balance between the energy input [right hand side of Eq. (52)] and the energy dissipated (left hand side), the above equality holds true. For an unstable system where the equality does not hold true,

$$E = 2\pi^2 S_o{}^2 a_o \int_t^{t+T} C_L\dot{\eta}dt - \frac{2\pi\zeta S_o}{\omega_o}\int_t^{t+T} \dot{\eta}^2 dt \qquad (53)$$

Thus, E = 0.0 corresponds to steady state with constant amplitude of oscillation; E > 0.0 corresponds to amplification; and finally, E < 0.0 corresponds to damping of oscillations. The variation of η, $\dot{\eta}$, $\ddot{\eta}$ and C_L in Eq. (44) as a function of time is shown in Figs. 51a-c. Figure 51a corresponds to the case where E > 0.0; Fig. 51b to E = 0.0; and Fig. 51c to E < 0.0. Clearly, the phase angle between the lift force and the velocity is smaller for the case of E > 0.0 than for E = 0.0. In fact, one can state that the said phase angle increases from a plus to a minus value. Only in the case of Fig. 51b is the phase angle such that the energy imbalance is for all intents and purposes zero. Furthermore, the stability of the system to small perturbations in amplitude is such that a small increase in amplitude leads to a decrease in phase between lift and displacement and thus to an increase in phase between lift and velocity. This, as noted earlier, leads to a decrease in amplitude. The reverse is true for a slight decrease in amplitude from a steady state oscillation.

3. Parametric Study of Synchronization

Numerical experiments have been performed for the ζ and a_o combinations given in Table II in addition to that already presented. The results for each set are presented in Figs. 52 through 54. All of the parameters shown in these figures display similar variations with ω_o or U_r. Furthermore, they are quite similar, at least in general form, to those experimentally obtained by Feng (see Fig. 47). A closer look at the experimental and calculated values show some differences, part of which may be attributable to the limitations of the numerical model and part to the limitations of the experimentation. In other words, all of the differences to be pointed out are not entirely consequences of the numerical model.

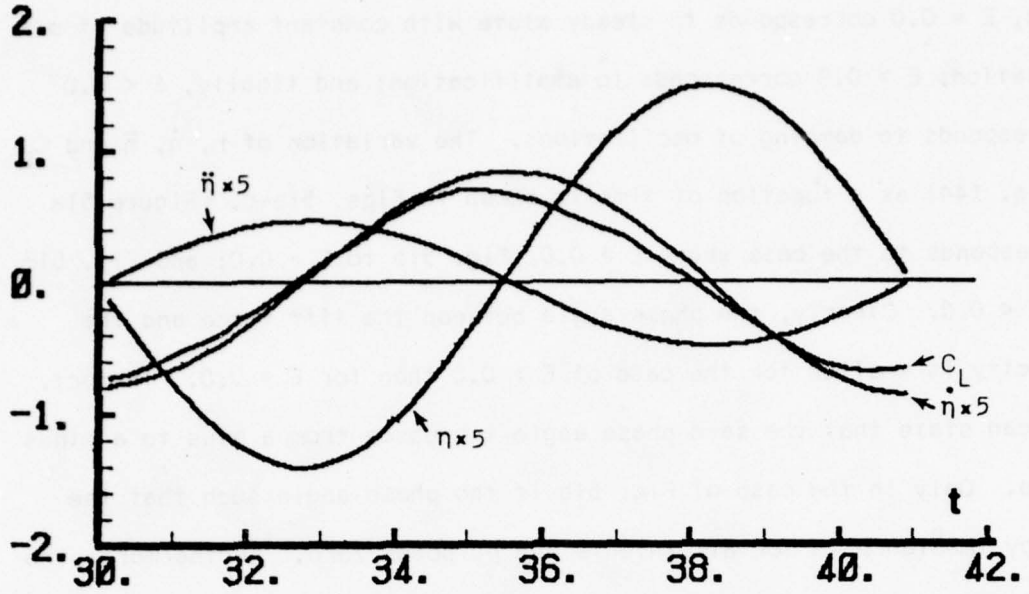

Fig. 51a. Variation of η, $\dot{\eta}$, $\ddot{\eta}$ and C_L versus time for E>0.0.

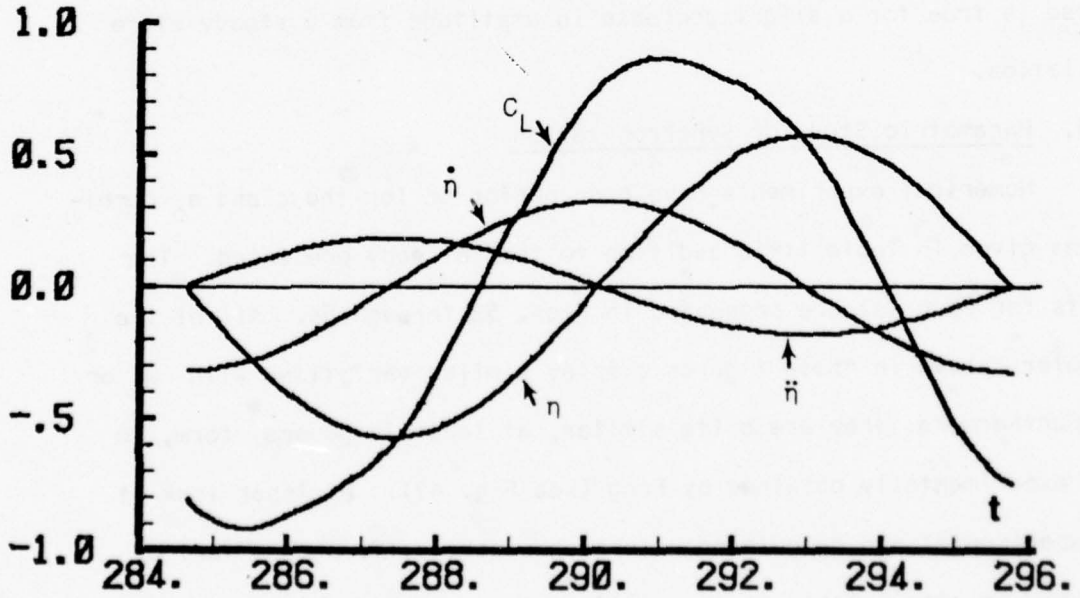

Fig. 51b. Variation of η, $\dot{\eta}$,$\ddot{\eta}$ and C_L versus time for E=0.0.

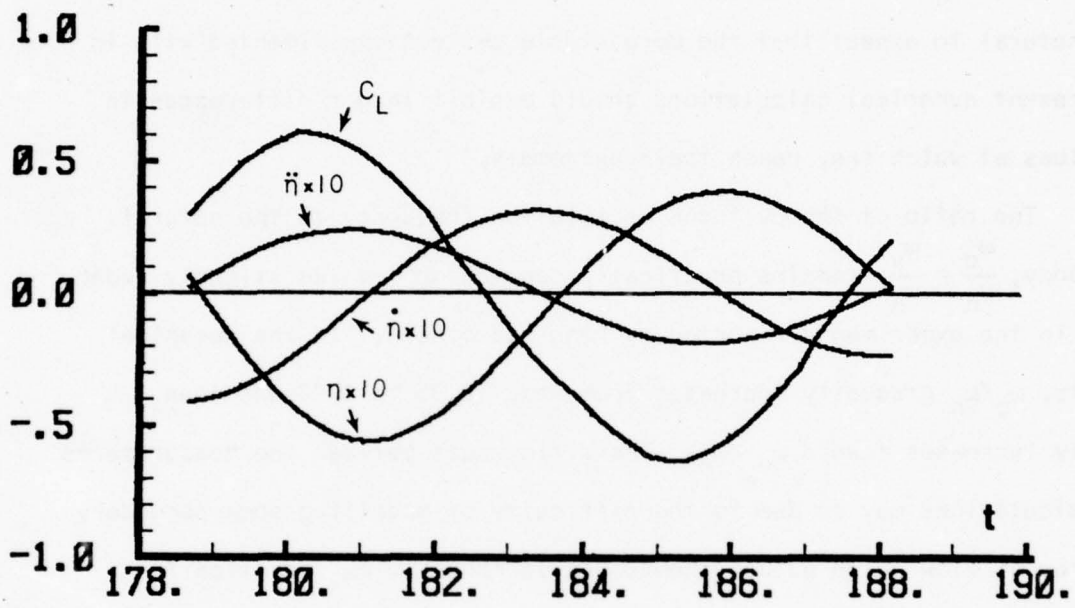

Fig. 51c. Variation of η, $\dot{\eta}$, $\ddot{\eta}$, and C_L versus time for E<0.0.

A comparison of Figs. 47 and 52 shows that the numerical model predicts a peak lift amplitude at a U_r value smaller than U_r^*. In Feng's experiments, the lift and oscillation amplitudes reached their peak at nearly identical U_r values. The reasons for this are not entirely clear. It may be conjectured that it is a consequence of the extremely low damping encountered in Feng's experiments ($\zeta \simeq 0.001$). In fact, mechanical systems with very small damping are much more finely tuned and more precariously balanced than those with larger internal damping. It is therefore natural to expect that the more stable systems experimented with in the present numerical calculations should exhibit larger differences in U_r values at which they reach their extremals.

The ratio of the cylinder oscillation frequency to the natural frequency, $\frac{\omega_c}{\omega_n} \simeq \frac{\omega_v}{\omega_n}$, remains practically constant at a value slightly under unity in the experiments reported by Feng and others. In the numerical results, ω_c/ω_n gradually increases from about 0.95 to 0.99 and then rapidly increases toward ω_{v_o}/ω_n. The differences between the measurements and calculations may be due to the difficulty of modelling some secondary features of flow which adjust themselves to render ω_c/ω_n practically constant.

The amplitudes of the lift coefficient and cylinder response cannot be compared with the experimental data because of the large differences in damping and mass parameters. However, it is interesting to note that the ratio of the maximum lift coefficient for the oscillating cylinders to the lift coefficient for the stationary cylinder (standard run) varies from 1.3 to 1.6 (see Figs. 48 and 52-54). This lift amplification is in conformity with most of the data reported in the literature [75]. The cylinder response shows a dramatic drop for a small change in ω_o or U_r,

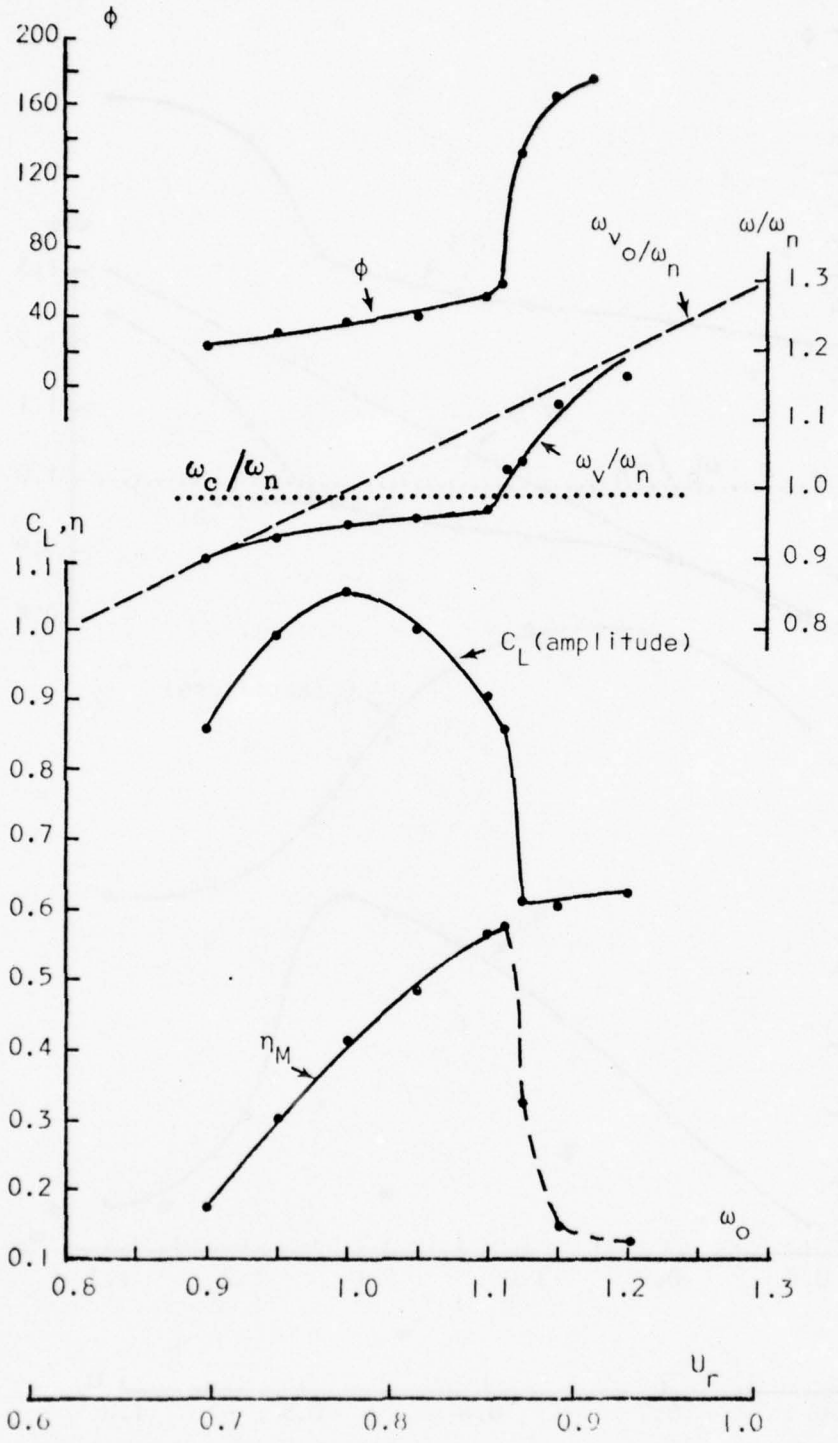

Fig. 52. Numerical results for self-excited transverse oscillations with ζ=0.04 and a_o=0.025.

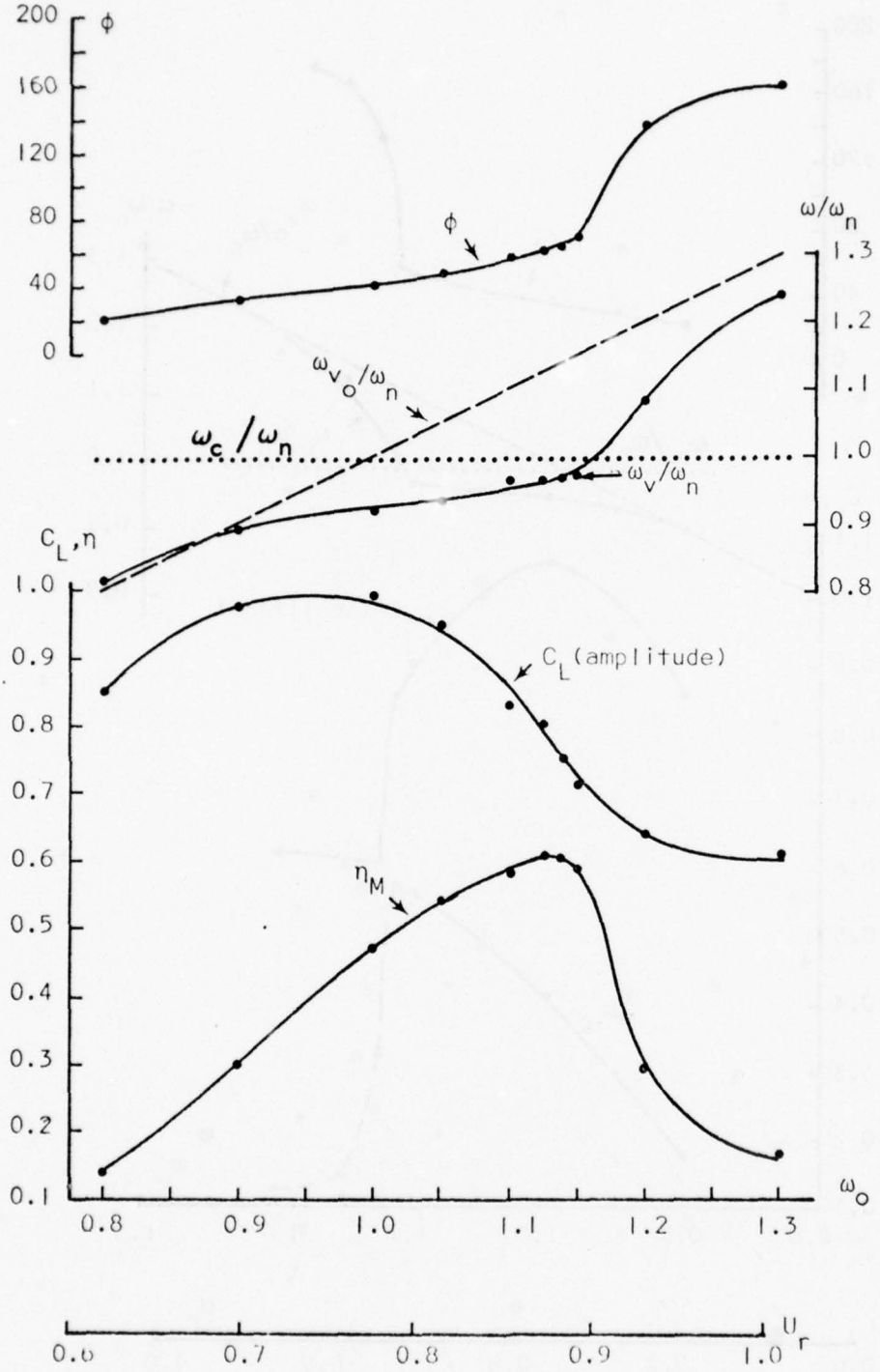

Fig. 53. Numerical results for self-excited transverse oscillations with $\zeta=0.08$ and $a_o=0.05$.

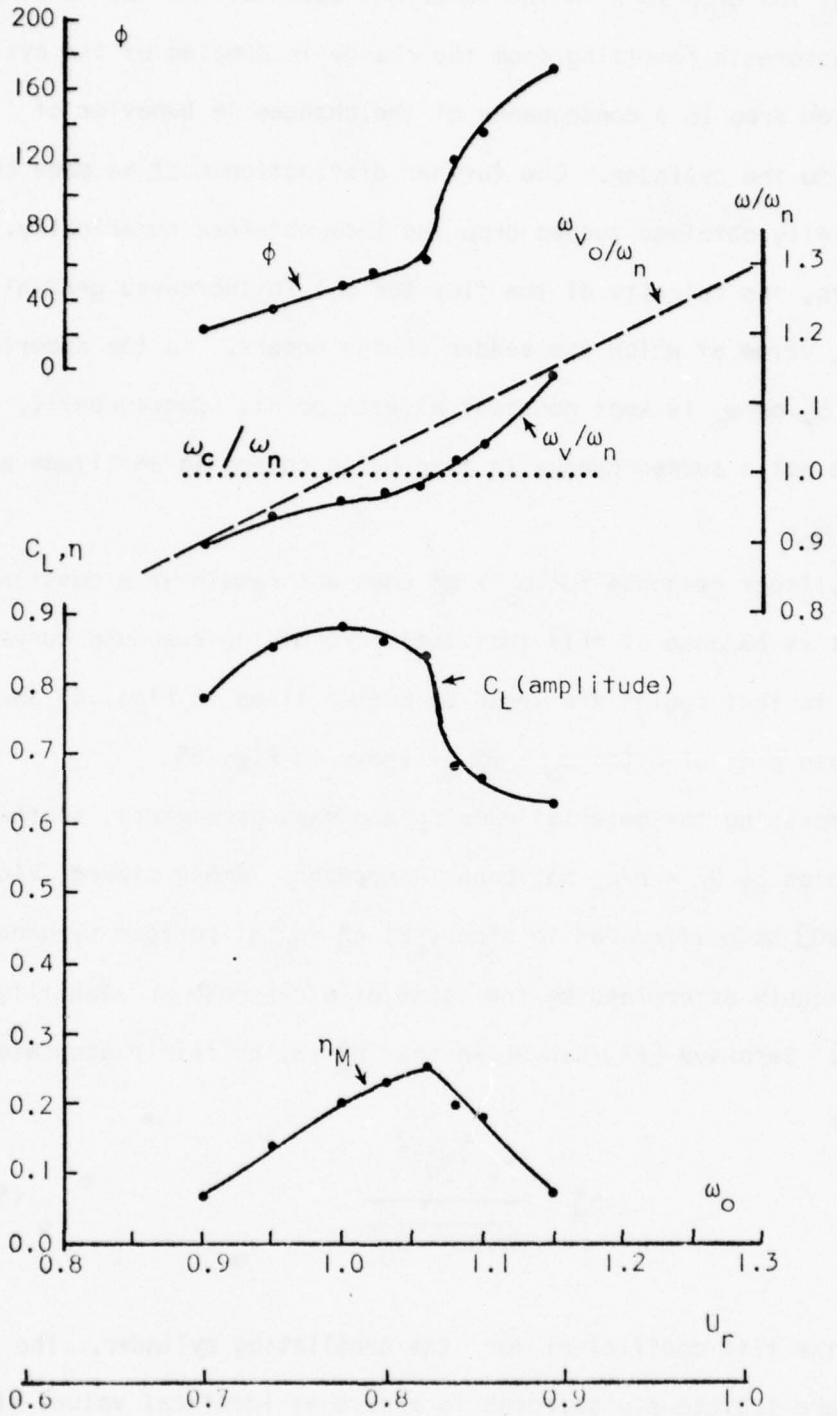

Fig. 54. Numerical results for self-excited transverse oscillations with ζ=0.04 and a_o=0.0125.

reminiscent of the hysteritic drop in Feng's data. It should, however, be emphasized that the drop in η in the numerical calculations has nothing to do with the hysteresis resulting from the change in damping of the cylinder. The sudden drop is a consequence of the changes in behavior of flow external to the cylinder. One further distinction must be made between the experimentally obtained sudden drop and that obtained numerically. In the experiments, the velocity of the flow (or U_r) is increased gradually through the U_r value at which the sudden change occurs. In the numerical calculations, U_r or ω_o is kept constant at each point. Consequently, what is observed is not a sudden change in time but a change in amplitude as a function of ω_o.

The cylinder response for $\omega_o > \omega_o^*$ does not remain at a constant amplitude. It is because of this fact that part of the response curves corresponding to that region are shown by broken lines in Figs. 48 and 52-54. A sample plot of η for $\omega_o > \omega_o^*$ is shown in Fig. 55.

In discussing the material damping and mass parameters, another parameter denoted by $S_G = \zeta/a_o$ has been introduced. Among others, Vickery and Watkins [80] have attempted to show that η_M^* (η_M at perfect synchronization) is uniquely determined by the value of a response or stability parameter, S_G. Sarpkaya [81] has shown that η_M^* may be fairly accurately represented by

$$\eta_M^* = \frac{C_L \, (\omega_o^*)^2}{\sqrt{0.06 + S_G^2}} \tag{54}$$

where C_L is the lift coefficient for the oscillating cylinder. The values of ζ and a_o were judiciously selected to arrive at identical values of S_G for three sets of calculations and twice the S_G value for one set of

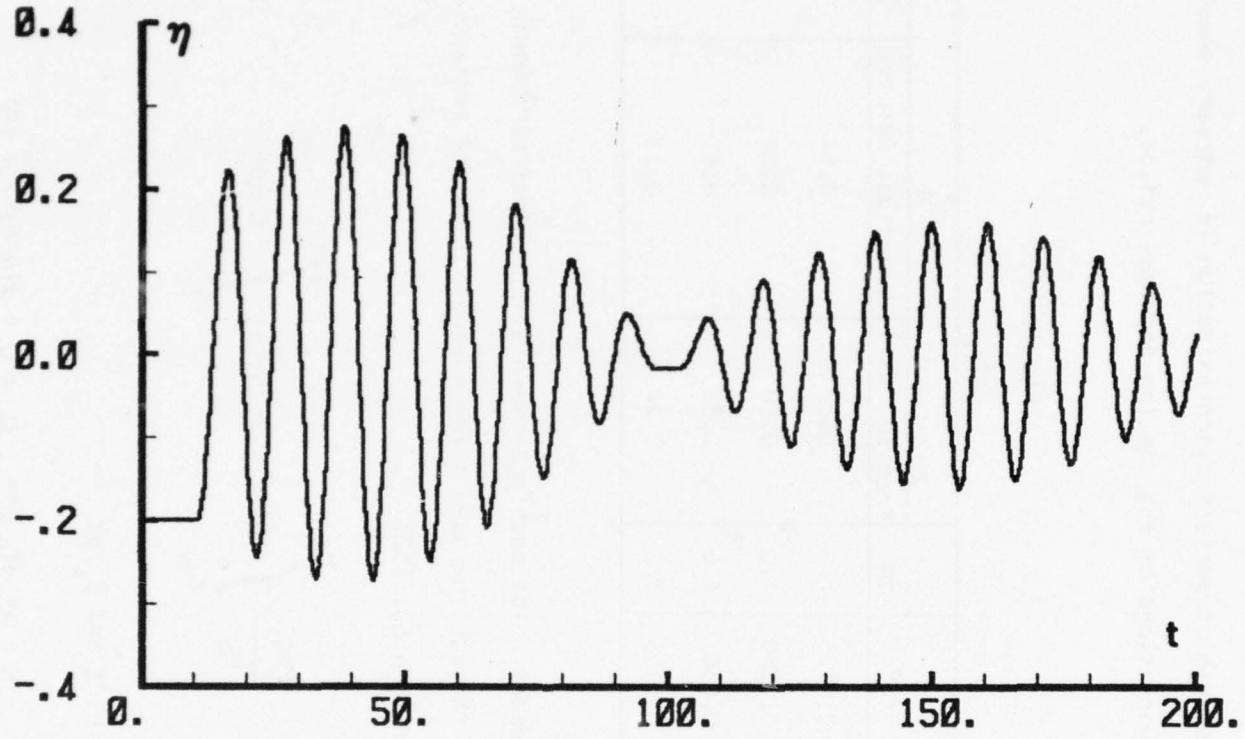

Fig. 55. Representative variation of cylinder displacement versus time for $\omega_o > \omega_o^*$.

calculations. According to the hypothesis advanced by Vickery and Watkins, η_M^* should be uniquely determinable by S_G. The results obtained through use of the model are tabulated below. The results in Table III show that cylinder response at perfect synchronization is not very sensitive to the individual variations of the damping and mass ratios.

TABLE III

SET	ζ	a_o	S_G	η_M^*		
				From Eq. (54)	Numerical Results	Eq. (56)
I	0.02	0.0125	1.6	0.52	0.54	0.56
II	0.04	0.0250	1.6	0.58	0.58	0.58
III	0.08	0.050	1.6	0.52	0.61	0.58
IV	0.04	0.0125	3.2	0.24	0.25	0.26

An exact relationship between S_G and other parameters may be established through the use of the energy balance at perfect synchronization. Re-writing Eq. (52)

$$\frac{2\pi\zeta S_o}{\omega_o}\int_t^{t+T}\dot{\eta}^2 dt = 2\pi^2 S_o{}^2 a_o \int_t^{t+T} C_L\dot{\eta}dt \qquad \text{(52 repeat)}$$

and expressing ζ and C_L as

$$\eta = \eta_M^* \sin\omega^* t \ , \ C_L = C_L{}^* \sin(\omega^* t + \phi^*)$$

where ϕ^* is the phase angle between the force and the displacement at perfect synchronization one has

$$S_G = \frac{\zeta}{a_o} = \pi \omega^*_o S_o \frac{\int_t^{t+T} C_L \dot{\eta} dt}{\int_t^{t+T} \dot{\eta}^2 dt} = \frac{\pi \omega^*_o S_o C_L^* \sin\phi^*}{\omega^* \eta^*_M} \tag{55}$$

or

$$\eta^*_M = \frac{\pi \omega^*_o S_o C_L^* \sin\phi^*}{\omega^* S_G} \tag{56}$$

Equation (56) shows that η^*_M is not a unique function of S_G. However, since ϕ^*, C_L^*, and ω^*/ω^*_o do not vary significantly, η^*_M varies approximately as S_G^{-1}. A comparison of Eqns. (54) and (56) shows that Eq. (56) requires the use of parameters which must be determined either numerically or experimentally whereas Eq. (54) requires only a knowledge of C_{L_o} and ω_o or U_r.

The results obtained through the use of Eq. (56) for the four sets of input parameters are also shown in Table III. Clearly the direct and indirect predictions of η^*_M are in excellent agreement, as would be expected.

The η^*_M-S_G relationship given by Eq. (56) is expected to hold true for values of ω_o other than ω^*_o provided ω_o is confined to the region of synchronization. Any small deviations between the predictions of

$$\eta_M = \frac{\pi \omega_o S_o C_L \sin\phi}{\omega S_G} \tag{56a}$$

from those directly calculated with the model are simply due to small modulations in the amplitude of oscillations. Numerical calculations which

can easily be performed through the use of Figs. 48 and 52-54 have shown that the predictions of Eq.(56a) are within a few percent of those obtained directly.

The transverse oscillations of a cylinder in uniform flow increase the affective projected area of the cylinder and hence the bluffness of the body. Consequently, hydroelastic oscillations of a cylinder, such as the strumming of a cable, not only cause alternating stress, fatigue, and noise but also increased drag.

The numerical model calculated two important characteristics of the fluctuating drag force: the mean drag and the amplitude of oscillation. Figure 56 shows the mean drag coefficient, $\overline{C}_D$, and the amplitude of the fluctuating component, $\Delta\overline{C}_D$, as a function of ω_o or U_r. Also shown in Fig. 56 is a data point obtained experimentally [81] for the corresponding ω_o and η_M values.

Figure 57 is a representative plot of the instantaneous value of C_D as a function of time. It shows, among other things, that the drag force oscillates at a frequency twice that of the lift force (for lift $T \simeq 10$ and for drag $T \simeq 5$).

The separation points on an oscillating cylinder oscillate with a frequency equal to that of the cylinder. Representative results presented in Fig. 58 show that the mean position of the separation angle remains practically constant at a value of $\overline{\theta}_s = 77$ degrees. The amplitude of the fluctuations follow a pattern very similar to that of η_M. The stagnation point undergoes similar oscillations. The results have shown that the instantaneous position of the stagnation point nearly coincides with that which would have resulted with a uniform flow at the instantaneous total velocity. In other words, the small oscillations of the stagnation

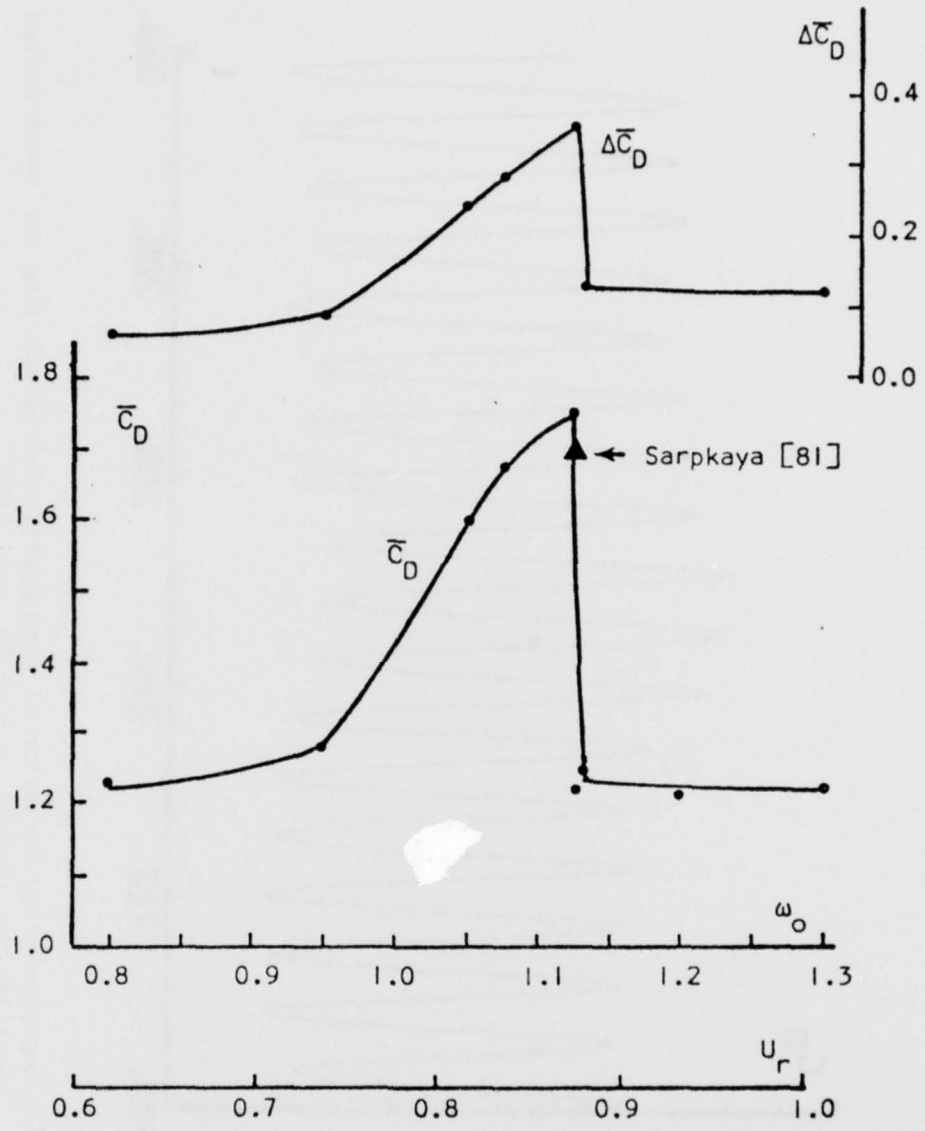

Fig. 56. Drag coefficient versus ω_o for ζ=0.02, a_o=0.0125.

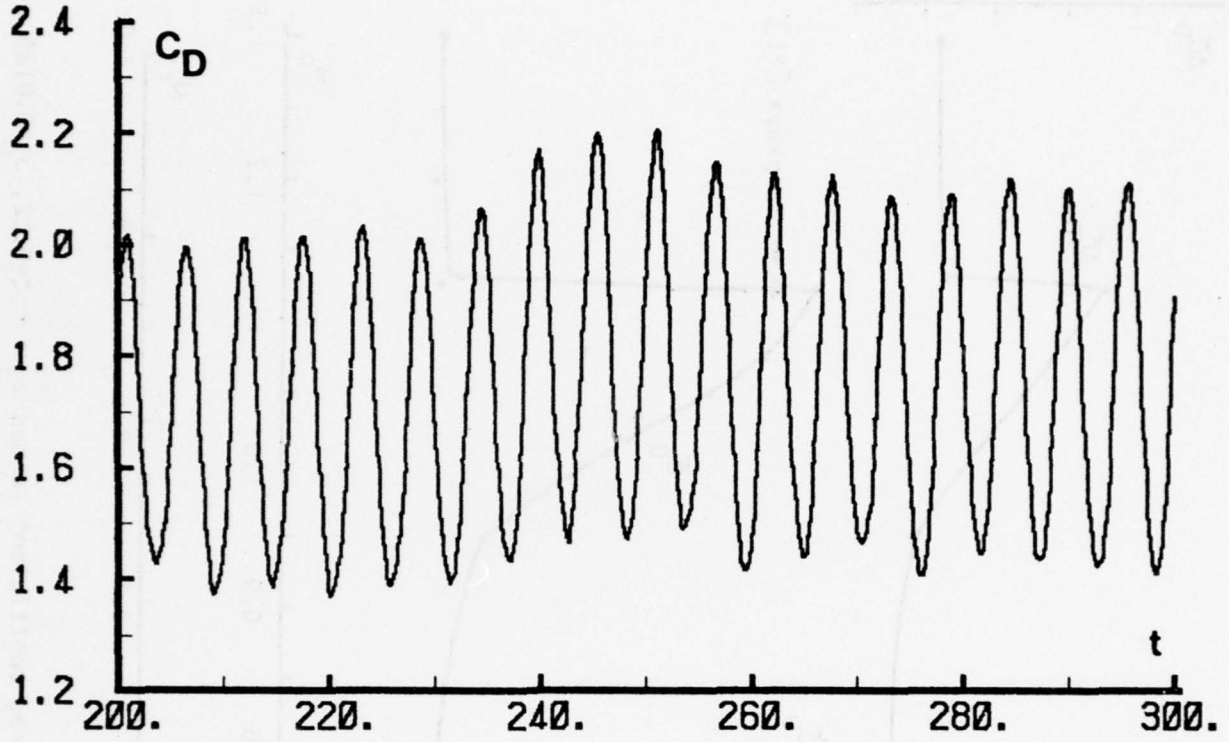

Fig. 57. Representative variation of drag coefficient versus time for synchronized oscillations (ζ=0.02, a_o=0.0125, ω_o=1.125).

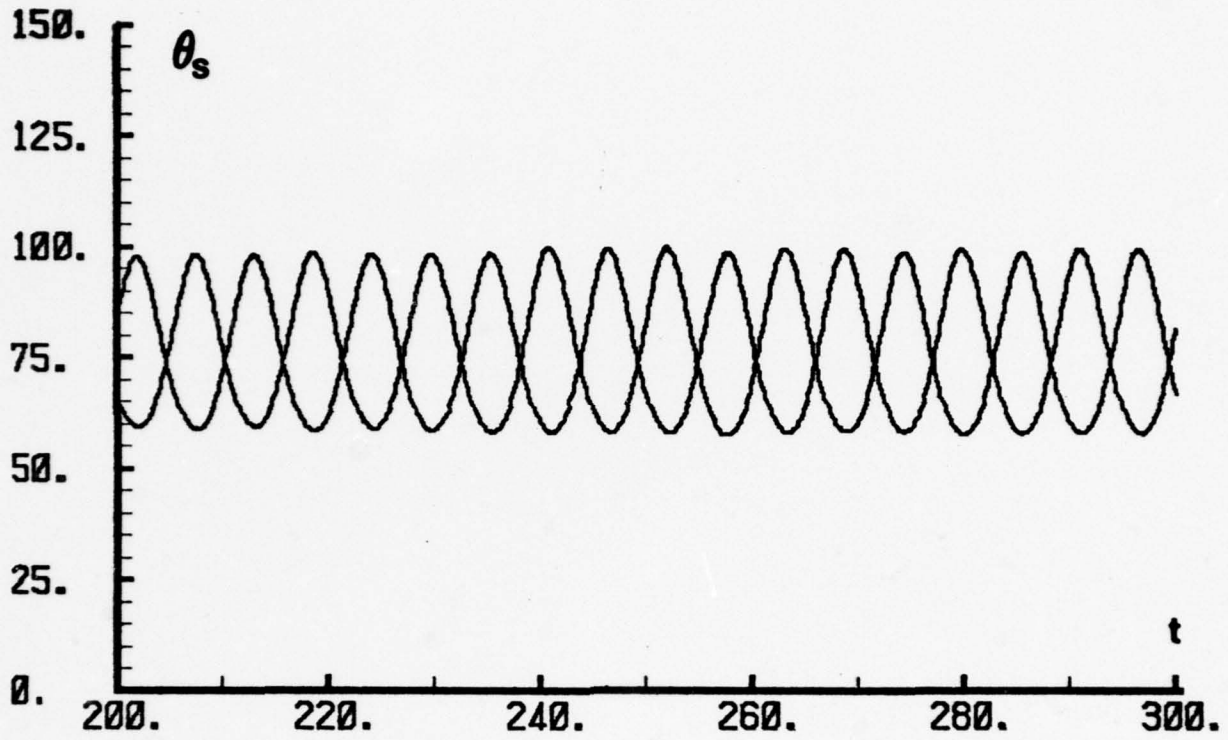

Fig. 58. Representative variation of separation angle versus time for synchronized oscillations (ζ=0.02, a_o=0.0125, ω_o=1.125).

point relative to the uniform flow are obscured by the larger oscillations resulting from the oscillations of the cylinder or of the ambient flow relative to the cylinder.

VII. CONCLUSIONS

The results presented herein warrant the following conclusions:

1. A discrete-vortex model based on the rediscretization of shear layers and the use of appropriate vorticity cancellation mechanisms can produce results which are in conformity with those obtained experimentally;

2. The numerical model allows experimentation with the variation of any one of the independent parameters and permits one to understand the governing physical mechanisms;

3. It has been shown that two major flow parameters, namely the drag coefficient and the Strouhal number, are least sensitive to changes in the characteristics of the wake. The Strouhal number is intrinsic to the shape of the bluff body and its magnitude cannot be varied more than a few percent by varying the strength of the vortices by physical means. Experiments over the past 50 years are in conformity with these conclusions;

4. The lift coefficient is the one most sensitive to the changes of flow in the near wake. This finding of the numerical model and the difficulty of obtaining consistent laboratory data for lift are in conformity with each other. The numerical model explains the physical mechanism as to why lift should be a strong function of the evolution of the near wake;

5. The discrete vortex model, as all other numerical methods attempting to model a turbulent region of a flow and its interaction with a laminar region, is in need of a hypothesis to properly simulate the circulation dissipation and the vorticity diffusion caused by turbulence.

Notwithstanding this fact, a very simple decay mechanism is capable of simulating the said consequences of turbulence;

6. The predictive powers of the numerical model have been put to test through its use in the study of self-excited oscillations of elastically mounted circular cylinders. The results were found to be in conformity with practically all observations and measurements made in recent years and led to the understanding of the mechanisms governing the synchronization phenomenon.

REFERENCES

1. Sacksteder, R., "On Oscillatory Flows," The Mathematical Intelligencer, v. 1, p. 45-51, 1978.

2. Roshko, A., On The Development of Turbulent Wakes from Vortex Streets, NACA Report 1191, Washington, D. C., 1954.

3. Bearman, P. W., "On Vortex-Street Wakes," J. Fluid Mech., v. 28, p. 625-641, 1967.

4. Calvert, J. R., "Experiments on the Low-Speed Flow Past Cones," J. Fluid Mech., v. 27, p. 273-289, 1967.

5. Simmons, J. E. L., "Similarities Between Two-Dimensional and Axisymmetric Vortex Wakes," The Aeronautical Quarterly, v. 28, p. 15-20, 1977.

6. National Physics Laboratory, Strouhal Number of Model Stacks Free to Oscillate, NPL Aero Report No. 1257, 1968.

7. Humphreys, J. S., "On a Circular Cylinder in a Steady Wind of Transition Reynolds Numbers," J. Fluid Mech., v. 9, p. 603-612, 1960.

8. Shih, S. and Hove, W., Hydrodynamic Loads on Circular Cylinders, Science Applications, Inc., Report No. SAI-79-548, 1978.

9. Wieselsberger, C., "Der Luftwiderstand von Kugeln," Z. Mech., v. 5, p. 140-144, 1914..

10. Fage, A. and Johansen, F. C., "The Structure of Vortex Sheets," Aeronautical Research Council R and M 1143, 1927.

11. Roshko, A., On the Drag and Shedding Frequency of Two-Dimensional Bluff Bodies, NACA TN 3169, Washington, D. C., 1954.

12. Fage, A. and Warsap, J. H., "The effects of Turbulence and Surface Roughness on the Drag of a Circular Cyclinder," Aeronautical Research Council R and M 1283, 1929.

13. Achenbach, E., "Influence of Surface Roughness on the Cross-Flow Around a Circular Cylinder," J. Fluid Mech., v. 46, p. 321-335, 1971.

14. Güven, O., Surface Roughness Effects on the Mean Flow Past Circular Cylinders, Iowa Institute of Hydraulic Research Report No. 175, May 1975.

15. Szechenyi, E., "Supercritical Reynolds Number Simulation for Two-Dimensional Flow Over Circular Cylinders," J. Fluid Mech., v. 70, p. 529-542, 1975.

16. Sarpkaya, T. and Isaacson, M., Waves and Wave Forces-in Theory and Application, (to be published), 1979.

17. Bublitz, P., "Messung der Drücke und Kräfte am ebenen, queranges-trömten Kreiszylinder, Teil I; Untersuchungen am ruhenden Kreis-zylinder," AVA-Bericht, 71 J11, 1971.

18. Collins, W. M. and Dennis, S. C. R., "The Initial Flow Past an Impulsively Started Circular Cylinder," Quart. J. Mech. Appl. Math., v. 26, p. 53-75, 1973.

19. Yang, K. T., "Unsteady Laminar Boundary Layers Over an Arbitrary Cylinder With Heat Transfer in an Incompressible Flow," J. Appl. Mech., v. 26, p. 171-178, 1959.

20. Thoman, D. C. and Szewczyk, A. A., Numerical Solutions of Time-Dependent Two-Dimensional Flow of a Viscous Incompressible Fluid Over Stationary and Rotating Cylinders, Notre Dame Mechanical Engineering Report No. 66-14, 1966.

21. Schwabe, M., "Über Druckermittlung in der Instationären ebenen Strömung," Ing.-Arch., v. 6, p. 34-50, 1935; also, NACA TM 1039, 1943.

22. Sarpkaya, T., "Separated Flow About Lifting Bodies and Impulsive Flow About Cylinders," AIAA Journal, v. 4, p. 414-420, March 1966.

23. Sarpkaya, T., Impulsive Flow About a Circular Cylinder, Naval Post-graduate School Report No. NPS-69SL-78-008, Monterey, California, March 1978.

24. Gerrard, J. H., "The Mechanics of the Formation Region of Vortices Behind Bluff Bodies," J. Fluid Mech., v. 25, p. 401-413, 1966.

25. Birkhoff, G., Hydrodynamics - A Study in Logic, Fact, and Simili-tude, Princeton Univ. Press, Princeton, N. J., 1950.

26. Iverson, H. W. and Balent, R., "A Correlating Modulus for the Fluid Resistance in Accelerated Motion," J. Applied Physics, v. 22, No. 3, p. 324-328, 1951.

27. Keim, S. R., "Fluid Resistance to Cylinders in Accelerated Motion," J. Hydraulics Div., ASCE, V. 83, No. HY6, 1956.

28. Hamilton, W. S., "Fluid Force on Accelerating Bodies," Proceed. of the 13th Coastal Engineering Conference, ASCE, New York, v. III, p. 1767-1782, 1972.

29. Odar, F. and Hamilton, W. S., "Forces on a Sphere Accelerating in a Viscous Fluid," J. Fluid Mech., v. 18, p. 302-314, 1964.

30. Sarpkaya, T., and Garrison, C. J., "Vortex Formation and Resistance in Unsteady Flow," J. of Appl. Mech., v. 30, Series E, p. 16-24, March 1963.

31. Sarpkaya, T., "The Hydrodynamic Resistance of Roughened Cylinders in Harmonic Flow," Trans. The Royal Institution of Naval Architects, v. 120, p. 41-55, 1978.

32. Morison, J. R., "The Force Exerted by Surface Waves on Piles," Petroleum Transactions, v. 189, p. 149-157, 1950.

33. Ingham, D. B., "Note on the Numerical Solution for Unsteady Viscous Flows Past a Circular Cylinder," J. Fluid Mech., v. 31, p. 815-820, 1968.

34. Gallagher, R. H., Oden, J. T., Taylor, C. and Zienkiewicz, O. C. (eds.), Finite Elements in Fluids, Volumes 1 and 2, John Wiley & Sons, 1975.

35. Bretanow, T. and Ecer, A., "Finite-Element Analysis of Unsteady Incompressible Flow Around an Oscillating Obstacle of Arbitrary Shape," AAIA J., v. 11, No. 11, p. 782-795, 1973.

36. Fromm, J. E. and Harlow, F. H., "Numerical Solution of the Problem of Vortex Street Development," Physics of Fluids, v. 6, p. 975-982, 1963.

37. Nichols, B. D. and Hirt, C. W., "Numerical Calculation of Wave Forces on Structures," Proc. 15th Conference on Coastal Engineering, July 11-17, 1976, (ASCE, New York).

38. Rosenhead, L., "Formation of Vortices From a Surface of Discontinuity," Proc. Roy. Soc. A, v. 134, p. 170-192, 1931.

39. Birkhoff, G. D. and Fisher, J., "Do Vortex Sheets Roll Up?", Rc. Circ. mat. Polermo, Ser. 2, v. 8, p. 77-90, 1959.

40. Hama, F. R. and Burke, E. R., On The Rolling Up of a Vortex Sheet, Univ. Maryland TN no. BN-220, 1960.

41. Abernathy, F. H. and Kronauer, R. E., "The Formation of Vortex Streets," J. Fluid Mech., v. 13, p. 1-20, 1962.

42. Gerrard, J. H., "Numerical Computation of the Magnitude and Frequency of the Lift on a Circular Cylinder," Philosophical Transactions of the Royal Society, London, Series A, v. 261, No. 1118, p. 137-162, January 1967.

43. Sarpkaya, T., "An Analytical Study of Separated Flow About Circular Cylinders," Journal of Basic Engineering, v. 90, p. 511-520, December 1968.

44. Chorin, A. J. and Bernard, P. S., Discretization of a Vortex Sheet With an Example of Roll-Up, Univ. California, Berkeley Engng, Rep. FM-72-5, 1972.

45. Moore, D. W., "A Numerical Study of the Roll-Up of a Finite Vortex Sheet," J. Fluid Mech., v. 63, p. 225-235, 1974.

46. Fink, P. T. and Soh, W. K., "Calculation of Vortex Sheets in Unsteady Flow and Applications in Ship Hydrodynamics," Tenth Symp. Naval Hydrodynamics, Cambridge, Mass., 1974.

47. Deffenbaugh, F. D. and Marshall, F. J., "Time Development of the Flow About an Impulsively Started Cylinder," AIAA J., v. 14, p. 908, 1976.

48. Clements, R. R. and Maull, D. J., "The Representation of Sheets of Vorticity by Discrete Vortices," Prog. Aerospace Sci., v. 16, p. 129-146, 1975.

49. Milne-Thomson, L. M., Theoretical Hydrodynamics, 5 ed., MacMillian, 1968.

50. Sarpkaya, T., "Lift, Drag, and Added-Mass Coefficients for a Circular Cylinder Immersed in a Time-Dependent Flow," J. Applied Mech., v. 85, Series E, p. 13-15, March 1963.

51. Pohlhausen, K., "Zur Näherungsweisen Integration der Differentialgleichung der Laminaren Grenzschicht," Z. Agnew. Math. Mech., v. 1, p. 252-268, 1921.

52. Stratford, B. S., Flow in Laminar Boundary Layers Near Separation, ARC Tech. Rept. BSM No. 3002, 1957.

53. Thwaites, B., "Approximate Calculation of the Laminar Boundary Layer," Aeronaut. Quart., v. 1, p. 245-280, November 1949.

54. Curle, N. and Skan, S. W., "Approximate Methods for Predicting Separation Properties of Laminar Boundary Layers," Aeronaut. Quart., v. 8, p. 264, 1957.

55. Timman, R. A., "One-Parameter Method for the Calculation of Laminar Boundary Layers," Rep. Trans. Nat. Luchtv Lab, Amsterdam, v. 15, p. 29-45, 1949.

56. Loitianski, L. G., "Approximate Method for Calculating the Laminar Boundary Layer on the Airfoil," Dokl. (Proc.) Acad. Sci. USSR, v. XXXV, 1942.

57. Hiemenz, K., "Die Grenzschicht an Einem in der Gleichförmigen Flüssigheitsstrom Eingetauchten Geraden Kreiszylinder," Thesis, Gôttingen, Dinglers Polytech J., v. 326, p. 32, 1911.

58. Meksyn, D., New Methods in Laminar Boundary-Layer Theory, Pergamon Press, 1961.

59. Takada, H., "An Extension to the Critical Flow of Stratford's Theory for Predicting the Turbulent Separation Position," J. Physical Society Japan, v. 39, p. 1106-1112, October 1975.

60. Schuh, H., "Unsteady Boundary Layers," Z.f. Flugwiss Heft. 5, p. 123-131, 1953.

61. Schlichting, H., Boundary Layer Theory, 6th ed., McGraw-Hill, 1968.

62. Davis, D. M., An Analytical Study of Separated Flow About a Circular Cylinder, M. Sc. Thesis, Naval Postgraduate School, Monterey, California, 1970.

63. Gerrard, J. H., "The Measurement of the Formation Region of Vortices Behind Bluff Bodies," J. Fluid Mech., v. 1, p. 401-413, 1966.

64. Schaefer, J. W. and Eskinazi, S. W., "An Analysis of the Vortex Street Generated in a Viscous Fluid," J. Fluid Mech., v. 6, p. 241-260, 1959.

65. Griffin, O. M., "Effects of Synchronized Cylinder Vibration on Vortex Formation and Mean Flow," Flow-Induced Structural Vibrations (ed. Eduard Naudascher), Springer-Verlag, Berlin, 1974.

66. Davies, M. E., "A Comparison of the Wake Structure of a Stationary and Oscillating Bluff Body, Using a Conditional Averaging Technique," J. Fluid Mech., v. 75, p. 209-231, 1976.

67. Clements, R. R., "Flow Representation, Including Separated Regions, Using Discrete Vortices," AGARD Lecture Series on Computational Fluid Dynamics, No. 86, 1977.

68. Sarpkaya, T., "An Inviscid Model of Two-Dimensional Vortex Shedding for Transient and Asymptotically Steady Separated Flow Over an Inclined Plate," J. Fluid Mech., v. 68, p. 109-128, 1975.

69. Bloor, M. S. and Gerrard, J. H., "Measurements of Turbulent Vortices in a Cylinder Wake," Proc. Roy. Soc. A, v. 294, p. 319-342, 1966.

70. Schmidt, D. V. and Tilmann, P. M., "On the Development of the Circulation in Water of Circular Cylinders," Acustica, v. 27, p. 14-22, 1972.

71. Dwyer, H. A. and McCroskey, "Oscillating Flow Over a Cylinder at Large Reynolds Number," J. Fluid Mech., v. 61, p. 753, 1973.

72. Clements, R. R., "An Inviscid Model of Two-Dimensional Vortex Shedding," J. Fluid Mech., v. 57, p. 321-336, 1973.

73. Bublitz, P., "Unsteady Pressures and Forces Acting on an Oscillating Circular Cylinder in Transverse Flow," Flow-Induced Structural Vibrations (ed. Eduard Naudascher), Springer-Verlag, Berlin, p. 443-453, 1974.

74. Chen, Y., "Wake Swing and Vortex Shedding in a Cross Flow Past a Singular Circular Cylinder," Flow-Induced Structural Vibrations (ed. Eduard Naudascher), Springer-Verlag, Berlin, 1974.

75. Parkinson, G. V., "Mathematical Models of Flow-Induced Vibrations of Bluff Bodies," Flow-Induced Structural Vibrations (ed. Eduard Naudascher), Springer-Verlag, Berlin, p. 81-127, 1974.

76. Hartlen, R. T. and Currie, I. G., "Lift-Oscillator Model of Vortex-Induced Vibration," ASCE, EM5, p. 577-591, October 1970.

77. Feng, C. C., The Measurement of Vortex Induced Effects in Flow Past Stationary and Oscillating Circular and D-Section Cylinders, M. A. Sc. Thesis, U. British Columbia, 1968.

78. Davies, M. E., "A Comparison of the Wake Structure of a Stationary and Oscillating Bluff Body, Using a Conditional Averaging Technique," J. Fluid Mech., v. 75, p. 209-231, 1976.

79. Thomson, W. T., Vibration Theory and Applications, Prentice-Hall, 1965.

80. Vickery, B. J. and Watkins, R. D., "Flow-Induced Vibrations of Cylindrical Structures," Proc. of the First Australian Conference on Hydromechanics, Univ. of Western Australia, Nedlands, Australia, p. 213-239, 1962.

81. Sarpkaya, T., "Fluid Forces on Oscillating Cylinders," J. Waterway, Port, Coastal and Ocean Division, ASCE, v. 104, No. WW4, p. 275-290, 1978.

INITIAL DISTRIBUTION LIST

1.	Defense Documentation Center Cameron Station Alexandria, Virginia 22314	2
2.	Library, Code 0212 Naval Postgraduate School Monterey, California 93940	2
3.	Civil Engineering Laboratory Naval Construction Battalion Center Port Hueneme, California 93043 ATTN: Mr. Dallas J. Meggitt	20
4.	Prof. T. Sarpkaya Code 69SL Mechanical Engineering Naval Postgraduate School Monterey, Calif. 93940	20
5.	Library of Congress Science and Technology Division Washington, D. C. 20540	1
6.	Department Chairman, Code 69 Naval Postgraduate School Monterey, Calif. 93940	1
7.	Dean of Research, Code 012 Naval Postgraduate School Monterey, Calif. 93940	1
8.	Prof. G. V. Parkinson University of British Columbia Mechanical Engineering Vancouver, Canada	1
9.	Dr. Robert D. Blevins General Atomic Company San Diego, California	1
10.	Naval Research Laboratory Ocean Technology Division Code 8441 Washington, D. C. 20390 Attn: Dr. O. M. Griffin	1
11.	Prof. A. Roshko Department of Aeronautics California Institute of Technology Pasadena, California 91109	1

12. Prof. E. Berger
Technische Universität Berlin
1 Berlin 12
Müller-Breslau-Str. 8
Germany 1

13. Dr. D. J. Maull
Engineering Department
University of Cambridge
Trumpington Street
Cambridge CB2 1PZ
United Kingdom 1

14. Prof. E. Naudascher
Institut für Hydromechanik
Universität Karlsruhe
75 Karlsruhe, Kaiserstrasse 12
Germany 1

15. Prof. Dr. H. Schlichting
AVA
Bunsenstrasse 10
1000 Göttingen, Germany 1